# THE DEVELOPMENT, CHARACTERIZATION AND TESTING OF MG-RICH

# PRIMERS

A Dissertation
Submitted to the Graduate Faculty
of the
North Dakota State University
of Agriculture and Applied Science

By

Dante Battocchi

In Partial Fulfillment
for the Degree of
DOCTOR OF PHILOSOPHY

Major Program:
Materials and Nanotechnology

December 2011

Fargo, North Dakota

North Dakota State University

Graduate School

Title

THE DEVELOPMENT, CHARACTERIZATION AND TESTING OF MG-RICH PRIMERS

By

Dante Battocchi

The Supervisory Committee certifies that this *disquisition* complies with North Dakota State

University's regulations and meets the accepted standards for the degree of

DOCTOR OF PHILOSOPHY

SUPERVISORY COMMITTEE:

Gordon Bierwagen
_____

Chair

Erik Hobbie
_____

Xinnan Wang
_____

Chad Ulven
_____

Approved:

1-25-2012                                          Erik Hobbie
_____                _____

Date                                          Department Chair

# ABSTRACT

Aluminum alloys are widely used in aircraft industry for their strength and light weight. Those alloys that are hardened by precipitation, especially the Copper-rich of the 2000 series, are prone to corrosion and are protected against it using chromate containing coatings. The primary component of these coating systems is Chromium 6+ (CrVI) that has been found to be very toxic in the environment and carcinogenic, toxic and mutagenic in humans.

The Mg-rich primer development is the result of a successful multi-year project funded by the US Air-force with its objective the replacement of coatings based on CrVI with a class of coatings less toxic and with comparable protective performances. The Mg rich primer fulfilled the USAF requirements and it is currently undergoing commercial and military qualifications testing.

The use of Mg as one of the active pigments in coatings allows the primer to protect the underlying Al sacrificially, not considered possible for this substrate until now. Mg is anodic to most of the other structural metals and when particulate Mg became available commercially, the concept of the primer was first developed by analogy to Zn-rich coatings for steel. When Mg and Al are in contact and immersed in a corrosive environment, magnesium corrodes preferentially and protects the aluminum.

DEDICATION

To my wife Holly,
You make everything bright and happy!
I love you


To my mother Bruna, my brother Enrico, my sister Stefania,
for all your support, strong and safe, everywhere I am
I love you

To my brothers of the AGdR, my friends around the world and the Universe,
all together you make life beautiful and fulfilling
I love you


For Nino
I love you

*Non ti curar di lor ma guarda e passa*
*Dante Alighieri*

TABLE OF CONTENTS

LIST OF TABLES

LIST OF FIGURES

viii

ix

# LIST OF EQUATIONS

CHAPTER 1. INTRODUCTION TO THE MG-RICH PRIMERS STUDIES

Aluminum (Al) alloys are widely used in aircraft industry for their strength and light weight. Those alloys that are hardened by precipitation, especially the Copper-rich of the 2000 series, are prone to corrosion and are protected against it using chromate containing coatings. The primary component of these coating systems is Chromium $6^+$ (CrVI) that has been found to be very toxic in the environment and carcinogenic, toxic and mutagenic in humans.

The Magnesium (Mg)-rich primer (MgRP) development is the result of a multi-year project funded by the US Air-force with its objective the replacement of coatings based on CrVI with a class of coatings less toxic and with comparable protective performances. The Mg rich primer fulfilled the USAF requirements and it is currently undergoing commercial and military qualifications testing.

The use of Mg as one of the active pigments in coatings allows the primer to protect the underlying Al sacrificially, not considered possible for this substrate until now. The technology is based on the fact that Mg is anodic to most of the other structural metals and when particulate Mg became available commercially, the concept of the primer was first developed by analogy to Zn-rich coatings for steel. When Mg and Al are in contact and immersed in a corrosive environment, Mg corrodes preferentially and protects the Al. The following chapters detail the development work and characterization on this new class of coatings for the past several years and they have all been published in peer reviewed journals.

Chapter 2, Electrochemical characterization of a Mg-rich primer (Corrosion Science 47 (2005) 1165–1176), demonstrates the electrochemical behavior of the Mg-rich primer when used to protect Al 2024 T3 and Al 7075 T6. The coating system was formulated using Mg particles and epoxy resin and its electrochemical behavior has been studied using Electrochemical Impedance Spectroscopy (EIS), Open Circuit Potential (OCP) and potentiodynamic polarization. It was found that the MgRP provides sacrificial protection to the

Al substrate by a two-stage mechanism. In a first stage, corrosion of Al is prevented by cathodic polarization, and the precipitation of a porous barrier layer of Mg oxide was observed.

Chapter 3, The use of multiple electrochemical techniques to characterize Mg-rich primer for Al alloys (Progress in Organic Coatings, 59, 3, (2007), 172-178), refers to the use of multiple electrochemical techniques that have been utilized to characterize the behavior of this class of Cr-free coatings. This approach was taken to ensure that the corrosion protective behavior of Mg-rich primers over Al aircraft alloys was properly understood. The electrochemical testing was done in conjunction with the qualification testing of the primer materials for US Air Force and US Navy specifications so that as this new class of primers did not encounter any unexpected corrosion protection-related deficiencies. To confirm that the MRPs did indeed provide cathodic, sacrificial protection to these alloys, the Open Circuit Potential (OCP) was used to indicate when the potential of the alloy substrate is modified by contact with the Mg. The results were confirmed also by measuring the potential of the minimum corrosion current in a potentiodynamic scan of the coating system. Electrochemical Impedance Spectroscopy (EIS) and Electrochemical Noise Methods (ENM) were also used to characterize the system in immersion. Finally, the Scanning Vibrating Electrode Technique (SVET) was used to examine local damage protection by the Mg-rich primer about a deliberately induced scratch in the coating system.

Chapter 4, Comparison of testing solutions on the protection of Al alloys using a Mg-rich Primer (Corrosion Science, 48, 8, (2006), 2226-2240), is focused on the effect of the immersion environment on the coating performances. These coatings are capable of sacrificial protection, but assessment of their efficiency and durability can be strongly affected by the testing environment. In this chapter, two solutions commonly used in exposure studies are compared: 0.1% NaCl and Dilute Harrison Solution (DHS). The corrosion behavior of two aluminum alloys coated with a Mg-rich coating, of pure Mg and of the bare aluminum substrates was assessed in the two solutions using electrochemical techniques. It was found

2

that the corrosion rate of pure Mg was higher in DHS than in diluted NaCl, although the dissolution rate of the Mg embedded in the polymer matrix was not significantly affected.

Chapter 5, The Use of Mg Alloys as Pigments in Mg-rich Primers For Protecting Al Alloys (Corrosion 65, 318, 2009), was developed with the goal to determine how much the metal pigment alloy composition can be varied without sacrificing corrosion protection. To achieve that, three different primers based on Mg alloy powders as pigments were formulated with an epoxy-polyamide polymer binder at different pigment volume concentrations (PVCs). Their behavior was studied after cyclic exposure in Prohesion Chamber via electrochemical methods. Testing results from Electrochemical Impedance Spectroscopy (EIS) and Scanning Electron Microscopy (SEM) showed that the metal-rich primers with Mg alloys as pigments could provide cathodic protection, and precipitates formed from oxidation of Mg alloy particles were similar to the ones found in the pure Mg-rich primer system.

Chapter 6 and 7 compose the polymeric binder section of the dissertation, in which a two component binder was developed and the use of a new resin was discussed.

Chapter 6, The development of a two component Mg rich primer for controlling corrosion of Al alloys (J Coat Technol Res, Volume 7, Number 6, November 2010), presents the development of a new binder system to take the place of the original system that was not easily adaptable for military applications. The original polymer binder system, that enabled exceptionally good performance, was based on a three-component binder system comprised of an epoxy resin, di-isocyanate, and an amino functional silane. Due to its complexity, a two-component binder system was desired that could provide equivalent or better performance than the three-component system. As a result, research was conducted to develop a two-component Mg-rich primer that provides excellent corrosion protection to Al alloys. Electrochemical techniques were used to monitor the performances during accelerated exposure. The results showed that all of the variables investigated, which included epoxy resin molecular weight, curing agent functionality, and Mg content significantly affected the coating performance. An optimized formulation for the two-component primer was identified, which

showed very similar corrosion protection performance to the original primer based on the three-component binder.

In Chapter 7, Thermal stability of Mg-rich primers based on Glycidyl carbamate resins (Polymer Degradation and Stability 95 (2010) pg 1160-1166), a new polymeric system was used to formulate Mg-rich primers and coatings of outstanding thermal stability were obtained. Here, the Mg-rich primer technology was combined with a newly developed silane-modified glycidyl carbamate binder. The objective of the study was to evaluate the new binder system, specifically with respect to overall film properties in the Mg rich primer technology. However, during thermogravimetric analysis of samples, previously unobserved properties were observed. The samples transformed into an intact residue, with the amount of the residue ranging between 60 to 90% weight depending on the coating composition. This new property is essentially a function of the metallic pigment particles in the composite. The discovery of this outstanding thermal stability has the potential to increase the range of application for the primers. Electrochemical Impedance Spectroscopy was extensively used to test and study the Mg rich primer, and one of the options for data analysis is fitting and modeling.

In Chapter 8, Modeling of Electrochemical Impedance Data of a Mg Rich primer (Journal of The Electrochemical Society, 155, 10, E143-E149, 2008), interpretation of the EIS data has been accomplished using a transmission-line model. This model was developed for the study of Zn rich coating systems and it accounted for the contact impedance between the Zn particles, the impedance associated with the Zn dissolution, and the percolation resistance of the coating. The EIS experiments were conducted on a Mg-rich primer on a gold substrate placed under immersion in diluted Harrison's solution. The data were analyzed using the measurement model technique to determine the consistency with respect to Kramer-Kronig relationships. In addition to that, the transmission-line model was used to analyze the data to demonstrate its applicability for studying the protection afforded by the Mg-rich primer. The following table explains my contributions in each of the chapters.

Table 1. Chapters description

| | |
|---|---|
| **Chapter 2**: Electrochemical behaviour of a Mg-rich primer in the protection of Al alloys<br>D. Battocchi , A. M. Simões, D. E. Tallman, G. P. Bierwagen<br>*Corrosion Science 47 (2005) 1165–1176* | • Planned and conducted the experiments<br>• Interpreted the results<br>• Discussed the results |
| **Chapter 3**: The Use of Multiple Electrochemical Techniques to Characterize Mg-rich Primers for Al Alloys<br>Gordon Bierwagen, Dante Battocchi, Alda Simões, Anthony Stamness and Dennis Tallman<br>*Progress in Organic Coatings, Volume 59, Issue 3, 1 June 2007, Pages 172-178* | • Planned and conducted the experiments<br>• Interpreted the results<br>• Discussed the results |
| **Chapter 4**: Comparison of testing solutions on the protection of Al-alloys using a Mg-rich primer<br>D. Battocchi, A. M. Simões, D. E. Tallman and G. P. Bierwagen<br>*Corrosion Science, Volume 48, Issue 8, August 2006, Pages 2226-2240* | • Planned and executed the experiments<br>• Interpreted the results<br>• Discussed the results |
| **Chapter 5**: The Use of Mg Alloys as Pigments in Mg-rich Primers For Protecting Aluminum Alloys<br>Hong Xu, Dante Battocchi, Dennis E. Tallman and Gordon P. Bierwagen<br>*Corrosion 65, Issue 5, 2009, 318* | • Planned and conducted the experiments<br>• Interpreted the results<br>• Discussed the results<br>• Supervised the work of the student coauthor |
| **Chapter 6**: The development of a two component Mg rich primer for controlling corrosion of Al alloys<br>Jun Li, Jie He, Bret J. Chisholm, Missy Berry, Dante Battocchi, and Gordon P. Bierwagen<br>*J Coat Technol Res, Volume 7, Number 6, November 2010* | • Planned the experiments<br>• Interpreted the results<br>• Discussed the results<br>• Trained and supervised co-authors on measurement techniques and coating formulation |
| **Chapter 7**: Thermal stability of Mg-rich primers based on glycidyl carbamate resins<br>Neena Ravindran, Dipak Chattopadhyay, Dante Battocchi, Dean C. Webster, Gordon P. Bierwagen<br>*Polymer Degradation and Stability 95 (2010) pg 1160-1166* | • Planned the experiments<br>• Interpreted the results<br>• Discussed the results |

Table 2. Chapters description (Continued)

| | |
|---|---|
| **Chapter 8**: Modeling of Electrochemical Impedance Data of a Mg-Rich Primer Kerry N. Allahar, Dante Battocchi, Mark E. Orazem, Gordon P. Bierwagen, Dennis E. Tallman *Journal of The Electrochemical Society, 155, 10, E143-E149, 2008* | • Planned and conducted the experiments<br>• Interpreted the results<br>• Discussed the results<br>• Drawn the conclusions |
| **Chapter 9: Summary and Conclusions** | • Original chapter |
| **Chapter 10: Future work** | • Original chapter |

CHAPTER 2. ELECTROCHEMICAL BEHAVIOUR A MG-RICH IN THE PROTECTION OF AL ALLOYS

D. Battocchi[1], A. M. Simões[2], D. E. Tallman[1,3], G. P. Bierwagen[1]

## Abstract

The electrochemical behaviour of Mg-rich primer on Al Alloys, AA2024 and AA7075, has been studied via Electrochemical Impedance Spectroscopy (EIS), Open Circuit Potential (OCP) and potentiodynamic polarization. Results showed that the Mg-rich primer provides sacrificial protection to the Al substrate by a two-stage mechanism. In a first stage, corrosion of aluminium is prevented by cathodic polarization, whereas at a later stage the precipitation of a porous barrier layer of magnesium oxide was observed.
Keywords: Mg-rich primer, AA2024, AA7075, EIS, OCP, potentiodynamic polarization, sacrificial protection.

## Introduction

When two metals exposed to a corrosive environment are in put contact, the more active metal will corrode preferentially, providing sacrificial protection to the nobler one. This concept has been applied for many years to the protection of steel by the use of zinc-rich primers (ZRPs)[1,2] and trials using other compositions[3,4] and metals, including manganese,[5] have also been made. For aluminium, however, such sacrificial protection has not been applied. Aluminium is very close to the bottom of the galvanic series, below zinc, and therefore ZRPs would not be effective.

---

[1] NDSU, Department of Coatings and Polymeric Materials, Fargo, ND 58105-5376, USA

[2] IST, Chemical Engineering Department, Av. Rovisco Pais, 1049-001 Lisboa, Portugal

[3] NDSU, Department of Chemistry, Fargo, ND 58105, USA

Corrosion protection of aluminium surfaces is usually achieved by using chromate pre-treatments[6] or primers.[7] The severe restrictions to Cr use, dictated by its toxicity, require the development of environmentally less aggressive alternatives. The potential of Mg is negative of almost all the other structural materials,[8] including aluminium, and its use as a pigment presents therefore a possible alternative for the sacrificial protection of aluminium alloys. This new class of metal–rich primer for the protection of aluminium alloys can thus be formulated, in analogy to the formulation of Zn-rich primer for the protection of steel. To provide sacrificial protection, the Mg metal particles in the primer have to be in electrical contact with the substrate and also with each other. To achieve this requirement, the primer has to be formulated near or above the Critical Pigment Volume Concentration (CPVC) for the coating.[9] A Mg-based system for the protection of aluminium structures, based on this concept, has been developed and tested by Nanna and Bierwagen,[10] who have observed an excellent performance of aluminium panels sprayed with this Mg-rich primer in Prohesion testing.

Aluminium alloys AA 2024 T-3 and AA 7075-T6 are widely used in the aircraft industry for their high strength and low density. Their high strength is achieved by heat treatments that affect the microstructure of the alloys and lead to the formation of intermetallic precipitates. These precipitates, mostly rich in copper, are responsible for the generation of potential differences along the surface that make the alloys prone to localized corrosion.[11,12] The mode of protection of these alloys by Mg-rich primers is the concern of this work.

Electrochemical characterization of the system was obtained using electrochemical impedance spectroscopy (EIS), measurement of the open circuit potential (OCP) and potentiodynamic polarization. EIS is a technique that can simultaneously provide information on the corrosion mechanisms and quantitatively assesses corrosion protection provided by a coating to a metal substrate. For barrier coatings the impedance values should be above $10^6$ ohm cm$^2$, in order to decrease the corrosion rate, whereas for sacrificial coatings low impedance is required to ensure conductivity between the cathodic metal substrate and the anodic pigment.[13] When used together, potential monitoring and potentiodynamic polarization

8

can also provide valuable information about the status of the sacrificial protection provided by the primer, namely in what concerns the rate of Mg oxidation and the time evolution of the system. These two techniques were used and complemented by scanning electron microscopy (SEM).

## Experimental

Aluminium panels of AA 2024- T3 and AA 7075 – T6, with dimensions 150 x 75 x 2 $mm^3$, supplied by Q Panel Lab products (Cleveland OH) were used in the tests. The samples for the tests of the bare alloys were polished to grit 600 and then washed with distilled water and ethanol, whereas those coated with the Mg-rich primer were brushed with a wire brush and washed in distilled water and hexane. The magnesium-rich primer was made using a stabilized Mg particulate, of 30-40$\mu$m in average size, manufactured by Non Ferrum-Metallpulver GmbH, Salzburg, Austria. This particulate consists of Mg covered with a thin layer of MgO, intended to control the reactivity of magnesium[14] and thus prevent further oxidation under dry conditions. Dispersion was made using a silane-modified multi-layer/IPN polymer matrix[10]. In order to ensure electronic conduction, the Mg-rich primer was formulated at 50% PVC (approximately the CPVC of the system). The primer was applied through an air spray gun to a thickness of approximately 70 $\mu$m. A period of three days was allowed for complete drying before measurements were started.

A magnesium electrode was made by pressing the pigmentary magnesium particles using an International Crystal Laboratories (ICL) press at 20 MPa, which produced a pellet with surface area of ~1cm$^2$. For ease of handling, this pellet was glued onto an inert glass substrate using epoxy resin. Electric contact was made by a Pt wire embedded in the resin.

For both the bare and the coated aluminium, the electrochemical cell consisted of a glass cylinder reservoir clamped on the surface. Leaking was avoided by using an o-ring. The cylinder was filled with the electrolytic solution for the duration of the experiment. The exposed area of the working electrode was 7.06 cm$^2$. A saturated calomel electrode (SCE) was used as

the reference electrode (RE) and a Pt mesh with approximately 1 cm$^2$ area was used as counter electrode. Most of the electrochemical tests were made in 0.1 wt.% NaCl in distilled water. One of the experiments was conducted in Diluted Harrison's Solution, which emulates acid rain and consists of 0.35 wt% $(NH_4)_2SO_4$ and 0.05 wt% NaCl in distilled water.

A Gamry PC4/300 potentiostat/galvanostat with dedicated EIS 300 software (both from Gamry Instruments Inc.) was used to collect the electrochemical data. Impedance spectra were collected at the open circuit potential, using the frequency range of 50 kHz to 0.1/0.01 Hz. The signal amplitude was 5mV for the magnesium electrode and 10mV for all the other systems. All the currents presented are normalized to 1 cm$^2$. Potentiodynamic plots were obtained at a scanning rate of 5mV/sec, starting from the open circuit potential.

For SEM investigations, samples were mounted on aluminium mounts and coated with gold using a Technics Hummer II sputter coater. Images were obtained using a JEOL JSM-6300 Scanning Electron Microscope. EDAX information was obtained via a Thermo EDS detector using a VANTAGE Digital Acquisition Engine at 15KeV.

## Results and Discussion

### Coating structure

Macroscopically, the dry coating is matte to the sight and rough to the touch, as a result of the optically large metal particles used in its formulation. SEM inspection of the cross-section shows that the coating consists essentially of magnesium particles covered by a thin layer of binder. The distance between neighbour particles typically does not exceed 1$\mu$m – Figure 1.

### OCP

The solution pH was approximately 5. At this pH, Al becomes passive, as indicated in the Pourbaix diagram. The presence of inclusions and precipitates, however, can induce instability of the passive film and lead to localized corrosion, and so can the presence of aggressive ions, such as chlorides.
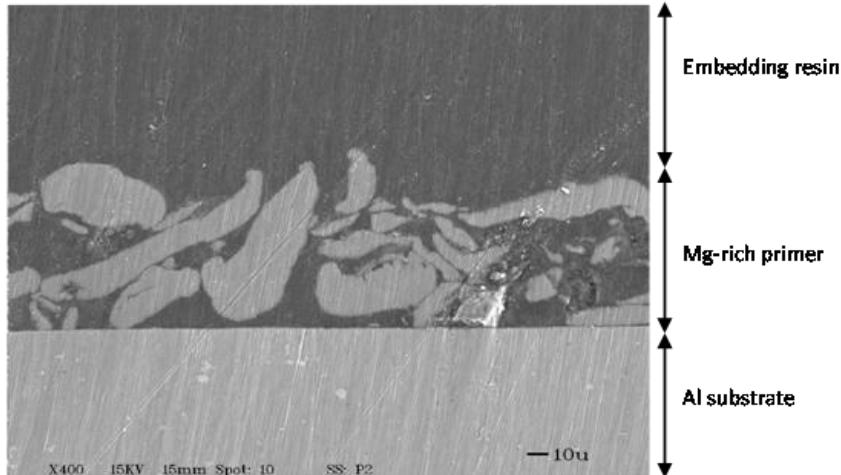
Figure 1. Cross-section micrograph of Mg-rich primer on aluminium alloy substrate

For the bare alloys the potential was stable from the first minutes of immersion, with the AA2024 potential higher than that of the AA7075 alloy by ~0.15V – Figure 2. Magnesium had a very negative potential, -1.6 V, and underwent fast corrosion, with visible bubbling on the surface due to the reduction of protons:

$$2H^+ + 2e^- \rightarrow H_2 \qquad \text{(Equation 1)}$$

which is the counter-reaction for the oxidation of Mg, which can occur either with the formation[15] of $Mg^+$ or by the direct oxidation to $Mg^{2+}$:

$$Mg \rightarrow Mg^{2+} + 2e^- \qquad \text{(Equation 2)}$$

The high rate of the cathodic reaction was assessed by measuring the pH on the Mg surface. With that purpose, the electrode was removed from the solution and pH coloured indicator paper was immediately put in contact with the surface. The pH measured in this way was approximately 11.

When the aluminium alloy was coated with the Mg-rich coating, the potentials achieved at steady-state were intermediate between those of the bare substrate and of the magnesium. They corresponded to the potential of the galvanic couple, in which magnesium polarized cathodically both of the Al alloys by approximately 0.35 V. This potential took approximately 1 hour to be achieved. At the beginning it started from a more anodic potential and then

fluctuated until a stable value was attained. This initial phase was probably due to the

activation of the sacrificial protection, which requires both the penetration of electrolyte to the

surface of the Mg particles and the dissolution of the MgO from the particle surface, leaving the

Mg exposed for oxidation.
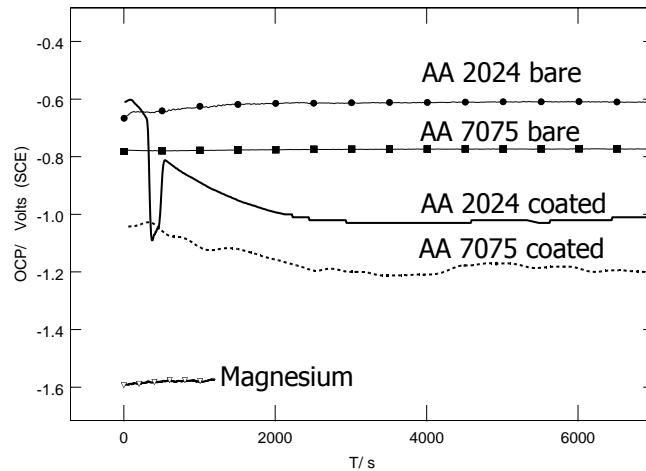


Figure 2. Open circuit potential of the bare substrates, of the magnesium-rich primer coated
substrates and of magnesium, in 0.1% NaCl

*DC potentiodynamic plots*

The dc potentiodynamic plot for Mg shows an approximately symmetrical curve around

the corrosion potential, revealing that the metal is in its active state – Figure 3. The corrosion

rate obtained by extrapolation of the Tafel lines is approximately $3 - 5 \times 10^{-4}$ A cm$^{-2}$. For the bare

Al alloys, the cathodic curves have a plateau corresponding to the diffusion-limited reduction of

dissolved oxygen, followed by a logarithmic increase of the current, probably due to reduction

of protons. Both alloys are very susceptible to localized corrosion at their open circuit potential,

since just a small anodic polarization leads to a current burst of several orders of magnitude,

corresponding to the quick growth of pits.
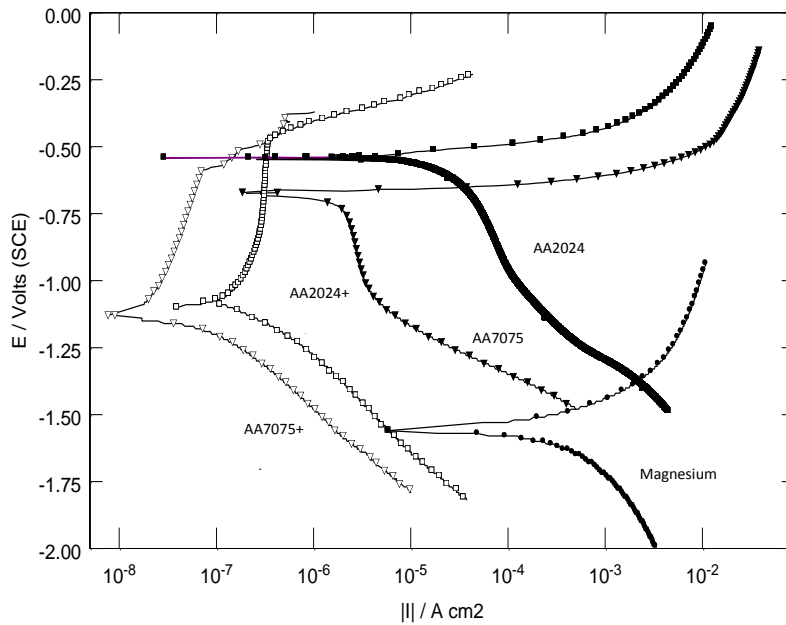
Figure 3. Potentiodynamic plots in 0.1% NaCl

For the aluminium substrates coated with Mg-rich primer, the cathodic branches of the plots are practically parallel, with a Tafel slope of 0.4V/decade, corresponding to the simultaneous reduction of oxygen and $H^+$. The anodic branch can be divided in two regions, corresponding to the behaviour of each of the materials. Below the pitting potential of the Al alloys the Tafel plot has a very high slope, ca. 0.8V/ decade, and reaches a limiting current with the coated 2024 alloy. Near the corrosion potential of the bare alloys, the slope of the curve decreases abruptly, probably revealing pitting of the substrate in parallel with the Mg oxidation. The slope of the first part of the anodic curve, i.e., the portion related with the oxidation of Mg, is considerably higher than that of bare magnesium. The relative values of the cathodic and anodic slopes on the bare Mg electrode show that magnesium dissolution proceeds under mixed cathodic-anodic control, whereas anodic control occurs when the magnesium particles are embedded in the polymer matrix. Thus, although in a normal situation of galvanic coupling the dissolution rate of the more active metal is accelerated, the use of

13

resin decreases the kinetics of magnesium oxidation, consequently prolonging its lifetime. Furthermore, pitting on either of these alloys is prevented by coupling to magnesium because of the cathodic polarization away from the pitting potential.

*Electrochemical Impedance Spectroscopy*

Corrosion of the Al alloys in 0.1% NaCl resulted in the formation of small pits. This was revealed in the impedance spectrum by a double layer capacitor in parallel with a resistor of several thousand ohm – Figure 4. Near the low frequency end of the spectrum another time constant, probably due to mass transfer control at the pits, was observed. This low frequency part of the spectrum was unstable at the beginning of exposure and became better defined with time. Apart from that, the shape of the spectrum was practically undisturbed during the immersion period, revealing only a rise of the total impedance.

Magnesium exhibited very low impedance with visible bubbling on the surface, corresponding to a high corrosion rate. The spectrum reveals only a simple Randles equivalent circuit (Figure 5) corresponding to active corrosion and the system seemed to be at approximately steady state. However, due to the rapid dissolution, the experiment was restricted to short times, and for that reason the spectrum presented refers to 1 hour of immersion. The impedance of magnesium was smaller than that of the bare aluminium substrate by approximately one order of magnitude (Figure 6), a conclusion that is in reasonably good agreement with the results from potentiodynamic polarization. When the Mg-rich coating was applied, the total impedance of the system increased significantly (Figure 6) again in good agreement with the potentiodynamic observations and showing that the sacrificial protection was manifested at a comparatively low Mg oxidation rate.

Unlike the bare magnesium and the bare aluminium alloy, the coated system impedance decreased with time (Figure 7). On the high impedance part of the spectra, there is an ill-defined capacitance, that goes out of the working frequency window and that is followed by a resistance at $\sim 10^4$ Hz.
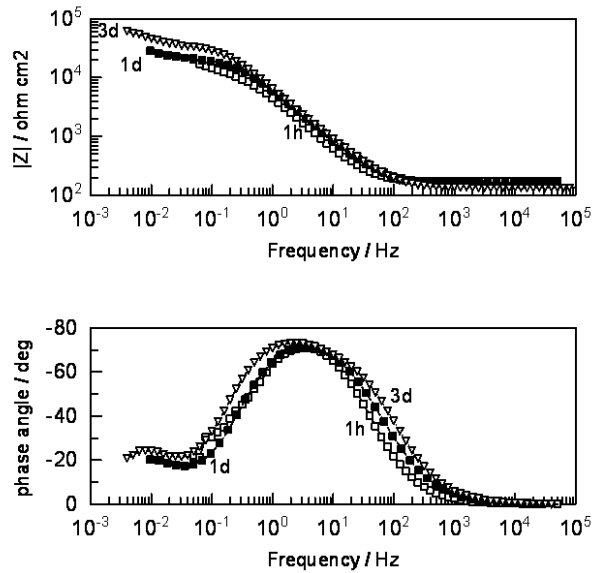
Figure 4. Impedance spectra of bare AA2024 after 1hour, 1 day and 3 days of immersion



a)                                                                                          b)
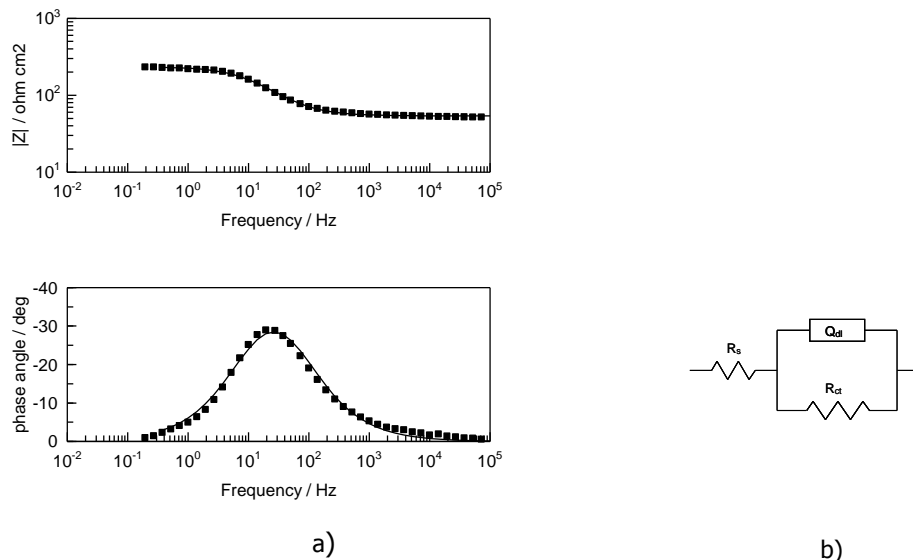
Figure 5. (a) Impedance spectrum of magnesium in 0.1% NaCl; dots: experimental; line: fitted. (b): equivalent circuit.  Fitted values: $R_s$=53.7 ohm cm$^2$, $Q_{dl}$=2*10$^{-4}$ F cm$^{-2}$ s$^{n-1}$, n=0.79, $R_{ct}$=180 ohm cm$^2$

This resistance exhibits values that are considered too high to be due to the solution

resistance and consequently both the resistor and the capacitor at the high frequency portion

of the spectrum can be interpreted as being due to the polymer phase in the coating, a

possibility that is corroborated by their change with time, i.e., due to water penetration.
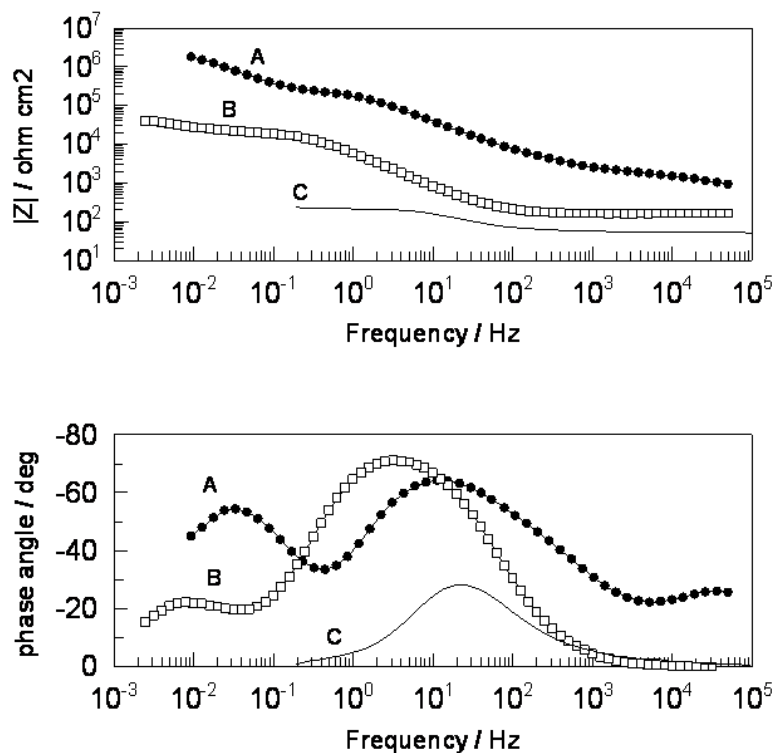


Figure 6. Impedance spectra of coated AA2024 (A); bare AA2024 (B); and pure magnesium
(C). For (A) and (B): after 1 day of immersion, for (C): after 1 hour

The capacitive region following in the spectrum, at intermediate frequencies, probably

corresponds to the double layer at the magnesium surface. Magnesium particles are initially not

only coated with the polymer, but also covered by a layer of magnesium oxide. As water

penetrates across the coating and the oxide becomes dissolved, the number of particles

exposed to water, and thus the total active area, will increase, leading to a higher capacitance.

This increase in the active area is also revealed in a charge transfer resistance drop,

also observed in Figure 7 in the decrease of the plateau at ~1 Hz.

16
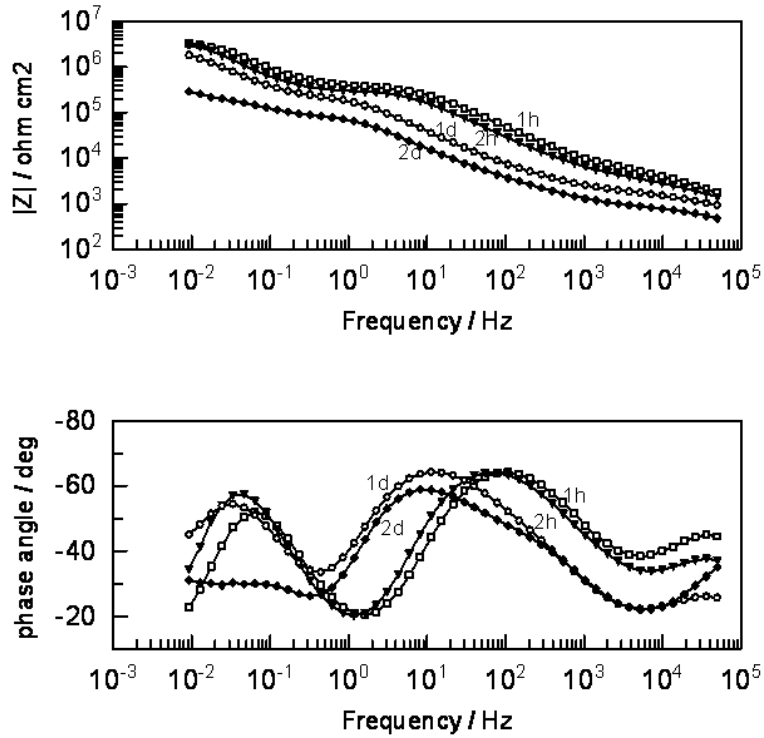
Figure 7. Impedance Spectra of Mg-rich primer on AA2024 at various exposure times

Fitting of the spectra requires a three time constant equivalent circuit as seen in Figure 8. For the polymer layer, i.e., at the high frequency part of the spectrum, the capacitance can be taken as 31 nF cm$^{-2}$, a value that is slightly high for a typical polymer film according to the equation for the capacitance of a dielectric layer:

$$C = \frac{\varepsilon \varepsilon_0}{d} A$$ (Equation 3)

in which $\varepsilon$ is the dielectric constant of the polymer, $\varepsilon_0$ is the permittivity of vacuum, $d$ is the thickness and $A$ is the area.

This capacitance can be increased by the increase of the real area $A$ of the electrode with respect to the geometrical area, i.e., the roughness, which is high in this system. Further, the SEM inspection of the sample (Figure 1) has shown that the thickness of polymer above magnesium particles can be less than 1 micrometer.

17
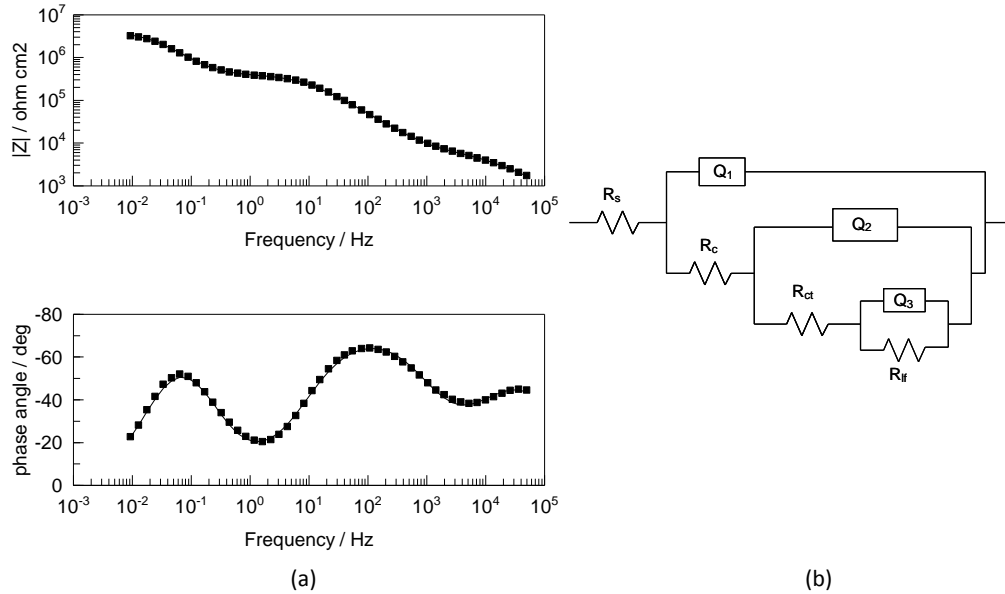
Figure 8. (a) Fitting of impedance spectrum of Mg-rich primer on AA2024 after 1hour of immersion; squares: experimental data; line: fitted spectrum; (b) equivalent circuit. Fitted values: $R_s$= 583 ohm cm$^2$; $Q_1$= 3.14*10$^{-8}$ F cm$^{-2}$ s $^{n-1}$; $n_1$= 0.79; $R_c$= 7173 ohm cm$^2$; $Q_2$=6.22*10$^{-8}$F cm$^{-2}$ s$^{n-1}$; $n_2$=0.85; $R_{ct}$= 4.05*10$^5$ ohm cm$^{-2}$; $Q_3$= 1.91*10$^{-6}$ F cm$^{-2}$ s$^{n-1}$; $n_3$= 0.93; $R_{lf}$= 3.49*10$^6$ ohm cm$^2$

These two factors account for the high capacitance measured. The physical meaning of the low frequency process is not totally clear. It can be due to the cathodic reaction proceeding on the aluminium exposed at the areas where the coating had voids and therefore water penetrated easily. If this is the case, it can be related to a mass diffusion process of charged species, possibly of $H^+$ or of $OH^-$. Abreu et al[16] obtained similar spectra with ZRP applied on steel substrates. They interpreted the EIS spectra of ZRP and concluded that the zinc oxide layer could lead to a capacitive loop in the spectrum.

The evolution of the coating parameters can be better observed in Figure 9. The drop of the coating resistance with time is consistent with a process of water penetration, whereas the charge transfer resistance decrease and the double layer capacitance increase reveal an increasing exposed area or corrosion rate of the magnesium particles. This is confirmed by SEM and EDAX inspection of the surface of exposed and non-exposed areas, presented in Figure 10.

The left half of sample seen in the micrograph was kept dry, whereas the right side corresponds to an area that was exposed for three weeks. The separation between the two areas consisted of the limit of the cup clamped on the surface.



(a)　　　　　　　　　(b)　　　　　　　　　(c)
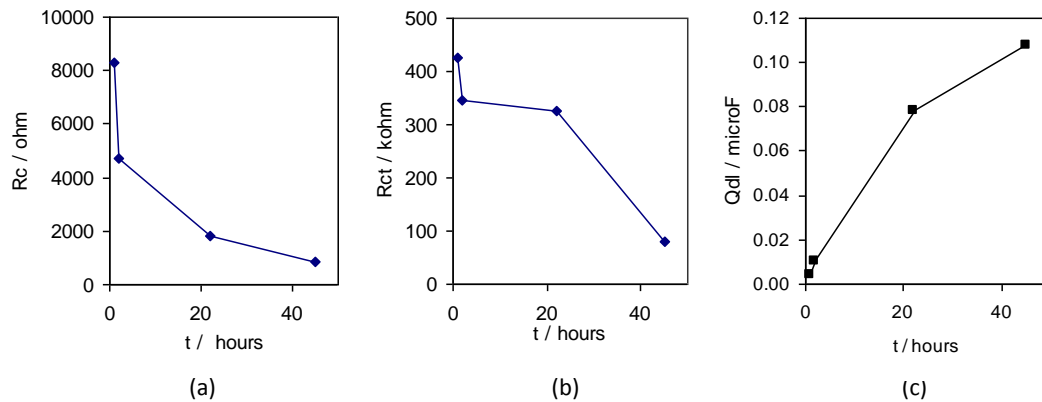
Figure 9. Evolution of parameters estimated from fitting of impedance data: (a) coating resistance; (b) charge transfer resistance; (c) double layer capacitance



(a)　　　　　　　　　　　　　　　(b)
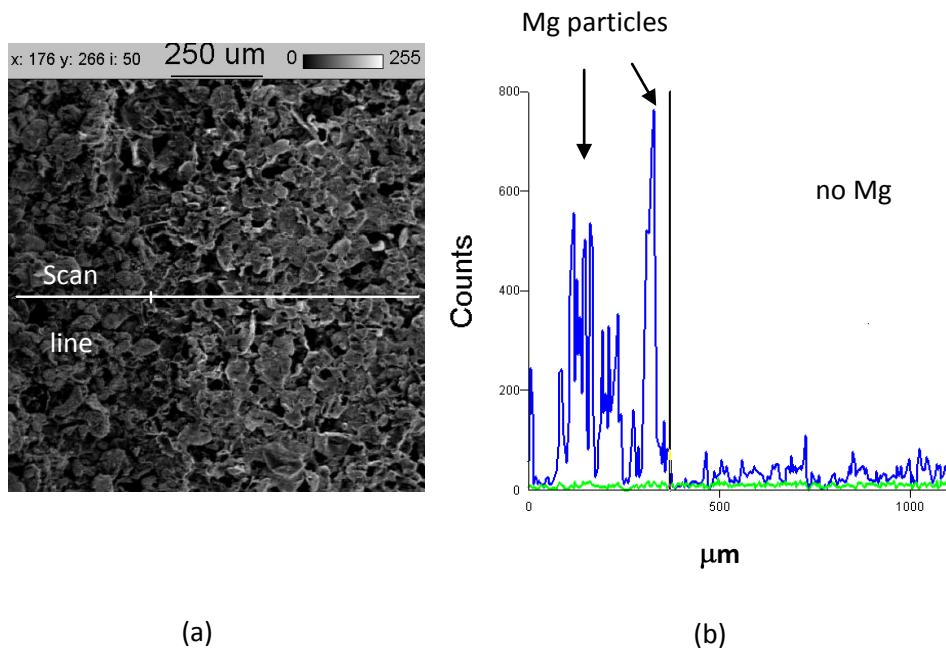
Figure 10. (a) SEM micrograph of primer at the edge of the exposed area, the exposed area being on the right part of the micrograph; (b) ED line scan made at the same area, showing the difference in Mg content

The micrograph reveals a significant difference in the structure of the surface, but the most striking feature consists of the line scan analysis, that reveals practically total depletion of magnesium at the exposed area.

*Mechanism of action at defective areas*

In order to assess the efficiency and protection mechanism at defective areas of the primer, a large scribe was induced with a knife on a coated sample, exposing an area of approximately $1cm^2$ prior to immersion in Dilute Harrison's Solution. The impedance of this sample was comparatively small in the first hour of immersion, but increased with time, becoming practically only capacitive in the range of frequencies of the spectrum after 10 days of immersion (Figure 11). Inspection of the scribed area at the end of the experiment by SEM and EDAX revealed the aluminium surface was covered by a precipitate of magnesium oxides.



(a)                                                                 (b)
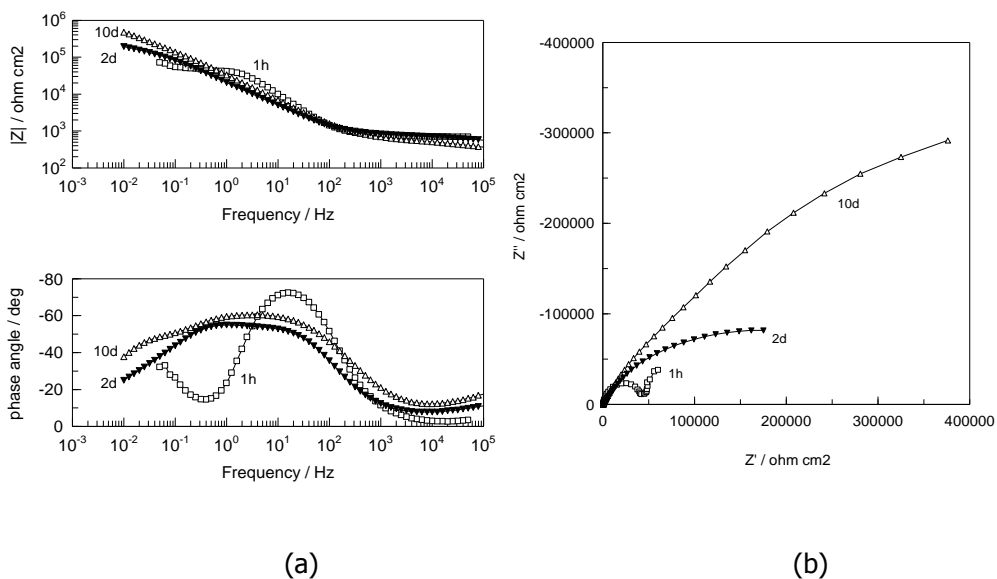
Figure 11. Impedance spectra of scratched Mg-rich primer on AA7075 at various exposure times, as Bode (a) and as Nyquist plot (b)

This precipitate was porous and had several flaws at which the substrate was exposed, as in Figure 12. These flaws, however, did not correspond to sites of pitting of aluminium.
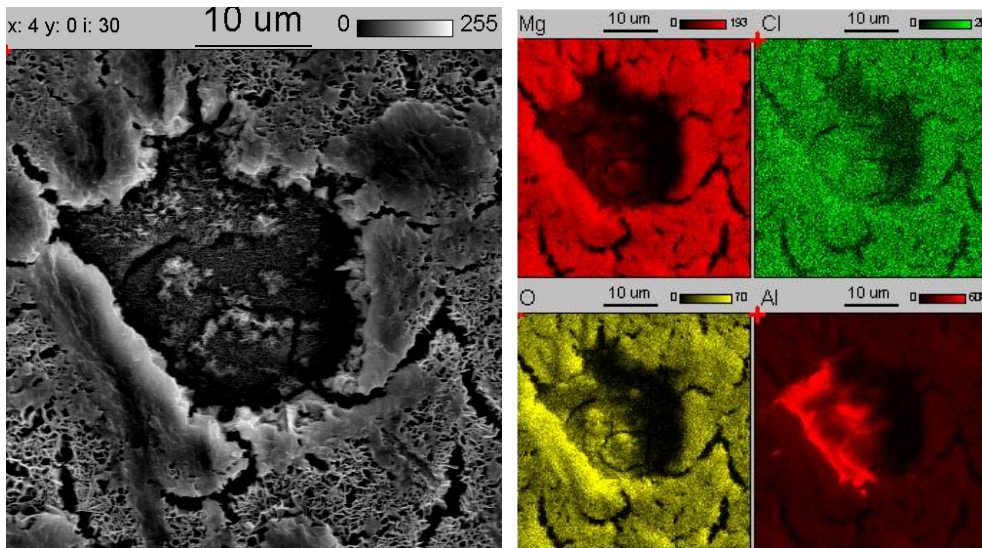
Figure 12. SEM micrograph (a) and EDAX elemental mapping of precipitates formed on a scratch on AA7075: (b) Mg; (c) Cl; (d) O and (e) Al

Discussion

One major requirement for the effectiveness of sacrificial metal-pigmented primers is that the metal particles be in electrical contact among themselves and also with the substrate. If this were not the case, then each particle would behave as an isolated cell, with the cathodic and the anodic reactions occurring on its surface, and no protection would be provided to the substrate. Our results have now shown that sacrificial protection is effective. In fact, the isolated electrochemical activity occurring at each particle would not be measured by the electrochemical techniques used in the work. Further, if the corrosion process measured by impedance were due only to the corrosion of the substrate, then also the potential would have to be due to the substrate only. The OCP measurements, however, have shown that the potential of the galvanic couple was lower than that of the bare alloys, and this has to be a result of cathodic protection. It is not possible to determine from our results what fraction of magnesium is actually used for the protection of the aluminium. Knowledge of that fraction would allow the determination of the coating lifetime, in terms of cathodic protection.

The oxidation rate of the sacrificial anode is another key factor in the viability of the protective system. Magnesium is at the bottom of the electrochemical series, which provides a high electromotive force for its oxidation by $H^+$ from the solution. Further, it does not undergo passivation at neutral pH. Unlike zinc, whose hydroxides precipitate at neutral pH, magnesium has a vast pH range over which it remains active.[17] This range includes not only the regions of stability of $Al^{3+}$ and $Al_2O_3$, but also overlaps the region of alkaline corrosion of aluminium, up to pH~ 11. Magnesium thus becomes oxidised at a high rate, which could lead to exhaustion of the coating after a relatively short exposure period. Mixing with the polymer, however, significantly decreased its corrosion rate, due to the barrier effect of the polymer. This will certainly extend the lifetime of the coating, for a period that is still uncertain at this point of the research.

For zinc-rich primers, it has been observed that zinc corrosion products precipitate inside the coating, around the zinc particles that originated them, blocking the pores of the coating and therefore increasing its barrier resistance.[18] Magnesium acts in a somewhat different way. Because at the near-neutral pH of the solution the magnesium ions are soluble, they actually diffuse out of the primer layer. Further, because of the high rate of the electrochemical reactions, the pH can become quite alkaline at the cathodic sites, particularly if there is a relatively small defect in the primer. When these ions reach the cathodic areas, they will then precipitate as $Mg(OH)_2$:

$$Mg^{2+} + 2OH^- \rightarrow Mg(OH)_2 \qquad \text{(Equation 4)}$$

$$Mg(OH)_2 \rightleftharpoons MgO + H_2O \qquad \text{(Equation 5)}$$
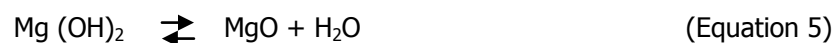
The mixture of the two oxides is thought to be the main composition of the layer that was observed on the scratched surface. The layer thus formed had a thickness of 1-2 micrometers and was highly porous. The oxide layer may therefore not be totally protective, but it can nevertheless provide some degree of barrier protection.

## Conclusions

The magnesium-rich coating used in this work has the capability of protecting alloys AA2024 and AA7075 against corrosion. The effect of magnesium is based upon two different mechanisms, each one associated with one stage. In a first stage, magnesium polarizes aluminium cathodically, shifting its potential below the pitting corrosion potential. The consequence of this polarization can be either the prevention of pit nucleation at the exposed aluminium areas, or the inhibition of pit growth for the nucleated pits. During this stage, any defects on the surface will become cathodic, whereas the magnesium particles will be anodic. At the cathodic areas, reduction of hydrogen and possibly dissolved oxygen increases the pH above the threshold for the precipitation of magnesium oxide. This precipitation leads to the formation of a porous layer that further inhibits corrosion by a barrier mechanism.

The typically high dissolution rate of magnesium is significantly decreased by its incorporation in the polymer.

## Acknowledgments

## References

[1] S. Feliu, Jr., M. Morcillo, and S.Feliu, Corrosion, 57 (2001) 591

[2] J.E.O. Mayne, Br. Corros. J. 5 (1970) 106- 111.

[3] H.Marchebois, S.Touzain, S. Joiret, J. Bernard, C. Savall, Prog. Org. Coat. 45 (2002) 415- 421.

[4] Wen-Ben Chen, Peter Chen, H.Y.Chen, Wen-Ta Tsai, Appl. Surf. Sci. 187 (2002) 154-164.

[5] M. Selvaraj, S.Guruviah, Prog. Org. Coat. 28 (1996) 271-277

[6] Y. Liu, A.M. Arenas, S.G. Garcia-Vergara, P.Skelton, G.E. Thompson, K. Shimizu, H. Habazaki, Corros. Sci. 47 (2005) 145-150.

[7] Jie He, V.J. Gelling, D.E. Tallman, G.P. Bierwagen, J. Electrochem. Soc. 147 (2000) 3661-3666.

[8] ASM Handbook, "Corrosion: Fundamentals, Testing, and Protection" Vol 13A, ASM International, Materials Park, OH (2003)

[9] C.Hare, J.Kurnas, J. Coatings Technology, 72 (2000) 21-27.

[10] M.E. Nanna, G.P. Bierwagen, J. Coatings Technology Research, 1 (2004) 69-80.

[11] Corrosion of Aluminum and Aluminum Alloys, J.R.Davis, Ed., ASM , OH, 1999.

[12] F.Andreatta, H.Terryn, J.H.W. de Wit, Electrochimica Acta 49 (2004) 2851- 2862

[13] J.R. Vilche, E.C. Bucharsky, C.A. Giúdice, Corros. Sci. 44 (2002) 1287-1309.

[14] P.F. George, J.J. Newport, J.L. Nichols, Corrosion 12 (1956) 627t-633t.

[15] M.G.López-Buisán Natta, Corrosion 57 (2001) 712-720.

[16] C.M. Abreu, M.Izquierdo, M.Keddam, X.R.Novoa and H.Takenouti, Electrochimica Acta 41 ( 1996) 2405.

[17] Marcel Pourbaix, Atlas of Electrochemical Equilibria in Aqueous Solutions, Pergamon Press, Oxford, 1966

[18] S. Feliu Jr., R.Barajas, J.M.Bastidas, M. Morcillo, S. Feliu, "Study of Protection Mechanisms of Zinc-Rich Paints by Electrochemical Impedance Spectroscopy", in *Electrochemical Impedance: Analysis and Interpretation*, ASTM STP 1188, J.R. Scully, D.C. Silverman and M.W. Kendig, Eds., American Society for Testing and Materials, Philadelphia, 1993, pp.438-449.

CHAPTER 3. THE USE OF MULTIPLE ELECTROCHEMICAL TECHNIQUES TO CHARACTERIZE
MG-RICH PRIMERS FOR AL ALLOYS

Gordon Bierwagen,[1] Dante Battocchi,[1] Alda Simões,[2] Anthony Stamness[1] and Dennis Tallman[1,3]

## Abstract

To insure that the corrosion protective behavior of Mg-rich primers over Al aircraft alloys is properly understood, multiple electrochemical techniques have been utilized to characterize the behavior of this class of Cr-free coatings. Many substitutes for Cr-containing pretreatments for Al alloys such as AA 2024 T-3 or AA7075 T-6 have been put forth as performing as well as the present Cr-containing materials, but none except Mg-rich primers (MRPs) have succeeded in passing the qualification testing required of these materials. The electrochemical testing was done in conjunction with the subjective "qualification" testing of the primer materials for US Air Force and Navy specifications so that as this new class of primers did not encounter any unexpected corrosion protection-related deficiencies.

To confirm that the MRPs did indeed provide cathodic, sacrificial protection to these alloys, one measures the mixed corrosion potential of the Al-Mg system ($E_{corr}^{mixed}$), also known as the Open Circuit Potential (OCP). This parameter indicates when the potential of the alloy substrate is modified by contact with the Mg to yield a potential cathodic to the Al Alloy ($E_{corr}^{alloy}$). This was done by a steady state measurement of the total system OCP in immersion and also by the measuring the potential of the minimum/free corrosion current ($i_{corr}$) in a potentiodynamic scan of the mixed system. Both methods yielded values in excellent agreement, but initial studies with a system with a high quality topcoat gave problems in OCP

---

[1] NDSU, Department of Coatings and Polymeric Materials, Fargo, ND 58105-5376, USA

[2] IST, Chemical Engineering Department, Av. Rovisco Pais, 1049-001 Lisboa, Portugal

[3] NDSU, Department of Chemistry, Fargo, ND 58105, USA

measurement due to exceedingly high impedance causing steady-state measurement difficulties.

Electrochemical Impedance Spectroscopy (EIS) and Electrochemical Noise Methods (ENM) were also used to characterize the system in immersion. Further, the Scanning Vibrating Electrode Technique (SVET) was used to examine local damage protection by the MRP about a deliberately induced scratch in the coating system. These results for the MRP system yield a very interesting, self-consistent set of data showing cathodic protection of one reactive metal (Al) by another more reactive metal (Mg).

## Introduction

*Problems Faced in the Protection of Aerospace Alloys*

The need for chromium-free methods of protecting Al and its alloys from corrosion is very urgent, especially with respect to high-strength aerospace alloys.[1,2] This current protection system of aircraft depends on chromates, both as metal pretreatments (e.g. Alodine®1200) before the coating process, and as $SrCrO_4$ pigments in the primer coating used beneath the urethane topcoat. Thus the painting, paint stripping, and re-painting of aircraft required by the normal maintenance cycle used by the military generates considerable hazardous chromium-containing wastes as well as possible workplace exposure problems. Both the military services and commercial aircraft manufacturers and users are thus expending considerable money and effort to circumvent the problems caused by chromate-based corrosion protection systems.[3]

The development within this laboratory of metal-rich primers based on Mg powder as their primary pigment[4] has shown that a system providing sacrificial, cathodic protection for Al and its alloys now exists and can stop corrosion in the two most difficult to protect and strategically important aerospace alloys, Al 2024 T-3 and Al 7075 T-6.[5,6] The use of various electrochemical techniques to characterize this new class of coatings has proven to be a very important part of our work on understanding and optimizing this Cr-free corrosion protection system.

*Complexity of Aerospace Alloys*

The high strength alloys of Al used for weight reduction in aircraft and aerospace vehicles of all types are very difficult to protect compared to pure Al because of their very complex metallurgical structures. There are many intermetallic phases and compositions present, especially in such tempered materials which derive much of their strength form the heterogeneities formed during their processing. This complexity of this structure is now beginning to be unraveled to the extent that the measurement of the electrochemical properties of the individual phases.[7] Because of this structure, the corrosion protection system of these alloys must provide protection under very difficult conditions.

*Uniqueness of Cr-Based corrosion protection*

The difficulty in replacing Cr-based systems in the corrosion protection of aerospace alloys is that these systems provide both anodic and cathodic protection to the alloys in a very complex manner based on the unique physical and chemical properties of $Cr^{6+}/Cr^{3+}$ oxide materials.[8,9] The characterization of chromate effects in aerospace systems by multiple-measurement methods by multiple investigators has been lead by Frankel,[10] while a study of just Cr-pretreatment on Al 7075 T-6 has be given by Meng and Frankel.[11] To date, an inhibitive system that provides both the passive corrosion protection and active damage area protection of chromate-based pretreatments and chromate pigments has not been developed and made commercially available.[12]

*Corrosion Protection by Metal-Rich Coatings. Introduction to Metal-Rich Coatings/Zn-Rich Coatings*

Metal-rich coatings (MRCs) are a class of corrosion protective coatings that inhibit corrosion by providing sacrificial, cathodic protection to the metal substrate over which they are applied. The most commonly used coatings of this type are of Zn-rich primer (ZRP) coatings.[13,14] These coatings are either organic or inorganic in nature, with organic polymer systems being the most common. The polymers used in these systems are coating polymers which are stable under the basic environment created by the metal oxide, hydroxide, etc,

formed from the oxidation of metal in the presence of electrolyte. The polymers must also adhere well to the metal substrate and be stable in a corroding environment. Common examples of the materials uses are epoxy-polyamide polymers or moisture-cure polyurethane systems. These are pigmented with the particulate metal or metal alloy, in either spherical or flake form. The metal used as pigment must be more reactive than the metal substrate to be protected (e.g. Zn for Fe/steel). The volume fraction of metal pigment (most commonly noted as the metal pigment volume concentration – PVC) in the coating should exceed or be near its critical pigment volume concentration (CPVC) in order for the coating to provide sacrificial/cathodic protection to the underlying metal substrate. With these conditions fulfilled, the metal particles are all in mutual contact as well as in electrical contact with the substrate.[13]

Evidence exists that the electrical connectivity of the metal particles carries over from the PVC = CPVC (circa 60-70% by volume) to PVC = Volume Percolation Threshold for the metal pigment[15] (~30% by volume for spherical particles), so some sacrificial protection occurs over this range even while the metal is being consumed by sacrificial oxidation. The percolation threshold for flake pigments may be different, depending on particle alignment.[16,17] The substrate metal and the pigmentary metal thus in electronic contact reach a mixed potential at the metal substrate surface. Examination of the corrosion potential/open-circuit potential (OCP) developed by the substrate surface is a key measurement in identifying the presence of cathodic-sacrificial protection.[14] These primer coatings often must be top-coated to function properly and to have a long field lifetime. With a topcoat, they provide both barrier and damage (sacrificial/ cathodic) protection to less reactive substrates.

*Protection by Metal-Rich Coatings (MRCs)*

The protection provided by MRCs is often called sacrificial protection or cathodic protection, in which the substrate to be protected becomes the cathode (the site of reduction reactions in the corrosion couple) and the metal pigment becomes the anode and is oxidized preferential to the substrate, "sacrificing" itself to protect the substrate. This is an extension of cathodic protection commonly used as a standard protection method by corrosion engineers.[18]

The basic requirement for sacrificial protection is for the sacrificial metal to be more electrochemically reactive than the metal substrate under the conditions of use. A guide to choosing a metal for sacrificial protection of another is their relative locations in the electrochemical series in the electrolyte most likely to occur in exposure. The standard electrochemical series in seawater is the most probable ranking for general corrosion protection use. With the electrical connection between the metal pigment particles themselves, and then between the metal-particles and the metal substrate, the substrate /coating interface is polarized to the mixed potential of the pigment metal/substrate metal mixed potential (cathodic relative to the OCP of the substrate metal itself).

Useful reviews of the mechanisms of MRC protection and method to characterize such coatings have been given by Scantlebury, et al.[19,20] Electro-chemically, one can verify this contact between pigment metal and substrate metal by an OCP measurement, and making the same measurement versus exposure time gives a measure of the extent of cathodic protection versus time, effectively providing a measure of the lifetime of cathodic protection provided by the MRC. [21]

*Mg-Rich Primers (MRPs)*

The first article on MRPs was published by Bierwagen and Nanna[4] and it described MRPs use in the first successful totally Cr-free coating system for aerospace alloys. The system has no use of Cr in either the coatings or pretreatment over Al 2024 T-3 and provides longer than 3000 hours of protection in Prohesion exposure. This system, with little or no pretreatment rather than surface degreasing, has the MRP applied by air spray, followed by spray application of the US Air Force Extended Life Topcoat (ELT™)[4]. This system continues to protect up to 6800 hours in this exposure, as well as greater than 6000 hours in ASTM B117 salt spray testing. MgO and related oxides, hydroxides, and oxy-chlorides have been identified by SEM and x-ray diffraction (XRD) studies in scribed areas of panels exposed in a cyclic test

---

[4] Deft 99 GY-001 ELT™, Deft, Inc., Irvine, CA

cabinet using the Prohesion test cycle. This primer system or close variations of it have also passed similar testing over 2024 T-3 in studies at the Air Force Coating Technology Integration Office (CTIO), Wright-Patterson Air Force Base, OH.[22]

Related studies have shown that systems very similar to the one described for 2024 T-3 pass most tests for corrosion protection in our lab over Al 7075 T-6. The coating formulation is described in ref.4, and followed "the rules for Metal Rich Coatings" as described above. The initial electrochemical studies performed on the MRPs were OCP and EIS measurements with accompanying qualitative exposure examination in Prohesion, plus SEM and EDAX examination of damaged area as well as in cross-section. The OCP data showed that for an MRP near its CPVC, cathodic protection was indeed being provided to the Al 2024 T-3 by this primer, with an OCP at steady state of *circa* -0.93 V vs SCE in 3% NaCl, between the ~ -0.65 V OCP for the 2024 T-3 and ~-1.65 for pure Mg. There were some difficulties in acquiring these measurements due the long time it took the system to reach steady state because of the high resistance of the (primer + topcoat) system. This was also seen in the accompanying EIS measurements with some $|Z|_{low\ freq}$ values exceeding $10^{10}$ $\Omega$-cm$^2$. SEM/ EDAX examination of the (primer + topcoat) in cross-section gave the results shown in Figure 13.

The Mg shows up in the primer, and Si shows up as silica in both the primer and ELT® topcoat, the Ti is from $TiO_2$ in the topcoat and Al shows up only in the substrate. The setting on the EDAX did not show the low concentration of Mg in the substrate. Another SEM view of the coating system in cross-section is given in Figure 14. A void is shown in the high PVC MRP, but particle-particle contact also appears. These successful results prompted further, more complete characterization of this unique primer system.

*Proposed Damage Protection Mechanism*

The damage protection mechanism proposed for all metal-rich coatings is that electrical connection between the reactive metal particles and the metal substrate causes
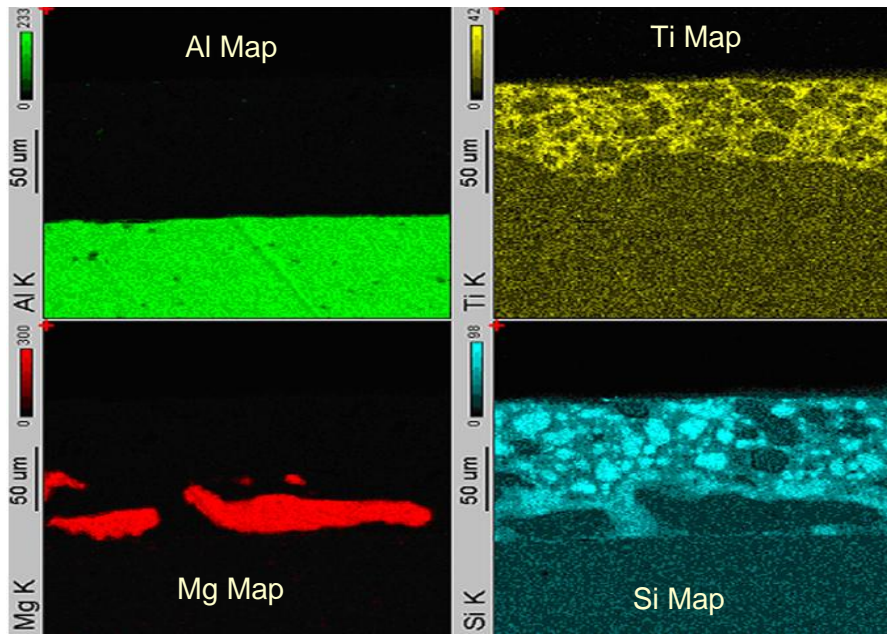
Figure 13. SEM/EDAX Maps from Mg-rich Coating System
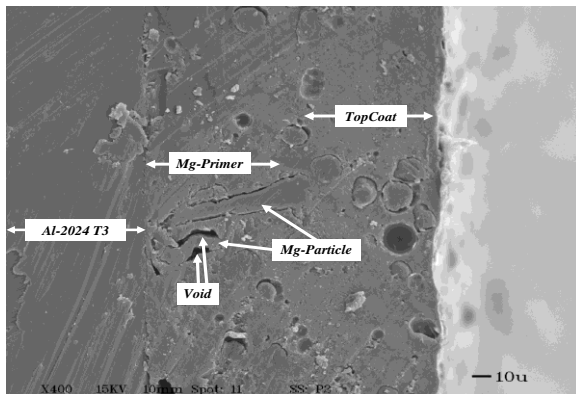


Figure 14. SEM of Structure of Mg-rich Primer (MRP) + Topcoat

galvanic corrosion of the metal pigment (the pigment particles, interconnected electrically near the CPVC, act in total as the anode) forcing the metal substrate to act as the cathode for the system, protecting it from corrosion. To examine whether this occurs in the MRP system, the Scanning Vibrating Electrode Technique (SVET) was utilized. This method has been used successfully in previous studies of this laboratory to examine damage protection mechanisms in chromate pigment-based systems.[23] Initial attempts to examine a scratched area of the

complete (MRP + topcoat) system under an electrolyte solution failed because of $H_2$ bubbles generated when water came in contact with bare exposed Mg particles in the damaged area.

These bubbles created unwanted fluctuations and flow making an instrument as sensitive as the SVET to fail to take meaningful readings. What was required was some way to prevent the direct contact of the electrolyte solution with the bare Mg particles of the primer, but still acquire meaningful readings with the SVET. The configuration of Figure 15 was proposed and it proved to be useful in acquisition of data concerning damage protection of the system. The thin layer of epoxy resin was low enough in resistance that data on current density distribution could be acquired in its presence, but it stopped the rapid direct reduction of water from direct contact of the Mg pigment with concomitant $H_2$ bubble formation.

The data that resulted from SVET characterization of the system shown in Fig. 15 are given in Figures 16 and 18. In Figure 16, the results of a SVET characterization of this system are shown immediately after exposed to dilute Harrison's solution. An anodic area as well as some area of cathodic activity form immediately in the scratch area, as shown in the two plots of Figure 16.

After the system come to steady state, in this case some time before thirty min, when the data for Figure 17 was acquired, the entire surface of the scratched are is cathodic. The sacrificial action of the Mg particles has caused the whole scribed area to become cathodic, and essentially no corrosion is occurring in the scribe. The protective action of the Mg-rich primer was thus confirmed locally in a scribe area as cathodic protection of the bare Al alloy.

The use of OCP measurements for characterizing the protective action of ZRPs has a long history.[21] The time period that the OCP (also termed "rest potential" or "corrosion potential" in the corrosion and protective coatings literature) in the cathodic protection range, at or below ~ -0.78V vs SCE for steel,[20] and estimated in this lab at ~ -0.9V vs SCE for Al 2024 T-3 (these OCPs of course depend upon the temperature and immersion electrolyte), is the clearest and simplest indicator of cathodic protection by MRPs.
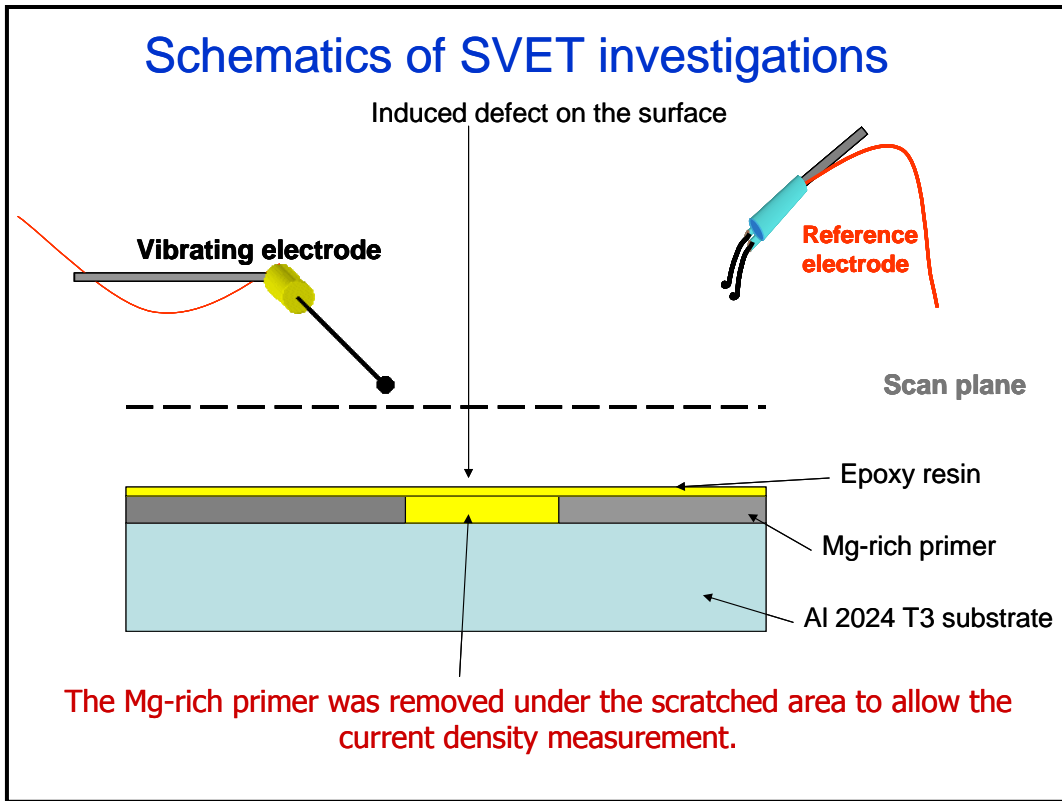
Figure 15. SVET Measurement Set-Up for Mg-Rich primer Investigation
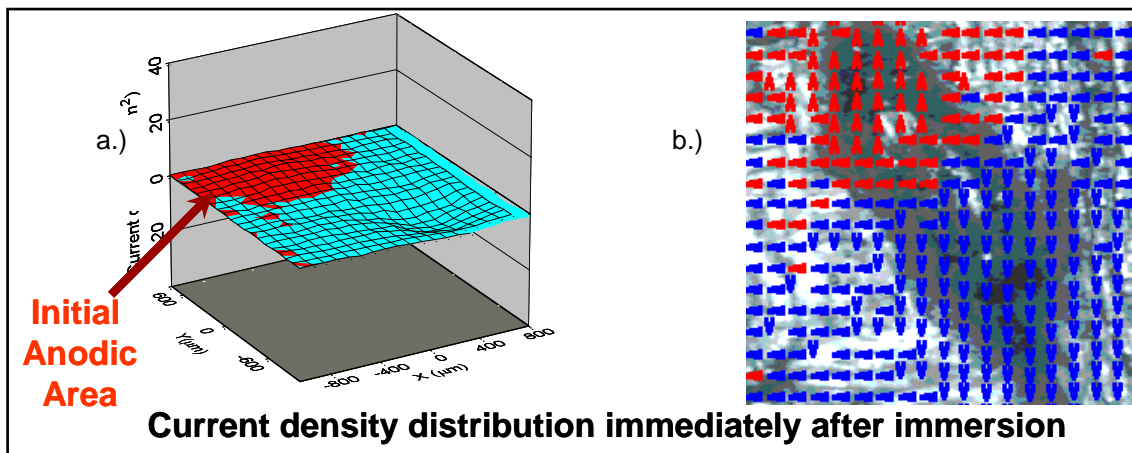


Figure 16. SVET Plots of Scratched Al 2024 T-3 initially after exposed to electrolyte. a.) Three dimensional plot of current density distribution in Scratch Area and b.) Planar photomicrograph of Scratch Area with superimposed arrows of Current Density Direction

**Current density distribution after 30 minutes of immersion**
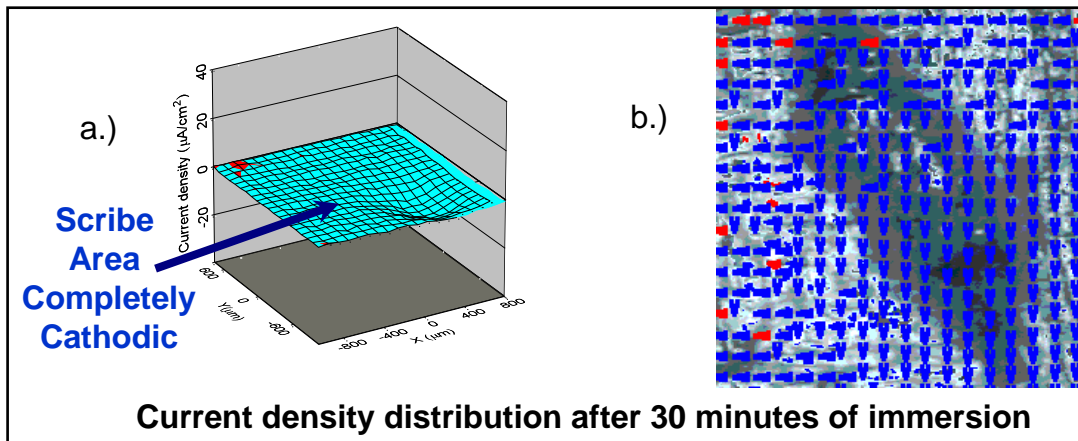
Figure 17. SVET Plots of Scratched Al 2024 T-3 30 minutes after exposed to electrolyte a) Three dimensional plot of current density distribution in Scratch Area and b) Planar photomicrograph of Scratch Area with superimposed arrows of Current Density Direction

*Open Circuit Potential Measurements. Use of OCPs in Zn-rich Paint Systems*

The lifetime of ZRPs is described in stages using OCPs measurement by many authors,[19,20,21,24] and the use of OCPs to characterize MRPs in general is very well established. The data of Birbilis and Bucchheit[7] give OCP values for the various phases of Al 7075 T-6 as well as the pure materials of this alloy, and they give a -1.59 V vs SCE for pure Mg in 0.1 M NaCl, and a -0.965 V vs SCE value for Al 7075 T-6 in 0.1M NaCl.

*OCP Measurements in (MRP + Topcoat) Systems*

As mentioned above, initial studies of the OCP of the Al 2024 T-3 substrate/MRP/topcoat system indicated that cathodic protection was being provided to metal by the MRP, but further details were not acquired other than SEM/EDAX verification of the oxidation of Mg particles in the primer near a scribed area. This is shown in Figure 18. Then OCP measurements were attempted on topcoated MRPs, but there were some difficulties in obtaining steady state values because of the high resistance of the topcoat originally used, the Deft Extended Life Topcoat (ELT™). When the data was properly acquired, the topcoated systems gave the OCP vs. exposure time in Prohesion exposure as shown in Figure 19.
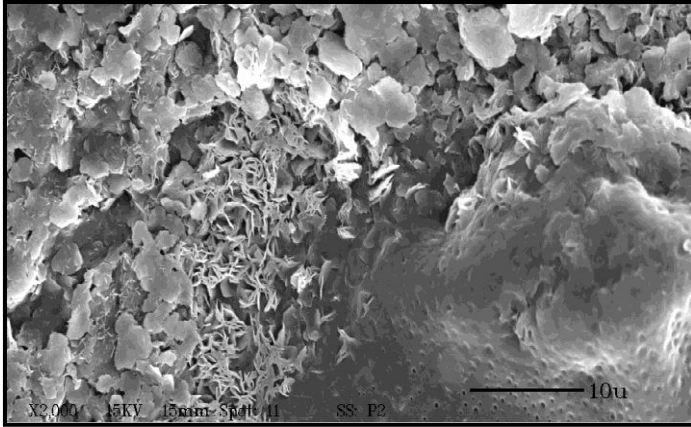
Figure 18. Structure of Mg-rich Coating in Dilute Harrison's Solution:  Underside of exposed Mg-rich primer with magnesium salts. 1) Hexahydrite ($MgSO_4*6\ H_2O$), upper left, 2) Brucite rosettes center, and 3) epoxy binder lower right

For the uncoated Al 2024 T-3 panels in Dilute Harrison's Solution (0.35 wt% $(NH_4)_2SO_4$ and 0.05 wt% NaCl in distilled water), the OCP has ranged for many different panels and samples from -0.5 V to -0.65V vs SCE as shown in Fig. 19.

Systems showing OCPs of < -0.90V would be expected to be under cathodic protection from any oxidation/corrosion. Figure 19 shows that the intact (MRP + topcoat) system provides cathodic protection for in excess of 3000 hours of Prohesion exposure, and show no signs of moving to the second stage of MRC protection where the cathodic protection no longer exists because of oxidation of the sacrificial metal, but the metal oxide provides some protection.[24] These OCP measurements were made in conjunction with EIS measurements where the sample has to be at steady state (stationary) before the EIS data is valid.

*Detailed OCP Studies in Mg-Rich Primers*

Detailed Studies of the OCP in Al 2024 T-3, Al 7075 T-6 panels with and without Mg-rich coatings, as well as the OCP of pure Mg have been reported elsewhere.[5] Some selected results of this study are presented here. OCP data taken in Dilute Harrison's Solution for the systems mentioned above are shown in Figure 20.

These studies also showed that the OCP values obtained were very sensitive to the composition of the electrolyte solution used in obtaining the measurements. A 0.300V difference was noted between DHS and 0.1 M NaCl, for example.[5]
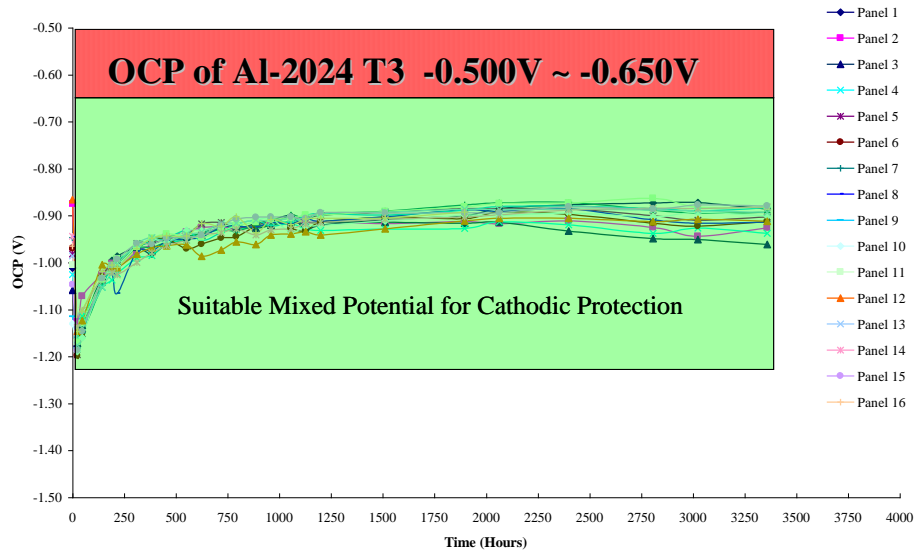


Figure 19. Open Circuit Potential (measured vs. SCE in DHS) data for 16 Topcoated Mg-Rich Primer Samples over Al 2024 T-3 Substrate vs. Exposure Time in Prohesion Cyclic Exposure

These data could be acquired more rapidly without the concern for reaching steady state by using potentiodynamic scans[24] as shown in Figure 21. This data for our MRPs shows the same values for the OCP values, in this case the potential at the lowest current in the Tafel region of the I-V curves, as the data of Figure 20. These data and the long times over which they have been observed (figure 19) verify that the systems is indeed under cathodic protection and this protection is maintained in excess of 3000 hours of Prohesion exposure.

*Electrochemical Impedance Spectroscopy Measurements On MRP Systems.*

EIS has been used quite often as a characterization tool for MRCs and has become a standard measurement technique for the study of corrosion protective coatings (see ref. 21 and references therein).
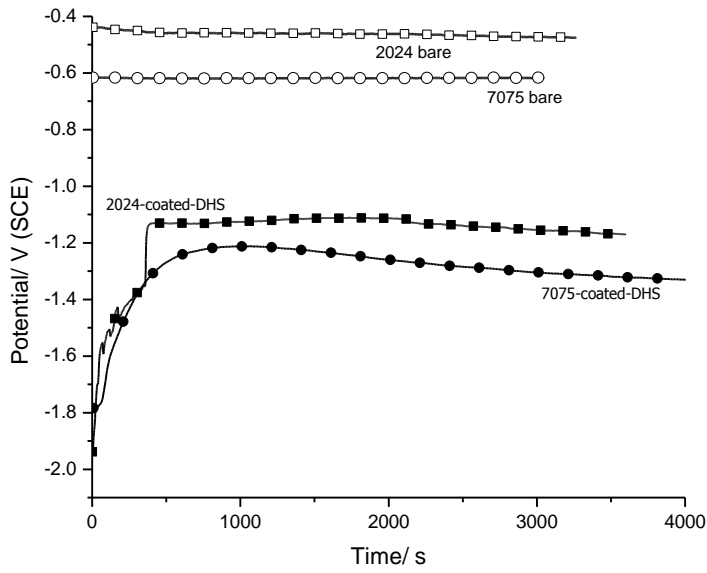
Figure 20. OCP Data versus Immersion Time for Al 2024 and Al 7075 Substrates Bare and Coated with the Mg-rich Primer in Dilute Harrison's Solution
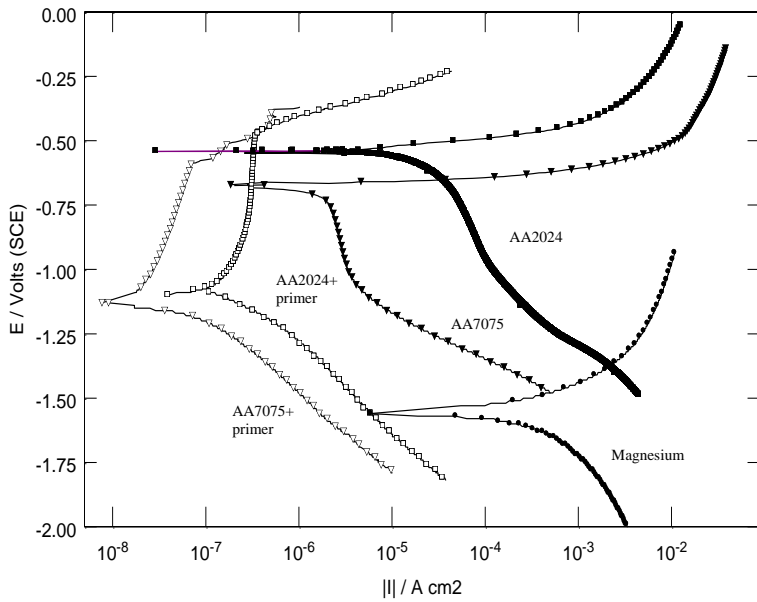


Figure 21. Potentiodynamic Scans for Al 2024 and Al 7075 and Mg Bare and Coated with the Mg-rich Primer

So from the beginning of our studies[4] EIS has been used to study the MRP-based protection systems. Initial data indicated that there was variation in the MRP performance due to the coating matrix polymer used in the primer formulation. This is shown in Figure 22. In Figure 22, the topcoat used for all systems was again the Deft ELT™ system. From studies in this laboratory,[25] it has been seen that the decay rate of the low frequency |Z| values with exposure is a measure of the protective lifetime of organic coatings. There were difficulties on getting the experimental systems to reach their OCP so that the EIS data could be properly acquired, but after these were overcome, the measurement provided considerable information.

The initial studies helped show that the lifetime of protection that the (MRP + topcoat) exceeded the system it was designed to replace which was based on chromate-based pretreatment and a primer based on $SrCrO_4$ pigmentation. The best system in these studies was the topcoated Mg-rich primer that had a binder that was the most resistant to water ingress as well as the best adhesion to the Al alloy substrate. These results will be examined by the analysis methods recently used by Touzain, et al. to study Zinc-rich powder-coating primers.[26,27,28,29]

<div align="center">Summary and Conclusions</div>

The value of multiple electrochemical and physical measurements on the newly developed Mg-rich primers for the chrome-free corrosion protection of Al alloys has been definitely been shown. The use of SVET, OCP, SEM, EDAX, and EIS measurements clearly show that the MRPs provide cathodic protection for alloys such as Al 2024 T-3 and 7075 T-6. SVET shows that in damaged areas of the protective coating system based on MRPs, the bare exposed substrate becomes cathodically protected shortly after exposure to the electrolyte.

The SEM and EDAX data show how the pigmentary materials in the coatings are distributed in the coatings system as well as provided some insight into the interaction of the polymer and pigments in the system.  SEM and XRD (XRD data described in ref. 4) helped identify the oxidation products of the Mg particles after exposure of MRP in damaged areas.

OCP measurements showed that the Mg particles were indeed electronically coupled to the Al alloy substrates, and by this connection the substrates were polarized to potentials that provided them cathodic protection.
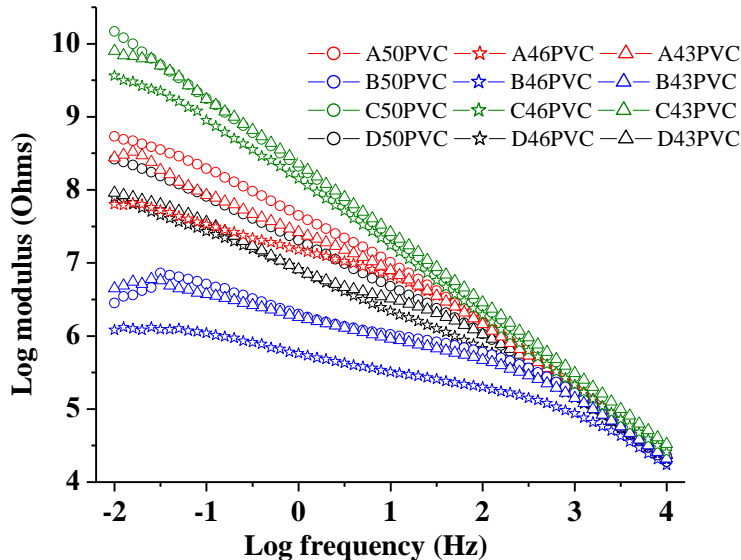


Figure 22. Bode Modulus plots of the four topcoated Mg-rich systems after 3 weeks continuous immersion in 3% NaCl: A) Epoxy-MDI hybrid;  B) Polyurea (MC-PUR); C) Epoxy-HMDI hybrid; D) Epoxy polyamide. Primers formulated at 46, 50, and 55 PVC

## References

[1] J. Janata, D. Baer, G.P. Bierwagen, H. Birnbaum, R. Buchheit, O. Davenport, H. Isaacs, F. Hedberg, M. Kendig, F. Mansfeld, B. Miller, A. Wieckowski, J. Wilkes, Issues related to chromium replacement, Meeting Abstracts, 187th Meeting of the Electrochemical Society, Pennington, NJ, 21–26 May, 1995, Reno, NV

[2] Gordon P. Bierwagen and Dennis E. Tallman, Prog. Organic Coatings, 41 (2001) 201-217

[3] Joseph H. Osborne, Kay Y. Blohowiak, S. Ray Taylor, Chad Hunter, Gordon P. Bierwagen, Brenden Carslon, Dan Bernard, and Michael S. Donley, Prog. Organic Coatings, 41 (2001) 217-225

[4] M.E. Nanna, G.P. Bierwagen, JCT Research, 1 (2004) 69-81

[5] D. Battocchi, A. M. Simões, D. E. Tallman, G. P. Bierwagen, Corrosion Science, 48, 5 (2006) 1292-1306

[6] D. Battocchi, A.M. Simões, D.E. Tallman & G. P. Bierwagen, Corrosion Science, 48, 8, (2006) 2226-2240

[7] N. Birbilis & R. G. Buchheit, J. Electrochem. Soc., 152 (2005) B140-B151

[8] John Sinko, Prog. Organic Coatings, 42 (2001) 267-282

[9] T. Prosek and D. Thierry, Prog. Organic Coatings, 49 (2004) 209-217

[10] William J. Clark, Jeremy D. Ramsey, Richard L. McCreery, and Gerald S. Frankel, Journal of The Electrochemical Society, 149 (2002) B179

[11] Q. Meng and G.S. Frankel, Corrosion, 60 (2004) 897

[12] M.W. Kendig and R.G. Buchheit, Corrosion, 59 (2003) 379

[13] C. Hare, Ch. 55 in *Uhlig's Corrosion Handbook,* 2nd Edition. R. W. Revie, Editor, John Wiley & Sons, New York (2000) pp.1023-1038

[14] S. Felix, R. Barajas, J.M.Bastidas, M. Morcillo & S. Feliu, in Electrochemical Impedance Spectroscopy, ASTM STP 1188, J.R.Scully, D.C.Silverman, & M. Kendig, eds., Amer. Soc. Testing and Materials (ASTM), Philadelphia, PA (1993) pp. 438-449

[15] S. Böhm, R.J. Holness, H.N. McMurray and D.A. Worsley, Eurocorr 2000, Queen Mary and Westfield College, London, 10th-14th September 2000

[16] A. Kalendová & A. Kuckacová, Macromol. Symp., 187 (2002) 377-386

[17] A. Kalendova, Prog. Organic Coatings 46 (2003) 324–332

[18] Jones D. A. Jones, Principles and Prevention of Corrosion, 2nd Ed., Prentice–Hall, Upper Saddle River, NJ (1996), Ch. 2

[19] D. Pereira, J. D. Scantlebury, M. G. S. Ferreira,and M. E. Almeida, Corrosion Sci., 30 (1990) 1135-1147

[20] S. E. Faidi, J. D. Scantlebury, P. Bullivant, N. T. Whittle, and R. SavinCorrosion Sci., 35 (1993) 1319-1328

[21] C. A. Gervasi, A. R. Di Sarli, E. Cavalcanti, O. Ferraz, E. C. Bucharsky, S. G. Real and J. R. Vilche, Corrosion Sci., 36 (1994) 1963-1972,

[22] Private communication, Dr. Joel Johnson, AFRL/MLBT, WPAFB, OH, USA

[23] Jie He, Victoria Johnston Gelling, Dennis E. Tallman, and Gordon P. Bierwagen, J. Electrochem. Soc., 147 (2000) 3661

[24] C.M. Abreu, M. Izquierdo, P. Merino, XR. Novoa, and C. Perez, Corrosion, 55 (1999) 1173

[25] Gordon Bierwagen , Dennis Tallman, Junping Li, Lingyun He, Carol Jeffcoate, Prog. Organic Coatings, 46 (2003) 148

[26] H. Marchebois, S. Joiret, C. Savall, J. Bernard and S. Touzain Surface Coatings Tech., 157( 2002) 151-161

[27] H. Marchebois, S. Touzain, S. Joiret, J. Bernard and C. Savall , Prog. Organic Coatings, 45 (2002) 415-421

[28] H. Marchebois , M. Keddam , C. Savall , J. Bernard and S. Touzain, Electrochimica Acta, 49 (2004) 1719-1729

[29] H. Marchebois, C. Savall, J. Bernard and S. Touzain, Electrochimica Acta, 49 (2004) 2945-2954

CHAPTER 4. COMPARISON OF TESTING SOLUTIONS ON THE PROTECTION OF AL ALLOYS

USING A MG-RICH PRIMER

D. Battocchi,[1] A. M. Simões,[2] D. E. Tallman[1, 3] and G. P. Bierwagen[1]

## Abstract

Magnesium-rich coatings present a new and challenging field of development for the corrosion protection of aluminum structures. These coatings are capable of sacrificial protection, but assessment of their efficiency and durability can be strongly affected by the testing environment. In this work two solutions commonly used in our studies are compared: 0.1% NaCl and Dilute Harrison Solution (DHS). The corrosion behavior of two aluminum alloys coated with a magnesium-rich coating, of pure magnesium and of the bare aluminum substrates was assessed in the two solutions using electrochemical techniques. The corrosion rate of pure magnesium was higher in DHS, although the dissolution rate of the magnesium embedded in the polymer matrix was not significantly affected. The impedance spectra of the scribed samples resembled that of the bare substrates in NaCl solution but not in DHS.

Keywords: corrosion, cathodic protection, aluminum alloys, Mg-rich primer, EIS.

## Introduction

Corrosion of Aluminum alloys is a matter of great concern for many applications and particularly for the aircraft industry. Sacrificial protection, when possible, has the great advantage of needing little supervision and is therefore a practical way to protect structures.[1]

---

[1] NDSU, Department of Coatings and Polymeric Materials, Fargo ND 58105-5376, USA

[2] ICEMS/ Chemical Engineering Department, 1049-001 Lisboa, Portugal

[3] NDSU, Department of Chemistry, Fargo, ND 58105, USA

For Aluminum, however, its low position in the galvanic series limits tremendously the choice of more anodic metals. One possibility described in previous publications was the use of organic coatings rich in magnesium, the only metal with acceptable properties and availability that is below Al in the galvanic series.[2]

In a previous study, a Mg-rich organic coating was applied on two different Al alloys, AA2024 and AA7075, and it was observed that in 0.1%NaCl the open circuit potential of the system took intermediate values between those of the bare alloy and of pure magnesium, due to the formation of a galvanic couple.

Additionally, the impedance revealed a global decrease of the corrosion rate of magnesium as a consequence of the barrier effect of the polymer.[3] Some of the corrosion tests employed on aeronautic alloys, however, use DHS, considered to be closer to the atmospheric conditions often encountered by airplanes (acid rain). In this work the behaviour of the Mg-rich primer and of the bare alloys are compared in 0.1% NaCl solution and in DHS.

## Experimental

Aluminum panels of AA 2024-T3 and AA 7075-T6, with dimensions 150 x 75 x 2 mm, supplied by Q Panel Lab products (*Cleveland OH*), were used in the tests. The samples for the tests on the bare alloys were polished to grit 600 and then washed with distilled water and hexane, whereas those coated with the Mg-rich primer were brushed with a wire brush and washed in distilled water and hexane. The magnesium-rich primer was made using a Mg particulate, of 30-40 $\mu$m average size, supplied by Ecka-Granules of America (Louisville, KY). This particulate consists of Mg covered with a thin layer of MgO, intended to control the reactivity of magnesium[4] and, thus, prevent further oxidation under dry conditions. Dispersion was made using a silane-modified multi-layer/IPN polymer matrix. In order to ensure electronic conduction through the coating bulk, the Mg-rich primer was formulated at 50% PVC (approximately the CPVC of the system2). The primer was applied through an air spray gun to

43

a thickness of approximately 70 $\mu$m. A period of three days was allowed for complete drying before measurements were started.

A magnesium electrode was made by pressing the magnesium particles using an International Crystal Laboratories (ICL) press at 20 MPa, which produced a pellet with surface area of ~1cm$^2$. The pellet surface had a shiny and apparently compact surface, with no significant porosity. The pellet was glued onto an inert glass substrate and electric contact was made by a Pt wire glued to the pellet with a conductive epoxy resin.

For both the bare and the coated aluminum, the electrochemical cell consisted of a glass cylinder reservoir clamped on the surface. Leaking was avoided by using an o-ring. The cylinder was filled with the electrolyte solution for the duration of the experiment. The exposed area of the working electrode was 7.06 cm$^2$. A saturated calomel electrode (SCE) was used as reference electrode (RE) and a Pt mesh was used as counter electrode. Experiments were conducted in two different electrolyte solutions: aqueous solution of 0.1 wt.% NaCl or in DHS, which consists of 0.35 wt% $(NH_4)_2SO_4$ and 0.05 wt% NaCl in distilled water. The pH of both solutions prepared in this way was 5.0.

A PC4/300 potentiostat/galvanostat with EIS 300 software (Gamry Instruments Inc.) was used to collect the electrochemical data. Impedance spectra were collected at the open circuit potential, using the frequency range of 50 kHz to 0.1/0.01 Hz. The signal amplitude was 5mV for the magnesium electrode and 10mV for all the other systems. Potentiodynamic plots were obtained at a scanning rate of 5mV/sec, starting from the open circuit potential. Fitting of impedance spectra was made using Zview software (Scribner Associates), capacitive responses were fitted by Constant Phase elements, Q, whose impedance is given by

$$Z_Q = \frac{1}{Y_0(j2\pi f)^n}$$
(Equation 6)

in which $Y_0$ is the CPE constant , j=$\sqrt{-1}$, f is the frequency (Hz) and the exponent n=$\alpha$/($\pi$/2), $\alpha$ being the phase angle of the CPE (radians).

Results and Discussion

*DC measurements*

The open circuit potential of the bare metals at steady-state can be divided in two groups: above –0.8 Volt, the aluminum alloys, and below –1.5 Volt, pure magnesium (Figure 23). Magnesium is thus anodic to both of the aluminum alloys with an electromotive force (EMF) of at least 0.7V. This high EMF is a major drawback for sacrificial protection, but it has been shown that the incorporation of the sacrificial metal in a polymer matrix significantly decreases the rate of the oxidation reaction.3 The OCP of the Mg electrode at steady state was approximately -1.6 V in the NaCl solution and it was shifted by approximately -0.25V in DHS. This shift is likely due to a stable complex, $MgSO_4$, or ion pair in the solution.[5,6]

For the bare alloys the influence of the solution was less relevant and acted in opposite direction, i.e., the potential became less negative by about +0.08V in DHS. In the samples coated with the magnesium-rich primer, the meaning of the open circuit potential depends on the existence of flaws in the coating and on the conductivity of the pigment particles across the coating layer. When both the pigment and the substrate are exposed and in electric contact with one another, it should correspond to the potential of a galvanic couple, as in the case of the scribed coatings.

After 1h of exposure, the potentials measured in the coated samples, with and without scribe, were always below those of the bare aluminum (Figure 24). The time for stabilization of the potential was in this case much longer, due to the need for the water and electrolyte to penetrate the polymer and reach the magnesium particles, making them active. The potentials were in the same range for both the scribed and the non-scribed samples and correspond to the galvanic potential for the aluminum-magnesium couple. The DHS solution led always to lower potentials, irrespective of the substrate and of the existence of the scribe, as a consequence of the anodic shift observed on pure magnesium.

The potentiodynamic behavior of the bare magnesium reveals a curve that is approximately symmetrical around the open circuit potential, revealing active uniform corrosion (Figure 25). The anodic branch corresponds to the oxidation of magnesium:

$$Mg \rightarrow Mg^{2+} + 2e^{-} \qquad \text{(Equation 7)}$$

whereas the cathodic branch reveals the reduction of water:

$$2H^{+} + 2e^{-} \rightarrow H_2 \qquad \text{(Equation 8)}$$
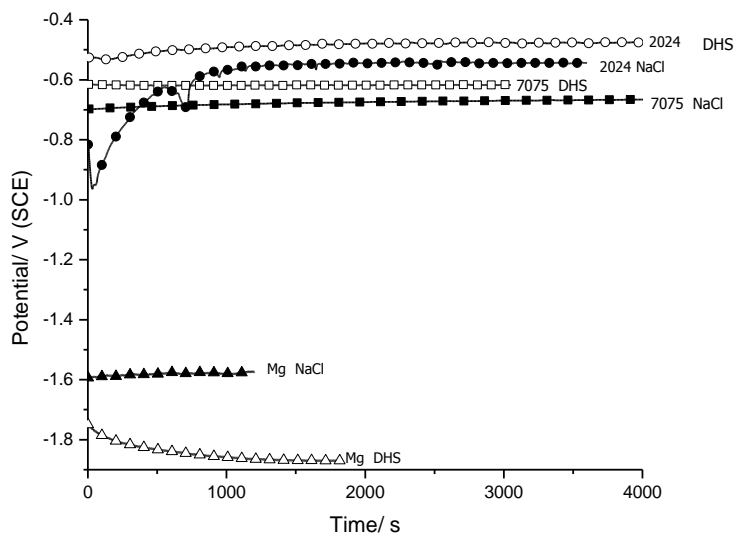


Figure 23. Open circuit potential of bare aluminum alloys and bare magnesium in 0.1% NaCl and in DHS

The shape of the curve was practically the same in the two solutions, although the currents were higher in DHS. The Tafel slopes are very high, circa 600 - 800 mV, possibly due to diffusion polarization. Corrosion currents estimated by extrapolation of the Tafel plots give values of roughly 0.1 - 1mA/cm$^2$, although this value has to be taken with care due to the high slopes of the curve.

46
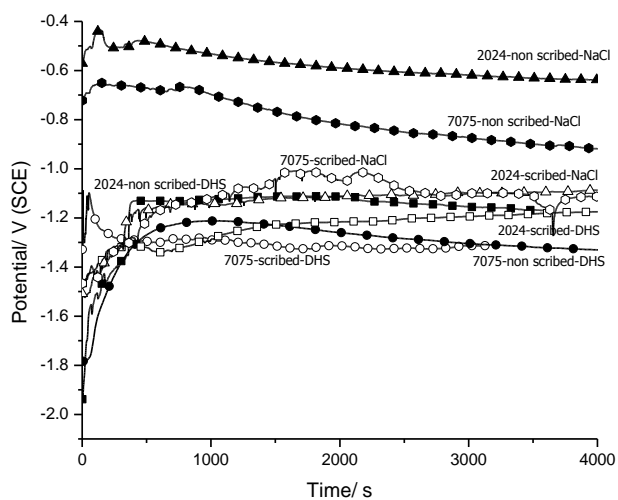
Figure 24. Open circuit potential of the Mg-rich coated alloys in 0.1% NaCl and in DHS
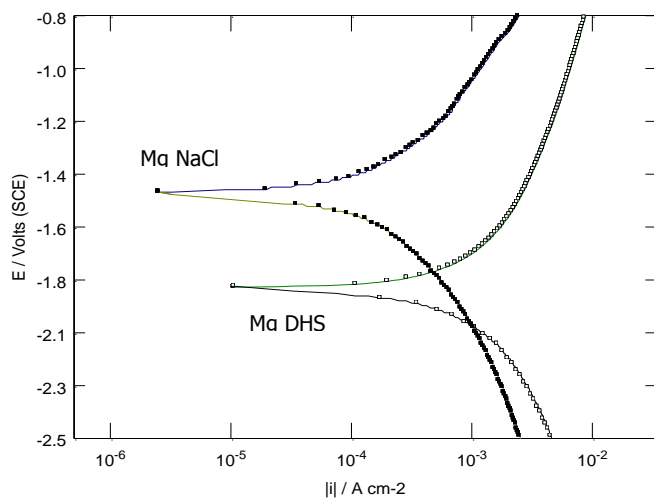


Figure 25. Potentiodynamic polarization plots of magnesium electrodes in 0.1% NaCl and DHS

For the bare alloys the polarization plots are quite asymmetrical (Figure 26), as expected for passive metals. The cathodic branch starts with a diffusion-controlled reduction of oxygen, followed by the reduction of hydrogen below ca. -1V. The anodic branch started with a fast increase of current and a limiting current was observed in the NaCl solution. Extrapolation

47

of the cathodic branch of the curve indicates a higher corrosion rate in DHS for the 7075 alloy.

On the 2024 alloy both the currents are less affected by the solution.
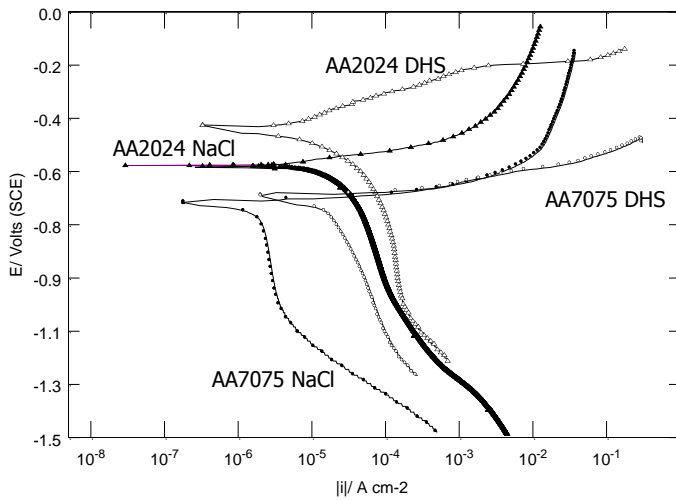


Figure 26. Potentiodynamic polarization plots of the bare alloys in different solutions

The potentiodynamic plots of the coated samples (Figure 27) are all shifted to lower

currents when compared to the bare metals, as observed previously.[3] Because of the lower

currents, the limiting current for oxygen reduction is not observed. The cathodic branch has a

well-developed Tafel region, probably associated with reduction of hydrogen. The anodic

branch can be divided in two parts: below the corrosion potential of the substrate, it reveals

the oxidation of magnesium, whereas above a critical value it is the oxidation of aluminum that

controls the process. This part of the curve is irregular, since it is associated with the formation

of anodic pits.

*E.I.S.*

The impedance spectra of magnesium (Figure 28) always presented a pseudo-inductive

loop at low frequencies, in agreement with the observations of other authors.[7,8,9] Our own

observations show that this is an artifact, due to non-linearity of the polarization plot, and can

48

be avoided by setting the low frequency limit at about 0.1Hz. The charge transfer resistance is quite small and can be safely detected above that frequency.
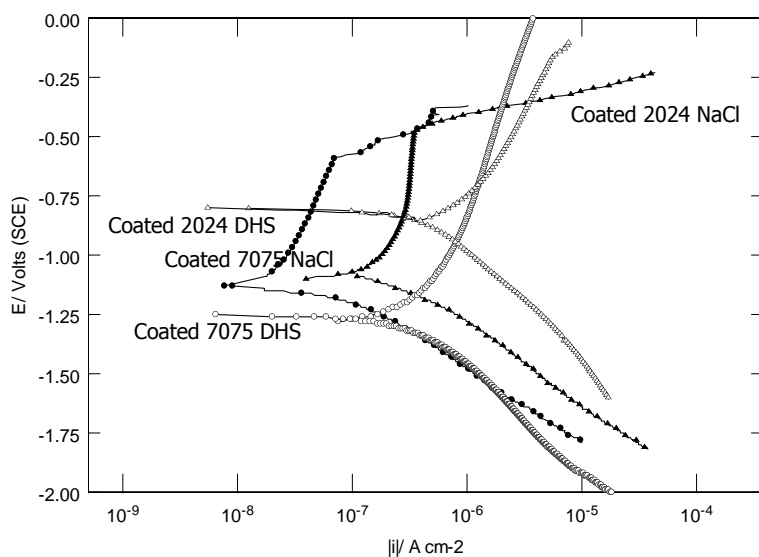


Figure 27. Potentiodynamic polarization plots for the Mg-rich primed alloys in different solutions

The spectra presented one capacitive loop in NaCl and two capacitive loops in DHS. Fitting of the spectrum obtained in NaCl (not shown) was made using only a RC network, in which the charge transfer resistance and the associated capacitance were approximately 180 ohm cm$^2$ and 0.2 mF cm$^{-2}$, respectively.

This capacitance is probably increased by a faradaic effect, due to the high current flowing across the electrode, and cannot thus be totally associated with the interfacial double layer. Fitting of the impedance spectrum obtained in DHS (Figure 29) was made assuming that the high frequency capacitive loop is due to the corrosion process.

For this loop, the charge transfer resistance gave ca. 60 ohm cm$^2$, revealing thus a higher corrosion rate in DHS, in agreement with the results from d.c. polarization. The meaning of the low frequency capacitive loop is not clear, but it may be associated with the precipitation of sulphates or with the finite diffusion of charged species.
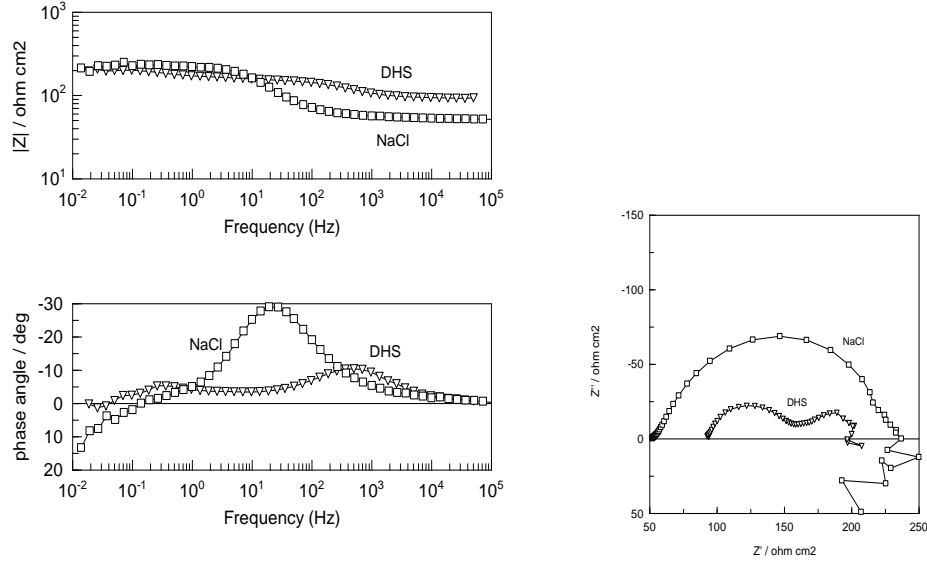
Figure 28. EIS spectra of Magnesium in 0.1% NaCl and DHS

Impedance spectra of the bare alloys were also obtained. The Nyquist plot of the bare 2024 revealed only one capacitive loop, although the Bode plot shows a second loop not well defined (Figure 30). The charge transfer resistance, obtained from the low frequency impedance, was slightly higher in the DHS solution, whereas the capacitance was lower.

Corrosion in this medium is associated with the nucleation and growth of active pits and therefore the double layer capacitance can be taken as a measure of the extension of pitting attack.[10,11] The DHS solution thus induced a less intensive attack when compared to the sodium chloride medium. The spectra of the 7075 alloy also revealed lower impedance in the NaCl solution. The spectra were quite different for the two solutions and also from the one observed in the 2024 alloy. In DHS the spectra had a capacitive loop followed by a pseudo-inductive loop (Figure 31). This loop was observed in both solutions but disappeared in NaCl after one day of immersion, being replaced by a second capacitive loop with capacitance of 1 μF, possibly related to diffusion. The reason for the loop is again non-linearity of the polarization plot, as described in the literature.[12]
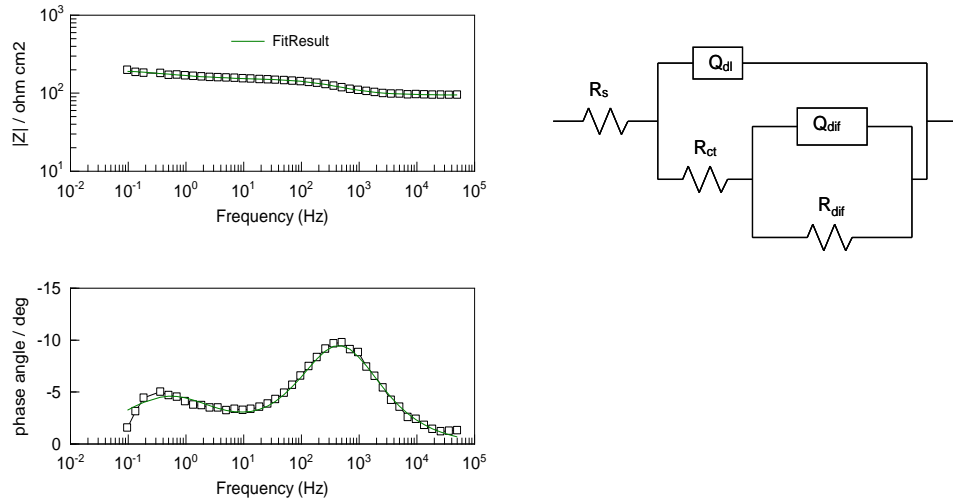
Figure 29. Fitting of spectrum and equivalent circuit of Magnesium in DHS (electrode area= 1cm$^2$)
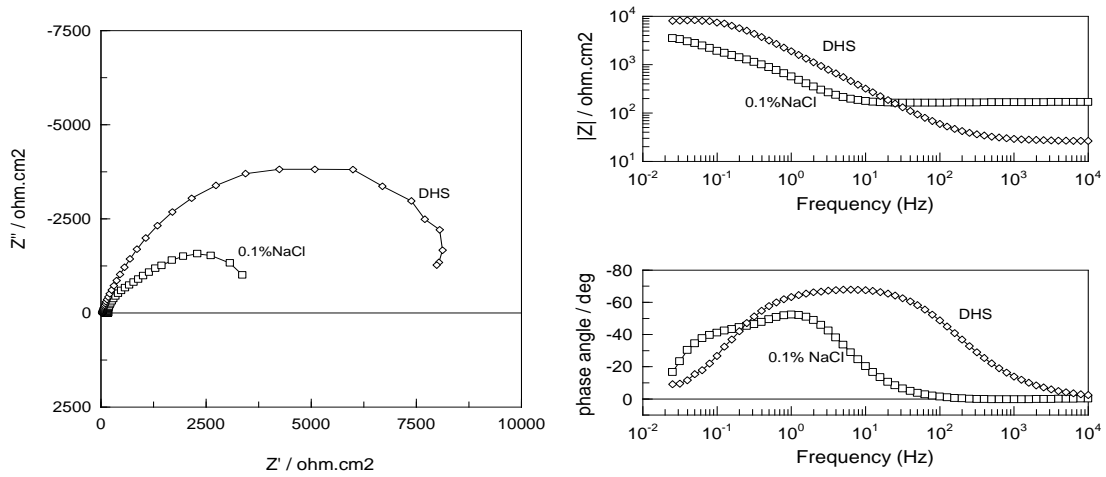


Figure 30. EIS of bare AA2024 in 0.1% NaCl and in DHS, after 1 day of immersion

The sample in NaCl solution revealed again a higher capacitance and a lower charge transfer resistance (taken as the diameter of the semi-circle in the Nyquist plot).
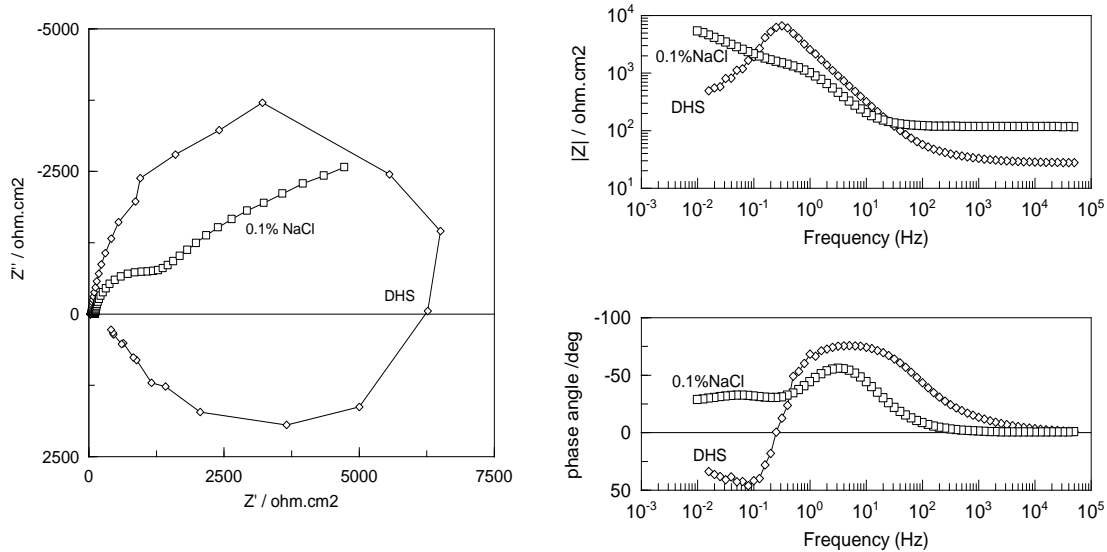
Figure 31. EIS of bare AA7075 in 0.1% NaCl and in DHS, after 1 day of immersion

A low frequency loop was attributed to mass transport of charged species. Visual inspection of the surface after 6 days of immersion revealed significant precipitation of dark corrosion products in the samples exposed to the NaCl solution, whereas the samples immersed in DHS presented a globally shiny surface with some localized corrosion. Analysis with the SEM (Figure 32) revealed that on the AA2024 in DHS the pits were localized and deep whereas on the AA7075 in the same solution, they were fewer in number and smaller in dimension. The samples immersed in 0.1% NaCl presented a number of shallow pits for both the alloys. A gel-like layer of alumina observed on the surface of all the samples could be responsible for the low frequency loop observed in some of the spectra. In a coating with good application the low frequency impedance remained above 10 kohm cm$^2$ for long exposure periods, meaning that the barrier effect prevailed over the sacrificial protection. The introduction of an artificial scribe on the coating lowered the potential and the impedance to active values (Figure 32).

Following previous results,[3,13] fitting of the spectrum was made considering the charge transfer process, plus the resistance of the polymer coating and a parallel resistor/CPE network to model the low frequency diffusion (Figure 34).

The spectra for the two alloys were very similar in the first hours of exposure (Figure 35), whereas after one day of immersion the differences became more evident between the two alloys (Figure 36). The major differences were observed in the DHS spectra, with an increase in the size of the high frequency semicircle, which probably is the combination of the charge transfer and diffusion. In the NaCl solution the spectrum remained practically unchanged, but the difference between the two solutions became larger in the 2024 sample.

The influence of the exposed substrate area on the EIS spectrum has been studied using three different scribes. The meaning of the impedance spectra in the scribed AA2024 is unclear, but it can be due either to the cathodic area, the anodic area or both.

To clarify the issue, three samples with increasing exposed substrate area (two with Mg-rich primer and one bare AA2024) were tested and are presented in Figure 37. The spectra of the scribed samples are identical in shape and only affected by an area factor. They all differ clearly from the spectra of the unscribed Mg-rich coated samples, suggesting that the impedance response is controlled by the cathodic reaction at the exposed aluminum surface and not by the oxidation of the Mg in the primer.

## Discussion

### Magnesium

The experimental results obtained with magnesium were consistent among the various techniques and reveal a fast process, activation-controlled, dependent on pH but also on the salts in solution. The difference in the OCP in the two solutions observed for magnesium agrees with the observations of Song[7] who reported that increasing NaCl concentrations caused an increase of $E_{corr}$, whereas $Na_2SO_4$ caused a decrease in $E_{corr}$.

a) AA2024 in 0.1%NaCl

b) AA7075 in 0.1%NaCl

c) AA2024 in DHS
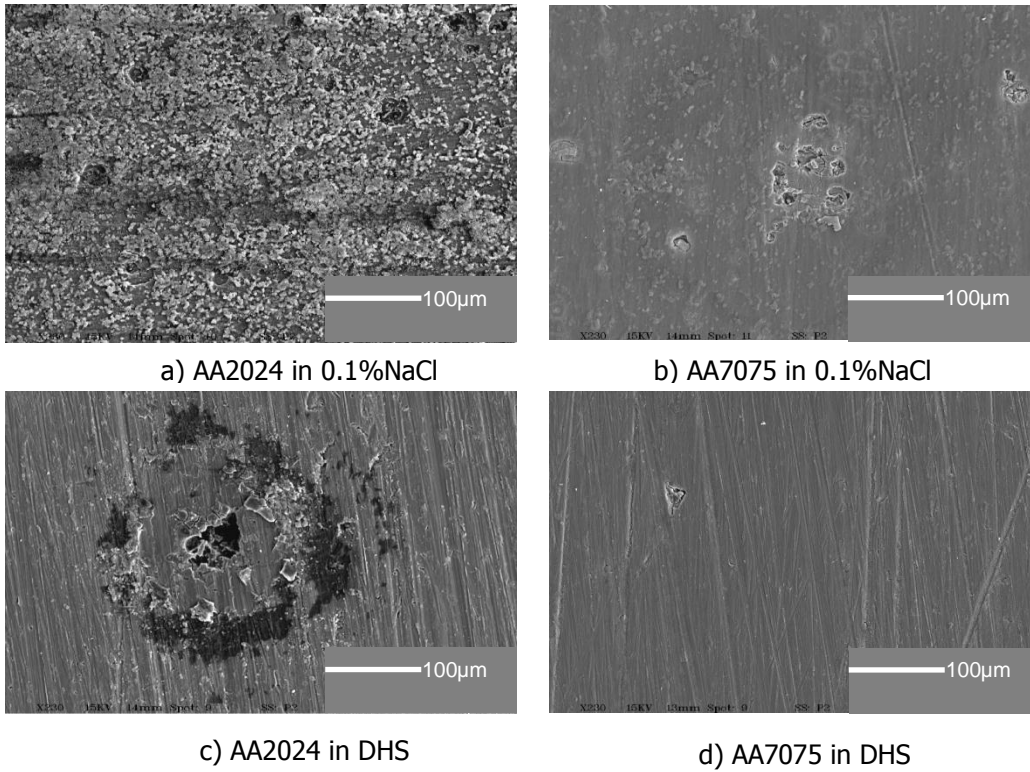
d) AA7075 in DHS

Figure 32. Morphology of the attack for the different alloys and solutions. a) AA2024 in 0.1% NaCl; b) AA7075 in 0.1% NaCl; c) AA2024 in DHS; d) AA7075 in DHS
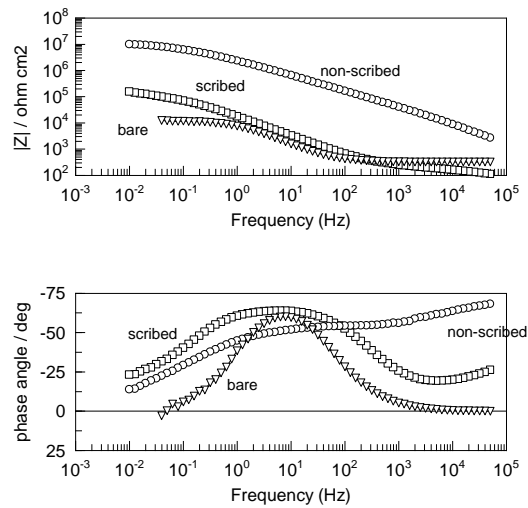


Figure 33. Effect of a scribe on the surface of the Mg-rich primer exposing the Aluminum substrate. Substrate: AA2024; solution: DHS; the spectrum for the bare alloy is also presented for comparison
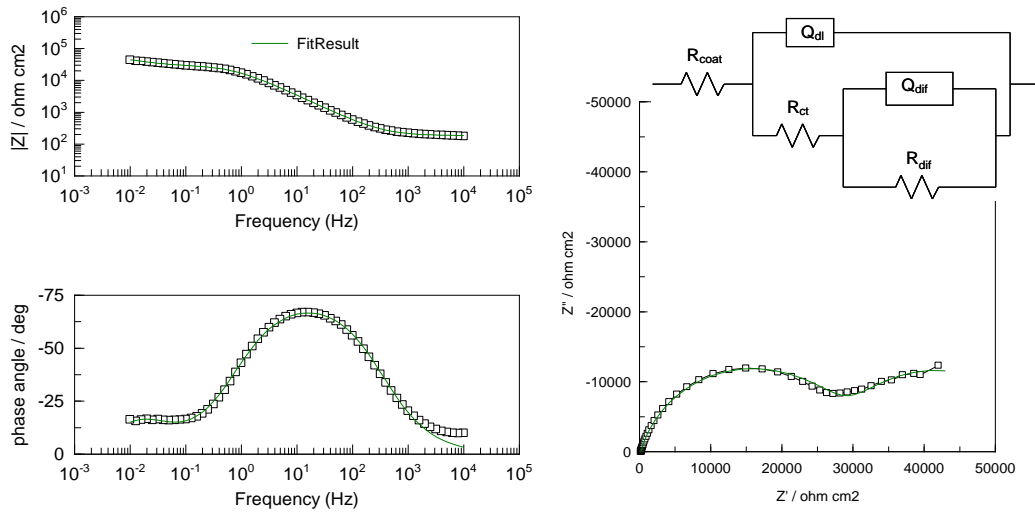
Figure 34. Fitting and equivalent circuit for scribed AA2024 in DHS. Values used in the fitting: $R_{coat}$= 183 ohm; $Q_{dl}$= 9.2*10^{-6}F s^{-n}; $n_{dl}$= 0.83; $R_{ct}$= 30.7 kohm; $Q_{dif}$= 4*10^{-4} F s^{-n}; $R_{dif}$= 25 kohm; values referred to 1cm^2



(a)



(b)
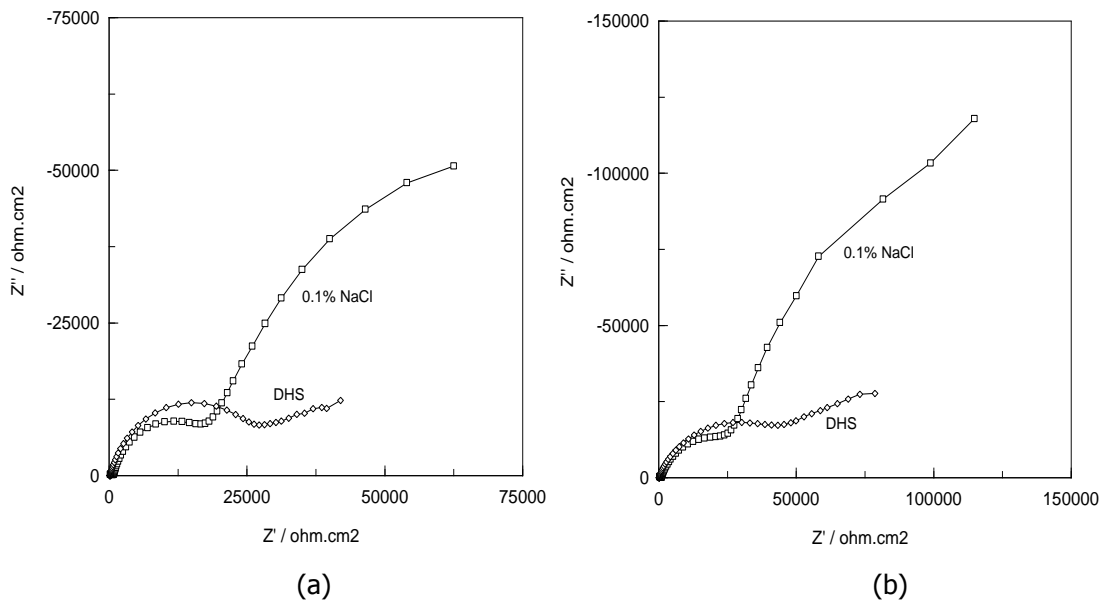
Figure 35. Nyquist plots of scribed coatings after 2h; AA 2024 (a), AA 7075 (b)

In the presence of sulphate ions the potential became more negative and the corrosion rate increased, suggesting that the rate-controlling may be the oxidation of $Mg^0$ to the soluble form.
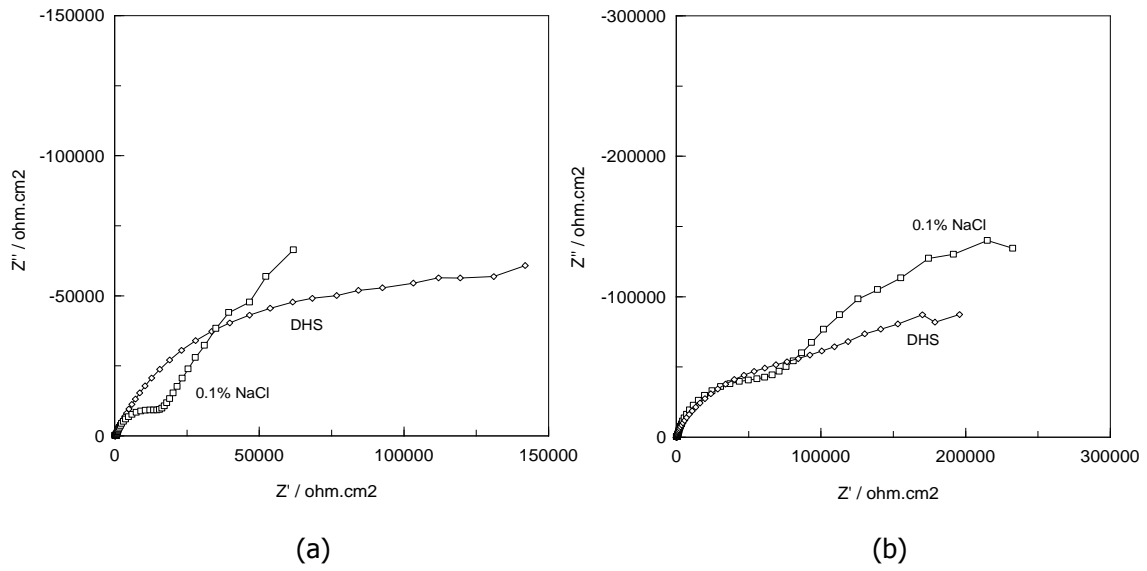
Figure 36. Nyquist plots of scribed coatings after 1 day of immersion; substrates: AA 2024 (a), AA 7075 (b)
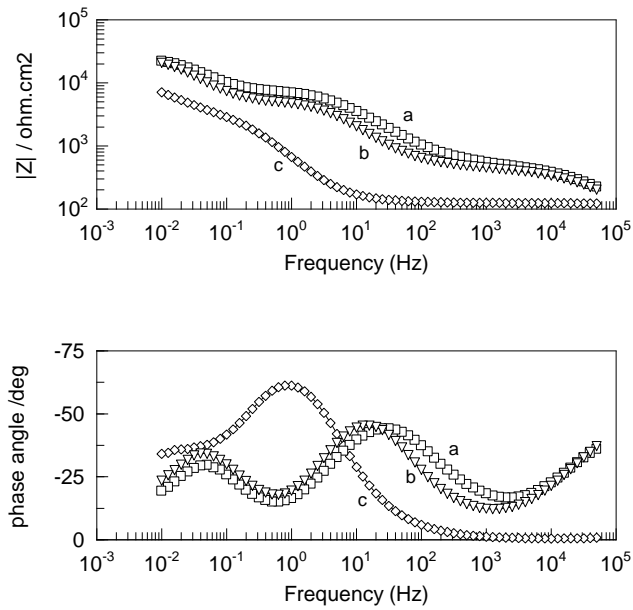


Figure 37. Effect of the exposed substrate area on the EIS spectrum; (a) scribe with 2mm$^2$ of area; (b) scribe with 4 mm$^2$; (c) bare substrate; substrate: AA2024 , coating: Mg-rich alloy, electrolyte: 0.1wt% NaCl

This result differs with reported data,[14] according to which an increase of the NaCl concentration and a decrease of the $Na_2SO_4$ concentration lead to an increase of the anodic and cathodic currents. Given the different chloride concentrations between the two solutions, it is not possible with the present results to establish which of the two effects predominate, although it is clear that the corrosion rate is higher in DHS.

*Aluminum Alloys*

For the bare aluminum alloys the results were not so clear. The OCP was more positive in DHS than in NaCl which, for a passive metal, usually represents a higher risk of pit nucleation. The polarization plots in DHS indicate a higher corrosion rate for the 7075 alloy, whereas the impedance revealed higher corrosion rates in the NaCl solution for both alloys. The morphology of aluminum corrosion, with pits that appear randomly at the surface, can be responsible for this difference in the results. The system can change dramatically with time, depending on the existence of pits on the surface, and reproducibility is low. The results show that sulphate had an opposite influence on the substrates and on the sacrificial metal: for magnesium the corrosion rate was higher and the potential was lower, whereas for both alloys the potential was shifted to nobler values and the reaction rate decreased.

*Scribed Samples*

In the scribed samples aluminum was cathodically polarized by approximately 0.4 Volt and therefore aluminum is protected from corrosion by the magnesium particles. The electromotive force between magnesium and the substrate is higher in DHS, but that does not lead to a higher protection current, according to the impedance measurements. The spectra obtained in the NaCl solution are similar to those obtained in the bare alloy (Figure 34). This is particularly evident in the 7075 alloy, for which the inductive loop is totally absent. The reason for this different behaviour is not totally clear, but it may be due to the different morphology of the attack.

On the bare alloys, both the cathodic and the anodic reactions occur on the alloy surface, with the anodic reaction taking place essentially inside pits. When the coating is

present, the two processes are physically separated, with the anodic process taking place at the coating particles and the cathodic process at the scribe. On the scribed samples, the high frequencies semicircle is related to the oxidation and reduction reactions on the surface. The shape of the spectrum, however, is remarkably similar to that observed on the bare aluminum alloy, and therefore the impedance measured may be due to the process occurring on the aluminum, which under cathodic protection is the reduction of hydrogen and possibly oxygen.

## Conclusions

Two different solutions were studied for the corrosion behavior of AA2024 and AA7075 aluminum alloys protected by a magnesium-rich coating. The change from 0.1% NaCl to Dilute Harrison Solution (DHS) affected the open circuit potential, the corrosion rates and the equivalent circuits of the systems studied. Nevertheless, the magnesium in the coating maintained its protecting properties, by cathodically polarizing the aluminum substrates away from their pitting potential.

It was observed that DHS caused pure magnesium to corrode faster, due to cathodic de-polarization, possibly due to formation of sulfate ion pair (or complex) of Mg, and it also caused an increase in the electromotive force for cathodic protection of aluminum alloys by the magnesium-rich primer. Nevertheless, the sacrificial protection in scribed samples followed the relative activity of the aluminum substrate, and consequently the charge transfer resistance for sacrificial protection was smaller in the NaCl solution. Further, the activity measured in DHS revealed a greater tendency to decrease after a few hours, whereas in NaCl activity remained higher for a longer period.

The shape of the EIS plots suggests that in the NaCl solution the impedance spectra may be determined mostly by the cathodic reaction on the scribe.

References

[1] J. E. O. Mayne, Br. Corr.J., 5 (1970) 106 -111.

[2] M. E. Nanna, G. P. Bierwagen, J. Coatings Technology Research, 1 (2004) 69-80

[3] D. Battocchi, A. M. Simões, D. E. Tallman, G. P. Bierwagen, Corrosion Science, 47, (2005), 1165–1176

[4] P. F. George, J. J. Newport, J. L. Nichols, Corrosion 12 (1956) 627t-633t.

[5] Kester, D. R., R. M. Pytkowicz. Limnology and Oceanography 13 (1968) 670-674

[6] Johnson, S. J., Pytkowitcz, R. M., Marine Chemistry, 8 (1979) 87-93

[7] G. Song, A. Atrens, D. St John, X. Wu, J. Nairn, Corrosion Science 39 (1997) 1981 – 2004

[8] M. Zidouane, M.-H. Grosjean, L.Roué, J.Huot, R.Schultz , Corrosion Science 46 (2004) 3041- 3055.

[9] G. Baril, N. Pébère, Corrosion Science 43 (2001) 471 – 484.

[10] ASM Handbook, "Corrosion: Fundamentals, Testing, and Protection" Vol 13A, ASM International, Materials Park, OH (2003)

[11] Corrosion of Aluminum and Aluminum Alloys, J.R.Davis, Ed., ASM , OH, 1999

[12] F. Mansfeld, J. C.S. Fernandes, Corrosion Science 34 (1993) 2105- 2108.

[13] C. M. Abreu, M. Izquierdio, M. Keddam, X.R. Nóvoa and H. Takenouti, Electrochimica Acta, 41 (1996) 2405- 2415.

[14] G. G. Perrault, Electroanal. Chem. Interfac. Electrochem. 27 (1970) 47.

CHAPTER 5. THE USE OF MG ALLOYS AS PIGMENTS IN MG-RICH PRIMERS FOR PROTECTING

AL ALLOYS

Hong Xu,[1] Dante Battocchi,[1, 2] Dennis E. Tallman [1] and Gordon P. Bierwagen [1, 2]

## Abstract

As an alternative to toxic Chromate coating, Mg-rich primers have been designed to protect Al alloys (in particular AA 2024 T3) and developed in analogy to Zn-rich primers for steel substrate. The Mg pigment present in the primer can provide cathodic protection to Al substrates and significantly deter Al alloy corrosion when damage occurs.[1]

In order to determine how much the pigment metal alloy composition can be varied without sacrificing corrosion protection, three different primers based on magnesium alloy powders as pigments were formulated with an epoxy-polyamide polymer binder at different pigment volume concentrations (PVCs). Their behaviour was studied after cyclic exposure in Prohesion Chamber via electrochemical methods.

Testing results from Electrochemical Impedance Spectroscopy (EIS) and Scanning Electron Microscopy (SEM) showed that the metal-rich primers with Mg alloys as pigments could provide cathodic protection, and precipitates formed from oxidation of Mg alloy particles were similar to the ones found in the pure Mg-rich primer system. Furthermore, the investigation of the properties of the three alloy pigments gave a good understanding of the effects of particle shape, particle size, particle size distribution and metal alloy chemical composition.

[1] NDSU, Coatings and Polymeric Materials Department, Fargo, ND, USA, 58105

[2] NDSU, Center for Surface Protection, Fargo, ND, USA, 58105

Introduction

Aluminum alloys, especially AA2024 T3, are widely used in the aerospace industry because of their high strength and stiffness combined with low density. However, Al alloys are very sensitive to corrosion environments due to their high copper content. Currently, chromate pre-treatment and chromate primer coatings are used to protect aluminum alloys from corrosive attacks.[2] However, with increasing environmental concerns, toxic chromate based coatings (including chromate pigments and chromate metal pretreatments) need to be replaced from coating systems and stringent regulations on their use are due to be enforced by the governments.

In analogy to the Zinc-rich primer coatings that keep steel from corrosion through cathodic protection, a promising alternative, Mg-rich primer coatings, were designed, examined and developed by M. E. Nanna, D. Battocchi and G. P. Bierwagen at NDSU.[3,4,5,6] By using pure magnesium pigment, which is more active than aluminum alloy substrate, Mg-rich primers were formulated around the Critical Pigment Volume Concentration (CPVC) to make sure there is good electrical conductivities among pigment particles and between pigment and substrate. The AA2024 T3 panels coated by the Mg-rich primer combined with a topcoat successfully passed 5000 hours of Prohesion exposure and exhibited excellent corrosion protection for aluminum alloy. Furthermore, various electrochemical techniques, such as electrochemical impedance spectroscopy (EIS), scanning vibrating electrode technique (SVET) and scanning electrochemical microscopy (SECM), were used to assess global or local corrosion protection mechanisms of the Mg-rich primer. It was proved that Mg-rich primer could provide good cathodic protection to AA 2024 T3 when damage occurred[1,7,8] and, further, present certain barrier protection ascribed to corrosion products.

Mg alloys, which contain different elements at various concentrations, show better mechanical properties than pure Mg. However, the corrosion resistance of Mg alloys are significantly affected by the added elements as well as alloys' micro morphology.[9, 10] For

example, trace amounts of iron or copper can increase Mg alloys' corrosion rate dramatically; however, addition of zinc or manganese in large amount can decrease the corrosion rate of Mg alloys. Therefore, it could be expected that by using Mg alloy pigments in place of pure Mg particles in Mg-rich primer system, different corrosion resistance performances of Mg-rich primers would be observed due to the effects of the Mg alloy pigments. Optimistically, we are interested in finding some suitable Mg alloy pigments for the Mg-rich primer system based on their various anti-corrosion behaviours. In this very initial work, we evaluate how much we can vary the pigment composition from pure magnesium in the Mg-rich primer system, as well as the effects of particle size and particle shape on the properties of the primer, without losing the protective behaviour.

Thus, three different Mg alloy particles as pigments were chosen for the first investigation. They were AM60, AZ91B and LNR91, which had different Al contents of 5%, 8.5% and 50%, respectively; in addition, they had dissimilar particle shape, particle size, particle size distribution (PSD) and oil absorption. Different metal rich primers were formulated by using the above three magnesium alloys as pigments in an epoxy-polyamide polymer matrix at different PVCs.

Electrochemical Impedance Spectroscopy (EIS) is a fast and useful method widely applied in monitoring and evaluating the performance of organic coatings, especially the corrosion protection abilities. In our study, EIS was used to characterize the electrochemical performances of different Mg alloy pigmented primers before or after certain exposure time. Scanning Electron Microscopy (SEM) was used to identify the shapes of the different Mg alloy pigments and the surface morphology of exposed Mg alloy pigmented primers. The measurement of particle size and PSD of the magnesium alloy pigments provided information useful for understanding their effects on primer behaviour.

## Experimental

*Property measurements of Mg alloy pigments*

Particle size and PSD of pigments were measured by using Accusizer 780 optical particle sizer (Lab Recyclers Inc., Gaithersburg, MD, USA), which is a single particle optical sensing (SPOS) method. The magnesium alloy particles suspended by acetone passed through a "photozone" one by one; meanwhile, the signal (a pulse) was recorded when an individual particle obscured the photozone with a certain area that is related to the mean diameter of the particle. The particle size distribution was obtained by comparing the single signal strength with a standard calibration curve.

Oil absorption of pigments was tested according to ASTM D281 by using the Spatula Rub-Out method. Linseed oil was added to a certain quantity of pigments drop by drop, and the pigments and Linseed oil were mixed thoroughly with the spatula. When the spatula could hold all the pigments together, the end point was reached. Oil absorption was expressed as gram of oil per 100 grams of pigment. Theoretical CPVC was calculated from the Oil absorption and pigment density.[11]

*Experimental flow*

A flow chart for the experimental procedures used in our studies is presented in Figure 38. All the AA2024 T3 panels supplied by Q Panel Lab products (Cleveland, OH, USA) were polished by 220 grit and 600 grit sand papers to remove the oxide layer and finally rinsed by hexane. The Mg alloys granulates were supplied by Reade (READE Advanced Materials, East Providence, Rhode Island, USA).

An epoxy-polyamide organic coating system, which has been used in Zn-rich primers for a number of years, was used as the polymer binder in magnesium alloy rich primer to provide good adhesion between primer and substrate, as well as certain barrier property. The Mg alloy primer paints were formulated at different PVCs but about CPVC in order to obtain good electrical conductivity among pigments and between pigment and metal substrate.
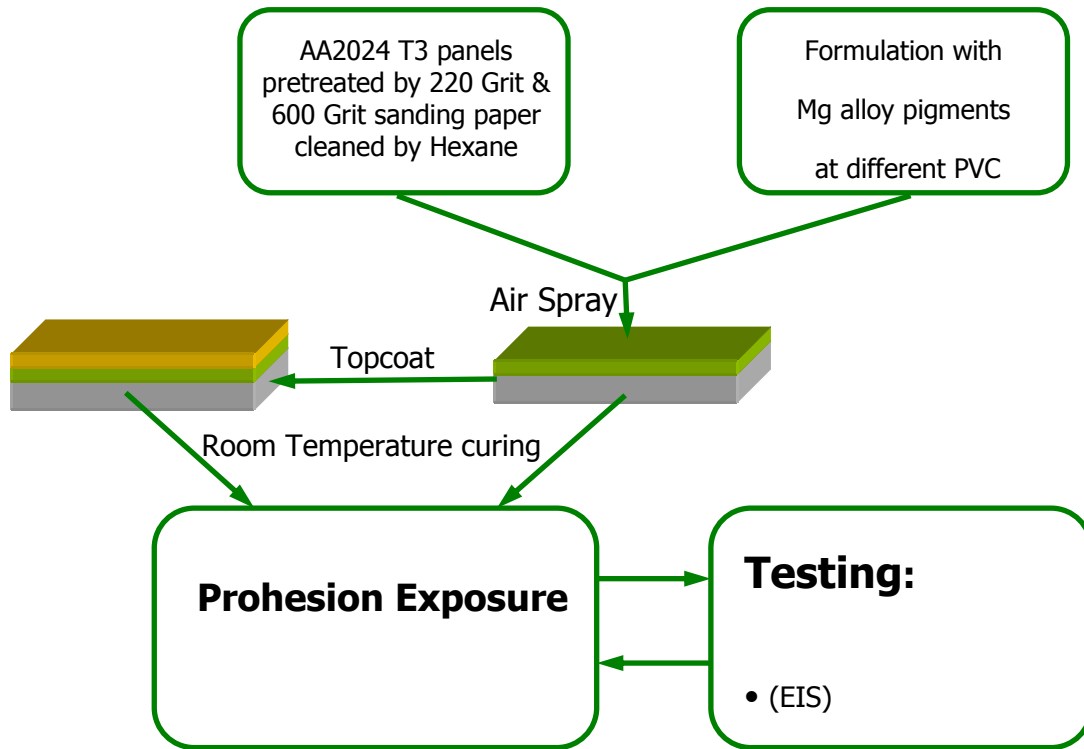
Figure 38. Flow of Experiments

Methyl Ethyl Ketone was used as solvent to give appropriate viscosity for spray application.

Formulated primers were applied on the panel surfaces by air spray. Eight different individual panels were prepared for each type of system. Primer coatings were cured at room temperature for two days and the thickness of dry primers was around 150 μm.

Four panels of each type were topcoated by 03-GY-321 topcoat (supplied by DEFT INC, Irvine, CA, USA) and cured at room temperature for two days. The thickness of dried topcoats was around 100 μm.

All the cured non-topcoated and topcoated test panels were put into a Prohesion chamber for accelerated exposure tests according to ASTM-G85-A5, which consists of one-hour fog cycle of Diluted Harrison's Solution (DHS) fog (0.05% sodium chloride and 0.35% ammonium sulphate ) at 25°C and one-hour dry-off cycle at 35°C. Once a week, the test

panels were removed from the Prohesion chamber for electrochemical testing (EIS) and returned to the chamber when the testing was concluded.

*Thermal analysis*

A TMA 2940 Thermomechanical Analyzer (TA Instruments Inc, New Castle, DE, USA) was used to detect the existence of primer film's post-curing. The procedure consisted of two test cycles: in the first test cycle, a free film sample of primer was equilibrated at 0°C, heated at a ramp rate of 5°C per minute to 140°C; after the same sample was cooled down and equilibrated at 0°C, then the second test cycle with the same conditions was run.

*EIS measurement setup*

A test panel was clamped to a glass cell with a 7.06 cm$^2$ exposure area and used as the working electrode; a saturated calomel electrode (SCE) was used as the reference electrode and a Pt mesh as the counter electrode; DHS was the working electrolyte. All the EIS data were collected through a frequency range from $10^5$ Hz to 0.01Hz by using a Gamry PCL4-300 in potentiostatic mode (Gamry Instruments, Inc. Warminster, PA, USA).

Experimental CPVCs of magnesium alloy rich primers were determined by measuring impedance at low frequency with changing pigment volume concentration (PVC).

*SEM measurement*

Scanning electron microscope (SEM) surface images of primers were taken by using a JEOL JSM-6300 (JEOL Ltd., Tokyo, Japan) with 15KeV acceleration voltage, at X3000 magnification for the 715 hours exposed samples.

## Results and Discussion

*Properties of Magnesium alloy pigments*

The data of particle size, PSD, oil absorption, density and chemical composition for the three magnesium alloy pigments, AM60, AZ91B and LNR91 are listed in Table 2.

We can see that the three magnesium alloy pigments have large particle size (above 60 μm); also they showed different shapes: AM60 has a plate-like shape with a smooth edge,

AZ91B has a chip-like shape and LNR91 has a cubic-like shape with a sharp edge. The oil absorption of LNR91 is the lowest, which indicates LNR91 pigments have smaller surface area or smoother surface. Although the mean particle size of LNR91 is smaller in comparison with the other two pigments, its PSD exhibited much broader range. Furthermore, LNR91 has the highest Al composition within the three.

*CPVC of magnesium alloy primers*

The predicted CPVCs for the three primers were estimated by the procedures outlined in the paper of Bierwagen et al.[11]

The estimated CPVCs of the three magnesium alloy pigments are listed on Table 3.The experimental CPVCs of magnesium alloy rich primers were determined by measuring the change in impedance at low frequency with change in pigment volume concentration.[12,13] With increasing PVC of a coating, the impedance of the coating decreases, because there is less polymeric binder to fill the voids between pigment particles, resulting in a more porous coating.

The plots of impedance at 0.01Hz versus PVC are shown in Figure 39. The ranges of CPVC of the three different Mg alloy primers are listed in Table 3.

Thus, in comparison with the thickness of coating film, the sizes of all the three magnesium pigments were too big to obtain good packing efficiency. Second, from the SEM images of pigments, we can see that the shape of pigment particle and particle size are not well controlled, and these may affect the pigment packing. Furthermore, some difficulties in the coating application processes, such as non-uniform film thickness, also can result in pigment packing problems.

Figure 40 shows changes with exposure time in the OCP of Mg alloy primer coated AA 2024 T3 panels (without topcoat). The data for a single panel of each sample set is reported since each is representative of the trend shown by the entire sample set.
It can be seen that  the OCP of panels increased with exposure time but fell mostly within a potential range that was higher than the OCP of pure Mg ( about -1.60 V) but lower than the OCP of bare AA2024 T3 substrate (-0.60V).

Table 2. Properties of three Magnesium alloy pigments
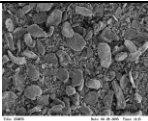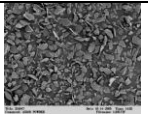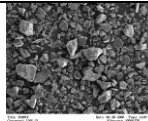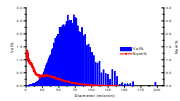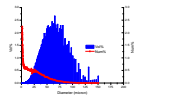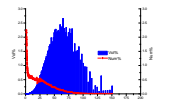
| Mg Alloy | AM 60 | | AZ91B | | LNR91 | |
|---|---|---|---|---|---|---|
| Particle shape (SEM) |  | |  | |  | |
| Comp. ( wt% ) | Al 5%, Mg 95% | | Al 9.5%, Mg 90.5% | | Al 50%, Mg 50% | |
| Oil absorption | 61.53 g/100g pig. | | 68.30 g/100g pig. | | 33.45 g/100g pig. | |
| Density (g/cm$^3$) | 1.80 | | 1.81 | | 2.22 | |
| Particle size plots |  | |  | |  | |
| Particle size | By Vol. ( µm ) | By Num. ( µm ) | By Vol. ( µm ) | By Num. ( µm ) | By Vol. ( µm ) | By Num. ( µm ) |
| Mean Diameter | 63.00 | 10.66 | 58.96 | 10.36 | 56.21 | 11.23 |
| Mode Diameter | 63.46 | 1.95 | 74.61 | 1.66 | 87.72 | 11.59 |
| Median Diameter | 60.12 | 5.02 | 55.45 | 4.16 | 49.78 | 8.39 |

Table 3. Theoretical and experimental CPVCs of three Mg alloy pigments

| Mg Alloy Pigment | AM 60 | AZ91B | LNR91 |
|---|---|---|---|
| Theoretical CPVC | 46% | 43% | 56% |
| Exp. CPVC | 31%< CPVC <34% | 31%<CPVC<34% | 39%<CPVC < 44% |

This mixed potential range indicated that the Mg alloy pigments could provide cathodic protection to Al alloy substrate.[2] Furthermore, at 0 hour exposure time, all the Mg alloy primer coated panels with different PVC had low OCP, between -1.50 V and -1.20 V, which might be due to the high content of Mg in fresh primer films.
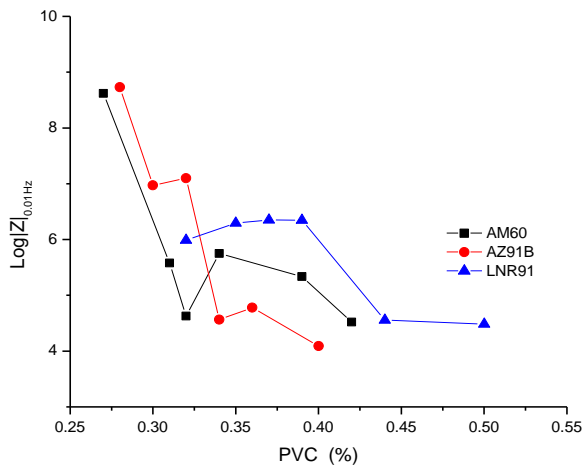
Figure 39. Impedance at 0.01Hz change with PVC of primers

*Open Circuit Potential (OCP) change with exposure time (Mg alloy primer coated panels without topcoat)*

With the increasing exposure time, the OCP increased, indicating the consumption of the active pigments. Among the primers, the OCP of the AM60 primer coated panels exhibited the lowest rate of increase and remained in a low OCP range for the longest time. This might be due to its highest Mg content and plate shape of its pigments. When the OCP of the panels reached the OCP of the bare substrate, the primers no longer provided sacrificial protection to the Al alloy substrate.

In addition, the OCP change also reflected the effects of PVC on primers. For the LNR91 primer coated panels, the OCP of the lowest PVC (35%) primer increased much more slowly; in contrast, the OCP of the highest PVC (50%) primer reached -0.60V very quickly. This might due to the lower barrier protection provided by polymer binder when PVC was higher than CPVC, where the electrolyte could easily penetrate into the coating film and speed up the corrosion of Mg pigments.
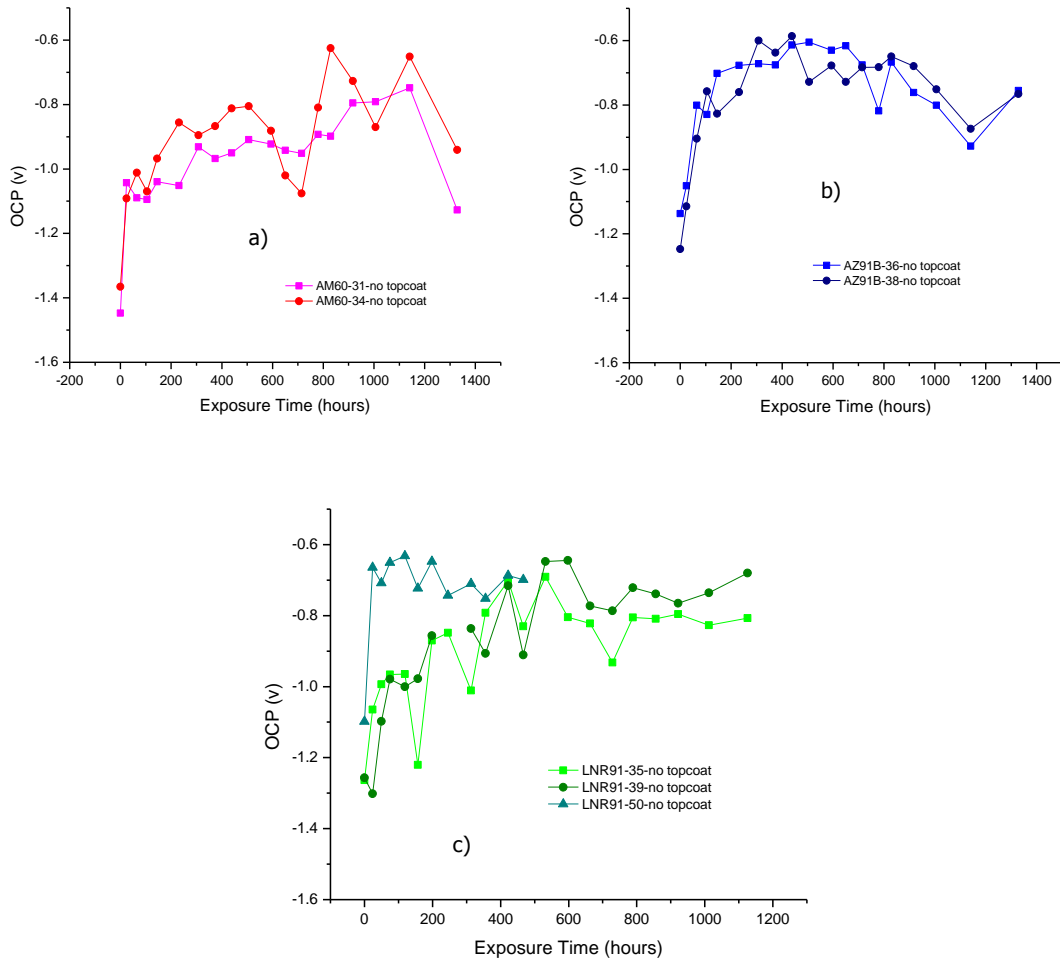
Figure 40. OCP of Mg alloy primer coated panels (without topcoat) change with exposure time. Different alloys (a) AM60; (b) AZ91B; (c) LNR91

*Mg alloy primer coated panels without topcoat (Impedances at 0.01Hz change with exposure time)*

In general, the impedance at low frequency is related to the sum of polarization resistance ($R_p$), pore resistance ($R_{pore}$) and solution resistance ($R_s$),[14] especially when some defects, such as pores, are present in the coating system. In fact, the non top-coated Mg alloy pigmented primer system was very porous due to the existence of the Mg alloy pigments. In addition, from Bode magnitude and phase diagrams of an AM60 31% PVC primer coated panel not shown here, it can be seen that the impedance at low frequency (0.01Hz) decreased with exposure time. Meanwhile, the phase angle at low frequency (0.01Hz) was about -10 degrees

in the first 100 hours exposure and increased to -40 degrees until 506 hours exposure; after

600 hours exposure, the phase angle dropped to -20 degrees. Figure 41 A and B show the

Bode magnitude and  phase diagrams of the different Mg alloy primer coated panels, along

with an unpigmented (clear) primer coated panel (black lines).

After 550 hours of exposure, the phase angles of the panel with a clear coating and

panels coated with primers having higher PVC (such as AZ91B at 36%PVC and LNR91 at 50%

PVC) were all less than -10 degree at low frequency, while the other panels were between -20

degree and -40 degree.

That the phase angle was not 0 degree at low frequency indicates that the capacitance

in the primer system also contributed to the impedance at low frequency, but we can assume

that the change of the impedance at low frequency (0.01Hz) reflects primarily the alteration of

the coating resistance because the range of the phase angles at low frequency didn't vary

significantly and the phase angles decreased further with the increasing exposure time.

The plots of impedance at 0.01Hz for the panels coated with Mg alloy primers versus

exposure time are shown in Figure 42. We can see that, with exposure time increasing, the

impedance at low frequency slowly decreased. This may be due to the decrease of the pore

resistance and the polarization resistance (solution resistance is normally very low and can be

ignored).

When the electrolyte penetrated the coating film through the porous paths and

reached the interface between the coating and the substrate, the pore resistance decreased.

On the other hand, with the presence of the electrolyte and the electrochemically active

species, the under-film corrosion was initiated and caused the decrease of polarization

resistance.

Sometimes, a sharp increase in impedance at low frequency could be observed,

especially during the first 24 hours. This phenomenon could be due to the post-curing of the

primer films. Figure 43 shows the results of thermal mechanical analysis (TMA) of the ambient

cured or 60°C oven cured Mg alloy primers. It can be seen that, with increasing temperature,

the primer film with ambient curing exhibited much larger dimensional changes (156.16 μm) than the one oven cured at 60°C  (87.59 μm), which meant the ambient cured primer film had much bigger volume shrinkage than the one oven cured at 60°C .
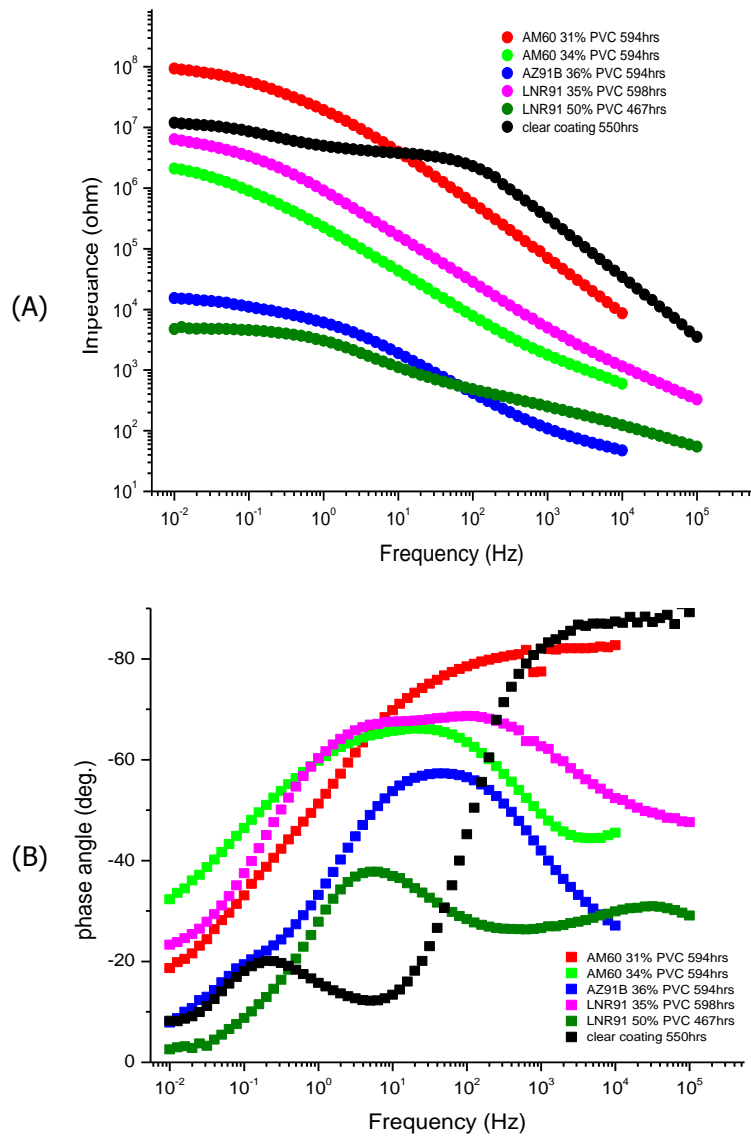


Figure 41. Impedance spectra of Mg alloy primers coated panels. (A)(B) Bode magnitude and phase diagrams, respectively, for different primers coated panels and clear coating panel after about 600hrs exposure
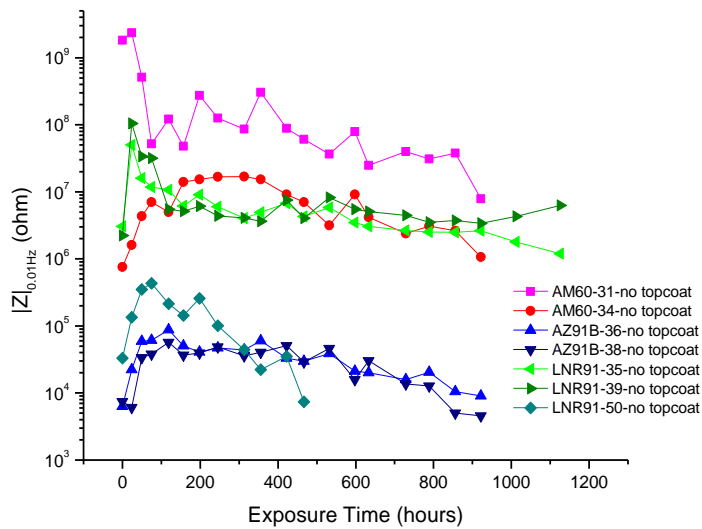
Figure 42. Impedance at low frequency of Mg alloy primer coated panels (without topcoat) as a function of exposure time

In addition, a second TMA cycle of either the ambient cured or the 60°C oven cured primer film showed no additional shrinkage after being exposed at high temperature. These TMA data indicate that the ambient cured primer film had lower degree of cure than the 60°C oven cured primer film,[15, 16] and the high temperature exposure (higher than 125°C) resulted in more fully cured primers. Thus, it was possible for the primers to continue to crosslink further in the Prohesion chamber.

Figure 44 shows a SEM surface image of Mg alloy primer after 715 hours exposure. The Mg precipitates were observed around the Mg alloy pigment.

The morphology of the Mg precipitate was very similar to that observed previously in the exposed primer containing pure Mg powder pigment, where the formation of the Mg precipitate was found to affect the impedance of the primer film and the film barrier properties.[6, 8] The confirmation of the actual chemical composition of the precipitate as well as its effects on barrier protection are currently being studied.
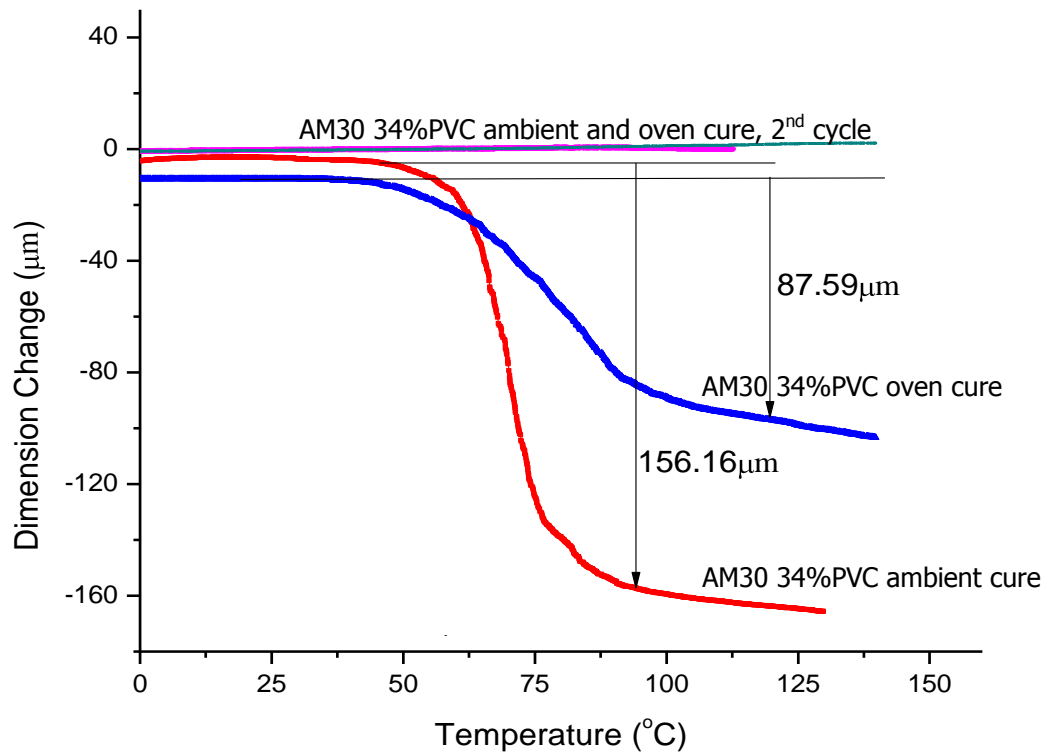
Figure 43. TMA plots of ambient cured or 60°C oven cured Mg alloy primer films

*Mg alloy primers coated panels with topcoat (OCPs change with exposure time)*

Mg alloy rich primer was designed to be used with a topcoat in field application. Thus, the effects of the topcoat on the Mg alloy primers were studied to understand the anti-corrosion behaviour and the possible lifetime of the whole aerospace coating system exposed to an electrolyte. The OCP changes with exposure time are shown in Figure 45. At 0 hour exposure, the OCPs were generally low; with increasing exposure time, the OCPs slowly increased.

These results indicate that, even when covered by a layer of topcoat, the Mg alloy primers still exhibited good cathodic protection to AA 2024 T3 substrates, suggesting that the barrier protection provided by topcoat didn't retard the cathodic protective function of primers.

The effect of PVC on OCP change by topcoated primers was different from that observed with the non-topcoated primers.
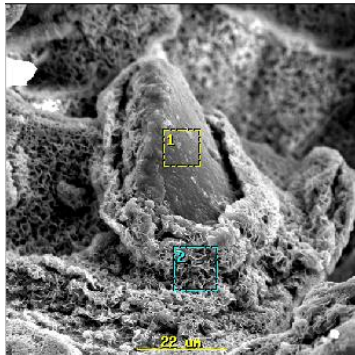


Figure 44. SEM surface image of AM60 primer coated panel (34% PVC, 715 hours exposure); Area 1) Mg alloy pigment; Area 2) Structure of Mg precipitate

In Figure 45, it can be seen that, when covered by the topcoat, the panels with higher PVC (such as AM60 at PVC 34% and AZ91B at PVC 38%) had the lower OCPs combined with a slower increase in OCP than the ones containing AM60 at PVC 31% and AZ91B at PVC 36%. This is attributed to the topcoat providing barrier protection for the porous primer and reducing the oxidation rate of the Mg pigments.

Figure 46 shows the impedance at low frequency as a function of exposure time for the topcoated Mg alloy primer panels. In general, the impedance of these panels followed a trend with respect to pigment composition very similar to that observed with the non- topcoated Mg alloy primers. However, the topcoated panels showed less variation in impedance with exposure time than non-topcoated ones, with the sharp increases and/or decreases observed in Figure 42 no longer observed in Figure 46.

*Mg alloy primers coated panels with topcoat (Impedances at 0.01Hz change with exposure time)*

This is hypothesised that the effect of the epoxy-polyamide binder in the primer may be masked by the presence of the topcoat and the topcoat mainly contributes to the barrier protection of this aerospace coating system. The effects of the pigments though manifested in cathodic protection, is possibly delayed as the topcoat presents the initial barrier protection for the substrate. The lifetime of the coating can be significantly extended when the inherent

barrier property of the topcoat is combined with the excellent topcoat compatibility with the

primer binder.
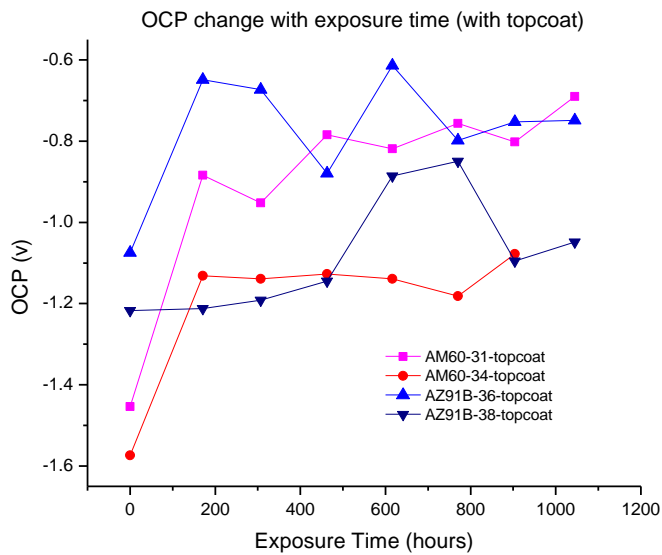


Figure 45. OCPs of Mg alloy primer coated panels (with topcoat) change with exposure time.
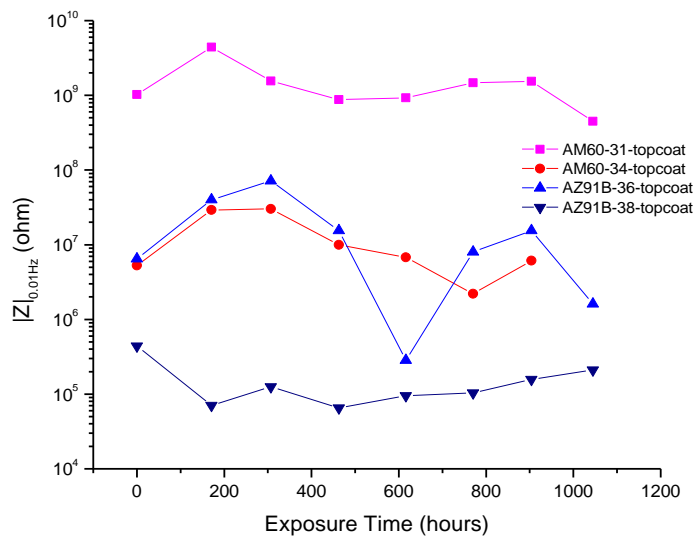


Figure 46. Impedance at 0.01Hz of Mg alloy primer coated panels (with topcoat) as a function of exposure time

## Conclusions

Similar to the pure magnesium pigment, the magnesium alloy pigments formulated in primer coatings can provide cathodic protection for Al alloy substrates. EIS results showed that the metal-rich primers with the Mg alloys as pigments had the mixed potentials between the OCPs of Mg alloys and the bare Al 2024 T3, which indicated the Mg alloy pigments provided sacrificial protection to the Al alloy substrates.

The changes in impedance at low frequency with exposure time for the non-topcoated samples indicated that the electrolyte penetrated the coating films and reached the interface between the primer coating and the substrate, eventually initiating under-film corrosion. Similar observations were made with the topcoated samples although this penetration process was retarded by the good barrier protection of topcoat. Scanning electron microscopy (SEM) showed the existence of Mg precipitates. Furthermore, the investigation of the properties of the three alloys gave a good understanding of the effects of the particle size, the particle shape and the chemical composition on the particle packing efficiency, CPVC and electrochemical behaviour of the primer system, suggesting that pigments with smaller particle size and better controlled shape would result in a better primer system.

## Acknowledgements

## References

[1] Battocchi, D.; Simoes, A. M.; Tallman, D. E.; Bierwagen, G. P., Corrosion Science 2006, 48, 1292-1306

[2] Knudsen, O. O.; Steinsmo, U.; Bjordal, M., Progress in Organic Coatings 2005, 54, 224-229

[3] Nanna, M. E.; Bierwagen, G. P., JCT Research  2004, 1, 69-80

[4] Bierwagen, G. P.; Nanna, M. E.; Battocchi, D. Magnesium rich coatings and coating systems. 2004-US33089, 2005051551, 20041007., 2005

[5] Bierwagen, G.; Tallman, D.; Nanna, M.; Battocchi, D.; Stamness, A.; Gelling, V. J., Polymer Preprints (American Chemical Society, Division of Polymer Chemistry) 2004, 45, 144-145

[6] Bierwagen, G.; Battocchi, D.; Simoes, A.; Stamness, A.; Tallman, D., Progress in Organic Coatings 2007, 59, 172-178

[7] Battocchi, D.; Simoes, A. M.; Tallman, D. E.; Bierwagen, G. P., Corrosion Science 2006, 48, 2226-2240

[8] Simoes, A. M.; Battocchi, D.; Tallman, D. E.; Bierwagen, G. P., Corrosion Science 2007, 49, 3838-3849

[9] B.A. Shaw, ASM Hand book 2003, 13A, 692-696

[10] G. Song; A.L. Bowles; D.H. StJohn, Materials Science and Engineering A 2004, 366, 74-86

[11] G.P.Bierwagen; R.S.Fishman; Storsved, T.; Johnson, J., Prog. Organic Coatings 1999, 35, 1-10

[12] Lobnig, R. E.; Villalba, W.; Goll, K.; Vogelsang, J.; Winkels, I.; Schmidt, R.; Zanger, P.; Soetemann, J., Progress in Organic Coatings 2006, 55, 363-374

[13] Asbeck, W. K., JCT CoatingsTech 2005, 2, 64-66

[14] Loveday, D.; Peterson, P.; Rodgers, B., JCT Coatings Tech 2004, October, 88-93

[15] Skrovanek, D. J., Progress in Organic Coatings 1990, 18, 89-101

[16] Skrovanek, D. J.; Schoff, C. K., Progress in Organic Coatings 1988, 16, 135-63

CHAPTER 6. THE DEVELOPMENT OF A TWO-COMPONENT, MAGNESIUM-RICH PRIMER FOR
CONTROLLING CORROSION OF ALUMINUM ALLOYS

*Jun Li,* [1] *Jie He,* [1] *Bret J. Chisholm,* [1] *Missy Berry,* [1] *Dante Battocchi,* [1] *and Gordon P. Bierwagen* [1]

Abstract

It has recently been shown that surface passivated magnesium particles can be used to produce primers that provide corrosion protection to aluminum alloys by serving as a sacrificial metal. The original polymer binder system that enabled exceptionally good performance was based on a three-component binder system comprised of an epoxy resin, di-isocyanate, and aminofunctional silane. Due to the complexity of the three-component system and variability in pot-life, a simpler one- or two-component binder system was desired that could provide equivalent or better performance than the three-component system. As a result, research was conducted to develop a two-component Mg-rich primer that provides excellent corrosion protection to aluminum alloys. As part of the investigation, several variables associated with the coating formulation were examined using open circuit potential measurements, electrochemical impedance spectroscopy, salt spray exposure testing, and scanning electron microscopy in conjunction with the energy dispersive X-ray technique. The results showed that all of the variables investigated which included epoxy resin molecular weight, curing agent functionality, epoxy/NH ratio, and Mg content significantly affected coating performance. An optimized formulation for the two-component primer was identified, which showed very similar corrosion protection performance to the extensively studied three-component, hybrid binder system for Mg-rich primers.

[1] North Dakota State University, Fargo, ND 58102

Introduction

Chromate containing coatings have been extensively used for corrosion control of aluminum (Al) alloys designed for aerospace applications. However, due to environmental concerns and adverse health effects surrounding use of chromates, there is an intensive effort to find suitable replacements for chromate-based coatings. Recently, a novel magnesium-rich (Mg-rich) primer coating specifically designed for corrosion protection of Al alloys was developed by Bierwagen and co-workers.[1, 2, 3] Corrosion protection for these coatings results from galvanic coupling between the Mg and Al. The Mg particles dispersed in the polymer binder serve as a sacrificial anode, which cathodically interacts with the Al substrate (as cathode) to protect it from corrosion.

The original Mg-rich coating, which showed excellent corrosion protection, was based on a three-component binder system comprised of an epoxy resin, di-isocyanate, and an aminofunctional silane. Due to the complexity of the three-component system and variability in pot-life, a simpler two-component binder system was desired. As a result, two-component epoxy-based binder systems were targeted for investigation.

In order for the Mg to provide cathodic protection to the aluminum substrate, it is necessary to create continuous electronic conduction pathways between Mg particles and the Al substrate. These pathways facilitate electron transfer between the two metals and can be controlled by optimizing Mg content. Qualitatively, if the Mg content in the coating is much less than the critical pigment volume concentration (CPVC), the Mg particles will not be in electrical contact with the Al and, as a result, cathodic protection will be significantly reduced. In contrast, if the Mg content far exceeds the CPVC, significant void space will be created within the coating, leading to relatively high permeability of the coating. As a result, Mg content optimization was also required to obtain a high performance, two-component Mg-rich primer.

<center>Experimental</center>

*Materials*

The Al alloy of interest was AA2024-T3 which is an aerospace aluminum. AA2024-T3 panels were obtained from Q-Panel Lab Products. A Mg powder obtained as a 52/48 vol./vol. blend of Eckagranules™ PK31 (mean particle size distribution (PSD) of 30 μm) and Eckagranules™ PK51 (PSD of 70 μm) was used as received from Ecka GmbH. The epoxides, Epon874-CX-90 and Epon1001-CX-75, and curing agents, Epicure3140 and Epicure3292-FX-60, were obtained from Resolution Performance Products®.

Both epoxides are bisphenol-A-based diepoxides with Epon874-CX-90 possessing a relatively low molecular weight (MW) and the Epon1001-CX-75 possessing a relatively high MW. Epon874-CX-90 contains 10 wt.% MIBK/xylene (50/50 vol./vol) while Epon1001-CX-75 contains 25 wt.% MIBK/xylene (65/35). Epicure3140 is a solvent less polyamide curing agent and Epicure3292-FX-60 is a polyamine curing agent containing 40 wt.% n-butanol/xylene (50/50). Table 4 provides a further description of the epoxy resins and curing agents. Dispersing agent, Aerosil® R974, was purchased from Degussa. Methylisobutylketone (MIBK) and xylene were obtained from Sigma-Aldrich Company. The topcoat used was DEFT MIL-PRF-85285C, which is glossy polyurethane.

The two-component Mg-rich coatings investigated were comprised of a component containing epoxy resin, Mg particles, MIBK, and dispersing agent and another component containing curing agent and xylene. Table 5 displays the composition of each of the coatings prepared. The acronyms used to identify the coatings were chosen to allow for easy identification of the coating composition. For example, the acryonym L-Ad-1-50 indicates that the epoxy resin used in the coating was based on the low molecular weight epoxy resin ("L"), amide functional curing agent ("Ad"), 1/1 mole/ mole epoxy/NH ratio ("1"), and 50 volume percent Mg ("50").

<center>80</center>

Table 4. Properties of the epoxy resins and curing agents utilized. [*]The capital letters indicate Gardner-Holdt viscosity according to ASTM D 1545-98. [†]Equivalent weight is grams of resin per mole of functional group

|  | Viscosity | Equivalent Weight [†] | Density | Amine Value |
|---|---|---|---|---|
|  | (Poise) |  | (lb/gal) | (mg KOH/g) |
| Epon874-CX-90 | $X-Z_1$[*] | 245-275 | 9.1 | ---- |
| Epon1001-CX-75 | $Z_1-Z_6$[*] | 450-550 | 9.1 | ---- |
| Epicure3140 | 30-40 | 95 | 8.1 | 360-390 |
| Epicure3292-FX-60 | $Z-Z_2$[*] | 140 | 8.5 | 390-420 |

Table 5.  Formulations of the primers investigated (PART I)

| Raw Material | L-Ad-1-40 | L-Ad-1-45 | L-Ad-1-50 | L-Ad-1-60 | L-Ad-0.87-45 | L-Ad-0.87-55 | L-Ad-1.18-45 |
|---|---|---|---|---|---|---|---|
|  |  |  |  | Weight, g |  |  |  |
| Epon874-CX-90 | 58 | 58 | 58 | 58 | 58 | 58 | 58 |
| Epon1001-CX-75 | × | × | × | × | × | × | × |
| Epicure3140 | 19 | 19 | 19 | 19 | 21.9 | 21.9 | 16.2 |
| Epicure3292-FX-60 | × | × | × | × | × | × | × |
| Mg powder | 72 | 88 | 108 | 163 | 93 | 139 | 85 |
| Aerosil® R974 | 0.7 | 0.9 | 1 | 1.6 | 1 | 1.5 | 1 |
| MIBK | 32 | 37 | 42 | 65 | 40 | 52 | 40 |
| Xylene | 7 | 9 | 10 | 16 | 9 | 15 | 8 |

*Procedures*

Substrate panels were pretreated prior to coating application by: 1) immersing them for 20 minutes at room temperature in an aqueous alkaline solution comprised of 0.4 wt.% sodium hydroxide, 2.8 wt.% tetrasodium pyrophosphate, and 2.8 wt.% sodium bicarbonate; 2) rinsing the panels with deionized (DI) water; 3) immersing in a deoxidizer solution comprised of 35% n-butyl alcohol, 25% isopropyl alcohol, 15% ortho-phosphoric acid (85%), and 25% DI water for 2 minutes at room temperature; 4) rinsing with DI water; and 5) allowing the panels to dry at ambient conditions.[4]

Table 6.  Formulations of the primers investigated (PART II)

| Raw Material | L-Ad-1.18-55 | L-Am-1-0 | L-Am-1-50 | H-Ad-1-20 | H-Ad-1-50 | H-Am-1-0 | H-Am-1-20 | H-Am-1-50 |
|---|---|---|---|---|---|---|---|---|
| | Weight, g | | | | | | | |
| Epon874-CX-90 | 58 | 58 | 58 | × | × | × | × | × |
| Epon1001-CX-75 | × | × | × | 67 | 67 | 67 | 67 | 67 |
| Epicure3140 | 16.2 | × | × | 9.5 | 9.5 | × | × | × |
| Epicure3292-FX-60 | × | 46 | 46 | × | × | 23 | 23 | 23 |
| Mg powder | 128 | × | 123 | 23 | 95 | × | 24 | 99 |
| Aerosil® R974 | 1.5 | 0.5 | 1 | 0.5 | 1 | 0.5 | 0.5 | 1 |
| MIBK | 52 | 20 | 60 | 22 | 45 | 20 | 30 | 45 |
| Xylene | 12 | 5 | 25 | 10 | 20 | 5 | 10 | 20 |

Primer compositions were applied to pretreated panels using a high volume/low pressure spray method.[5] Solvent flash and curing were done at ambient conditions. All primed specimens were allowed to cure for at least one week before top coating. The average dry film thicknesses of the Mg-rich primers were about 100±25 microns. The high gloss polyurethane topcoat was applied by spray coating and the average film thickness was 50±15 microns.

*Characterization*

Electrochemical impedance spectroscopy (EIS) was used to evaluate electrochemical properties of coated specimens using a Gamry Femtostat/PCI4 Electrochemical Workstation in conjunction with dilute Harrison's solution (0.35 wt% $(NH_4)_2SO_4$ and 0.05 wt% NaCl) as the electrolyte. A single sinusoidal potential 10 mV in amplitude was superimposed on the open-circuit potential (OCP). Measurements were made between 10 mHz and 100 kHz from high to low frequency. The sample area of the working electrode was 3.5 $cm^2$. A saturated calomel electrode (SCE) was used for the reference electrode and a platinum mesh was used as the counter electrode.

Scanning electron microscopy (SEM) and energy-dispersive X-ray (EDX) analysis were performed with a JEOL JSM-6300V microscope (JEOL, Ltd., Tokyo, Japan) equipped with a

Thermo EDS detector using a VANTAGE Digital Acquisition Engine. An accelerating voltage of 15 kV, a take-off angle of 29.08, and a 100 s count were used. Samples were mounted on Al mounts and coated with gold using a Technics Hummer II sputter coater.

*Testing*

Salt spray exposure tests were conducted according to ASTM B117 using a Q-FOG CCT-1100 salt fog chamber obtained from Q-PANEL.  The salt fog was generated from a 5 wt. % NaCl solution with a pH ranging from 6.5 to 7.2. The fog deposition rate ranged from 1 to 2 ml/h and the temperature of the chamber was kept constant at 35ºC. The coated specimens (3 inch by 6 inch) were scribed using a tungsten carbide cutter (Robert Bosch Tool Corporation). The scribe was X-shaped with a top width of 4 cm, a height of 10 cm, and width of 1 mm and penetrated through all coating layers to expose the substrate. The outer edges and backside of the specimens were protected by covering them with Polyken 231 tape (Covalence Adhesives). After a desired amount of salt spray exposure, specimens were removed from the chamber and rinsed thoroughly with DI water before visually inspecting the coatings for corrosion. In addition to visual inspection, EIS was conducted on some specimens. After visual inspection and an EIS measurement, specimens were immediately returned to the salt spray chamber for further testing.

## Results and Discussion

Since Mg is critical to corrosion protection, initial experimentation was focused on characterizing the effect of Mg content on coating properties using representative two component-binder systems and EIS to determine CPVC by measuring the change of coating pore resistance as a function of Mg volume content (PVC).[6] Low frequency impedance (0.01 Hz) of the coatings was used as an indicator of coating pore resistance. Figure 47 displays a representative plot of low frequency impedance as a function of PVC.

A distinct drop in impedance was observed when the PVC was changed from 45 to 50%, indicating that the CPVC lies within this range. From theoretical calculations made for the

three-component Mg-rich system, the calculated CPVC was 47.5 %, a value quite similar to our experimental result.[3] It is interesting to note that the impedance increased to some extent after the PVC exceeded CPVC, indicating that the polymer binder concentration was too low to completely coat all of the surface area of the Mg particles.

Due the presence of exposed Mg surfaces within the coating, it would be expected that rapid Mg oxidation would occur by reaction with water or ionic species (Cl$^-$, SO$_4^{2-}$, etc.) diffusing through the coating,[2] generating oxidation products that fill void space and therefore increase coating pore resistance. Similar behavior may be responsible for the increase in impedance that was observed at given PVC when electrolyte exposure time was increased beyond three days.
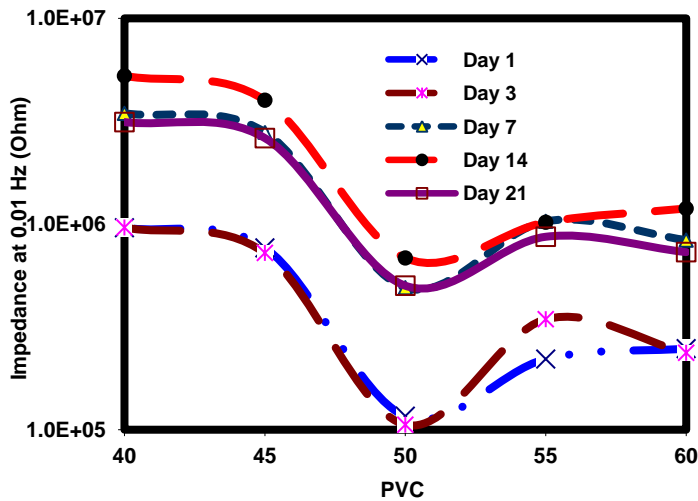


Figure 47. Impedance at low frequency (0.01Hz) as a function of PVC and exposure time for a series of Mg-rich primers based on the low MW epoxy resin, amide curing agent, and 1/1 epoxy/NH ratio

The galvanic coupling between the Mg particles in the coating and the Al substrate was also characterized by measuring OCP above and below the CPVC. As shown in Figure 48, galvanic coupling was only obtained for a short period of exposure (1 to 2 hours) for the coating containing 40% PVC. A large fluctuation of potential was also found during this period, indicating ineffective electrical contact between Mg particles and the Al substrate.[7] The OCP

stabilized at -0.7 V after about four hours of exposure, which is basically the OCP of Al 2024.

For the 50% PVC coating, a lower and more stable OCP was obtained, indicative of the

formation of effective electric contact between Mg particles and the Al substrate.  From these

results, it was clear that 50% PVC was approximately the optimum for the two component

primers of interest.
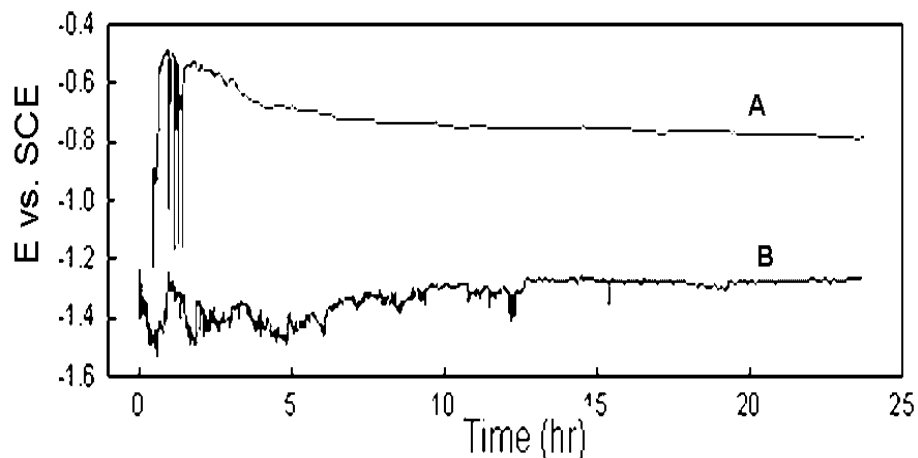


Figure 48. A short term OCP measurement for Mg-rich primers, L-Ad-1-40 (A) and L-Ad-1-50 (B), on Al 2024 using dilute Harrison's solution

After having determined the approximate Mg content needed to obtain galvanic

coupling between the Mg particles and Al substrate, the effect of the various factors associated

with polymer binder composition were investigated.  The factors investigated included

epoxy/NH ratio, epoxy resin MW, and curing agent functionality.

Figure 49 shows the effect of epoxy/NH ratio on coatings produced at different Mg

contents above and below CPVC. As expected, impedance of coatings containing 45% PVC

were higher than corresponding coatings containing 55% PVC because increasing the Mg

content above CPVC increases conductivity and coating porosity.  With regard to the effect of

epoxy/NH ratio, the data shown in Figure 49 shows that, at a given PVC, coatings formulated

using a 1/1 epoxy/NH ratio showed the highest impedance over the entire frequency range.

This behavior suggests that use of an equal molar ratio of epoxy groups to NH groups results in the highest crosslink density and, thus, the highest barrier properties.
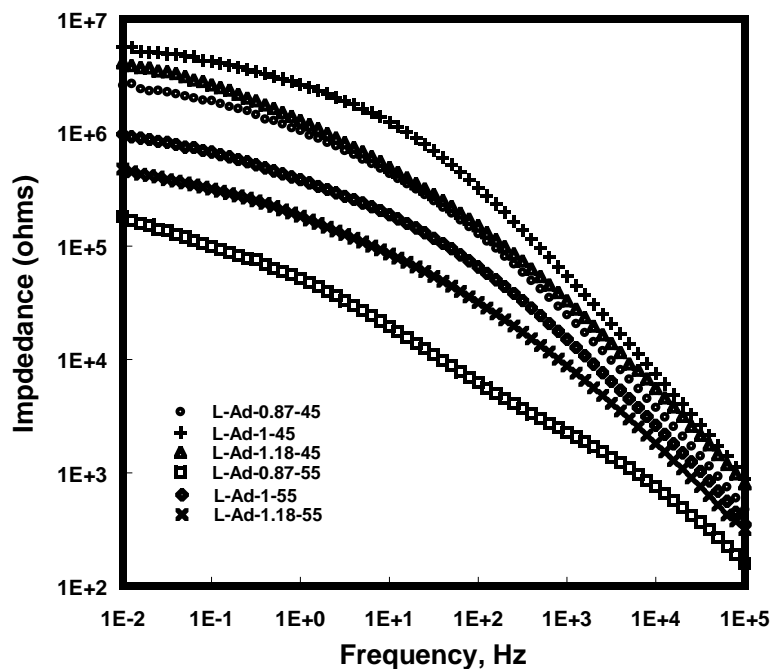


Figure 49. Bode plots of impedance for Mg primers exposed for 1 day to dilute Harrison's solution

Based on the results obtained with respect to the effect of epoxy/NH ratio, epoxy/NH ratio was held constant at 1.0 for further experimentation. The effect of epoxy resin MW on corrosion protection of topcoated samples was evaluated using EIS. As shown in Figure 50, before the exposure test and after two weeks of exposure to dilute Harrison's solution, the coating system based on the high MW epoxy resin showed significantly higher low frequency impedance than the coating system based on the low MW epoxy resin. This result indicates that the coating system based on the high MW epoxy resin possessed better barrier properties than the coating system based on the low MW epoxy resin. Since the higher MW epoxy resin possesses a higher epoxy equivalent weight (Table 4), the higher barrier properties for this coating system may be due to the lower concentration of the hydrophilic curing agent required to cure the resin.

86
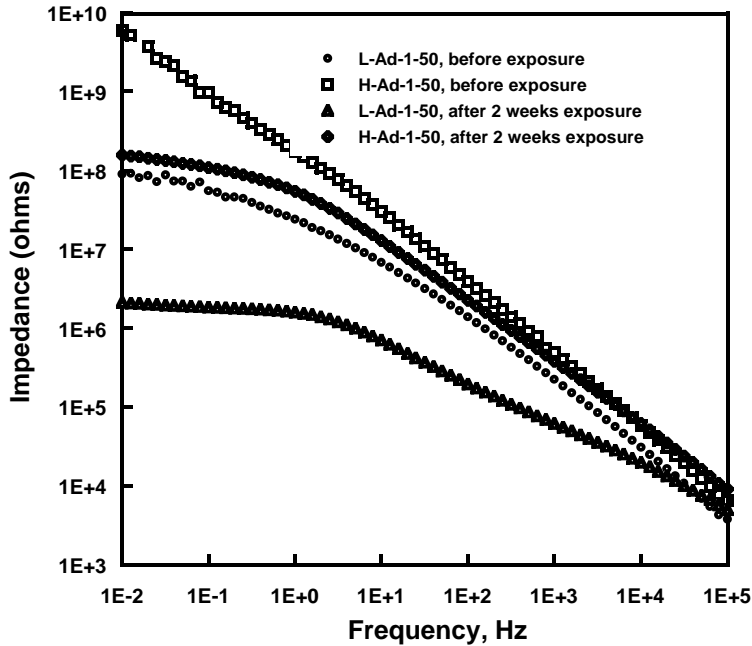
Figure 50. Bode plots for polyurethane topcoated samples illustrating the effect of epoxy resin MW in the Mg-rich primer layer

Using the high MW epoxy resin, the effect of curing agent composition on corrosion protection was investigated. The experiment compared an amino-functional curing agent to an amidofunctional curing agent using EIS and B117 salt spray to characterize corrosion protection. Figure 51 displays Bode plots for coatings as function of curing agent composition, Mg content, exposure time.

The coatings in their "as produced" state (prior to longer term exposure to dilute Harrison's solution) showed essentially no difference in impedance behavior with respect to the effect of curing agent composition. However, after two weeks of exposure, higher impedance was consistently found with the use of the polyamide curing agent suggesting that the polyamide cured epoxy provides better barrier properties than the amino-cured epoxy.

Figure 52 displays images of coating samples tested using 3000 hours of B117 salt spray exposure. All of the coating samples based on the amino functional curing agent exhibited blistering even at 50% PVC while samples prepared using the amide-functional curing agent generally showed much less blistering.
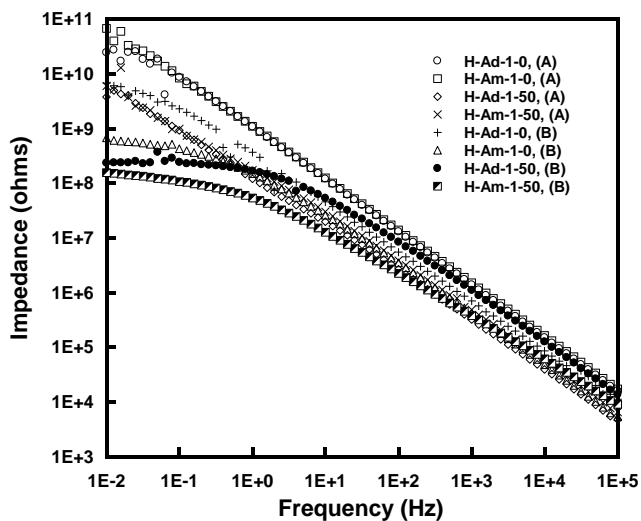
Figure 51. Bode plots of impedance for polyurethane topcoated epoxy primers on Al 2024 before (A) and after two weeks of exposure to dilute Harrison's solution (B)

For the coating system based on the amide-functional curing agent and 50% PVC, no blistering or corrosion was observed after 3000 hours of salt spray exposure. In addition to measuring the corrosion protecting capabilities of the coatings, the effect of primer curing agent composition on adhesion was measured. As shown in Figure 53, the coatings based on the amidofunctional curing agent consistently displayed higher adhesion than the coatings based on the aminofunctional curing agent. The superior corrosion protection provided by the polyamide curing agent may be at least partly due to better adhesion. Since the primary objective of the work described in this document was to develop a two-component Mg-rich primer that possessed the excellent corrosion protective attributes of the previously described three-component Mg-rich primer,[3] a comparison between the three-component and the optimized two-component Mg-rich primer was made using B117 salt spray. Figure 54 displays representative images before and after 3,000 hours of salt spray exposure for a sample based on the three-component Mg-rich primer and an analogous sample based on the optimized two-component Mg-rich primer (H-Ad-1-50).
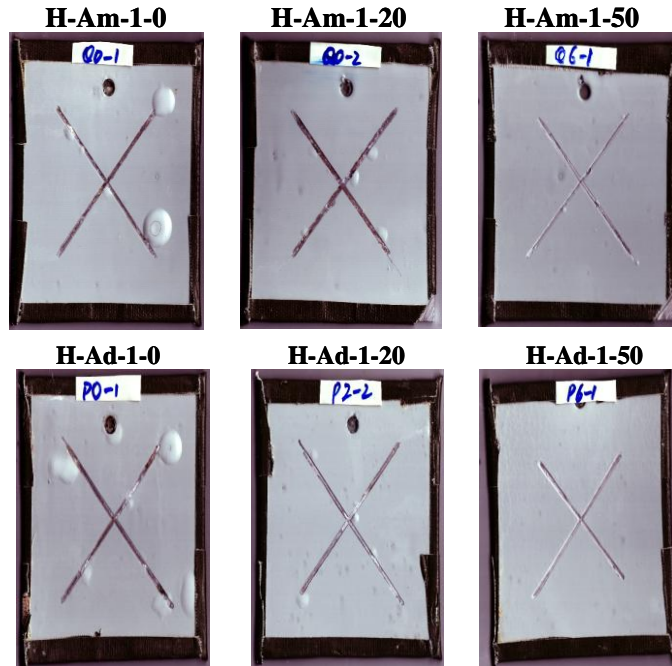
Figure 52.  Images of topcoated two-component Mg-rich primer samples after 3000 hours of B117 salt spray exposure
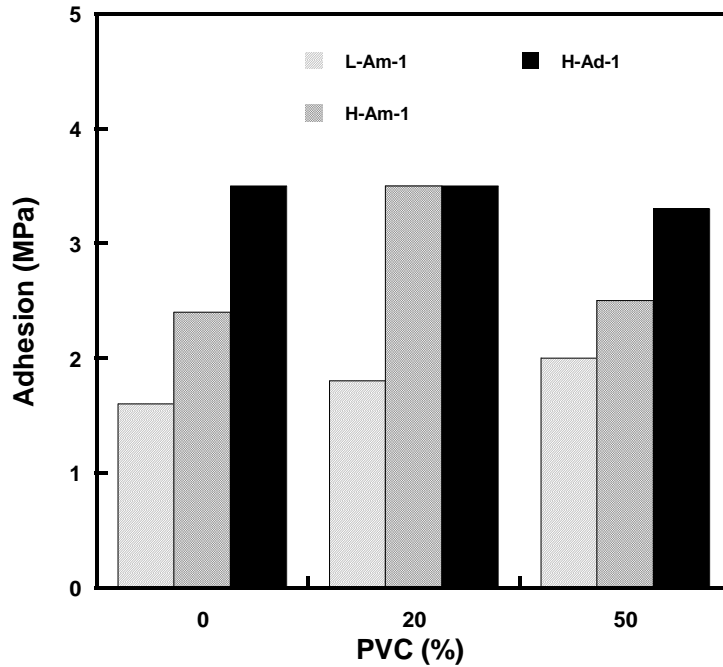


Figure 53. Pull-off adhesion results obtained for topcoated samples illustrating the effect of curing agent composition and PVC

After 3000 hours of salt exposure, no blistering or coating delamination was observed indicating that the two-component Mg-rich primer provides at least the same corrosion protection performance as the three-component Mg-rich system.

Based on the promising salt spray results obtained for the two-component Mg-rich primer developed, further characterization of this composition was conducted using electrochemical methods and SEM-EDX. A long term OCP measurement was conducted to observe the variation in conductivity with exposure time for the Mg-rich primer on Al 2024.
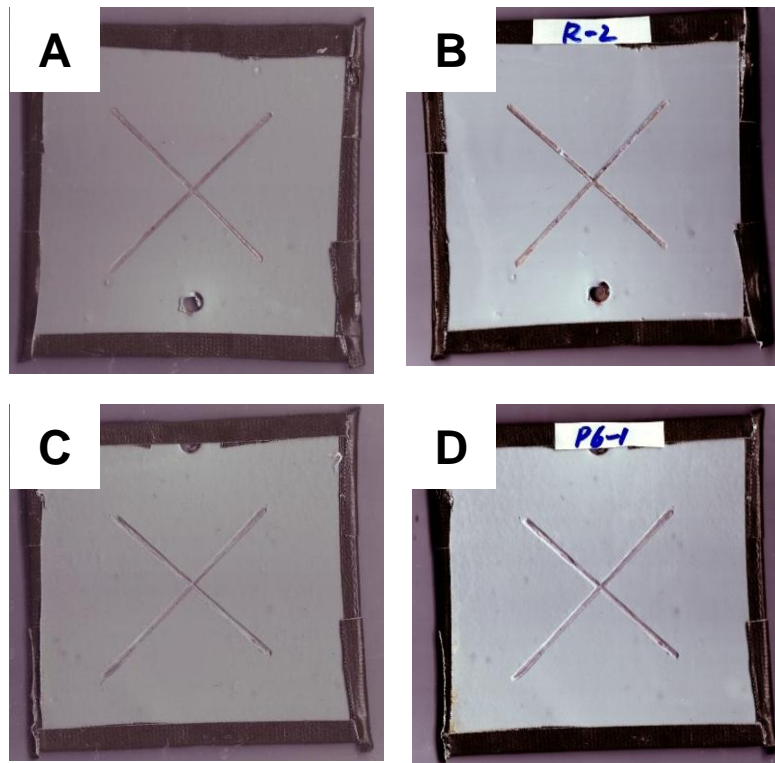


Figure 54.  Representative images before and after 3,000 hours of salt spray exposure for a topcoated three-component Mg-rich primer on Al 2024 (A = before salt spray and B = after 3,000 hours salt spray) and a topcoated two-component Mg-rich primer (H-Ad-1-50) on Al 2024 (C = before salt spray and D = after 3,000 hours salt spray)

As illustrated in Figure 55 and similar to the results previously observed by Bierwagen and co-workers,3 the OCP can be divided to three regimes. Regime 1 corresponds to the change in OCP during the initial 7 days of exposure in which the OCP was the mixed potential between pure Mg (-1.6 V) and bare Al 2024 (-0.6 V). During this time period, the Mg-rich

coating interacts with the Al substrate predominantly through a cathodic protection mechanism. After 7 days of exposure, the OCP slowly increased from -0.9V to -0.6V over a 43-day period (Regime 2). The slow increase in potential during Regime 2 was attributed to the consumption of Mg in the coating, reducing the galvanic interaction between Mg particles and the Al substrate.  The OCP shifted out of the cathodic protection domain and basically stabilized at -0.6V (OCP of bare Al 2024) after 50 days of immersion (Regime 3).
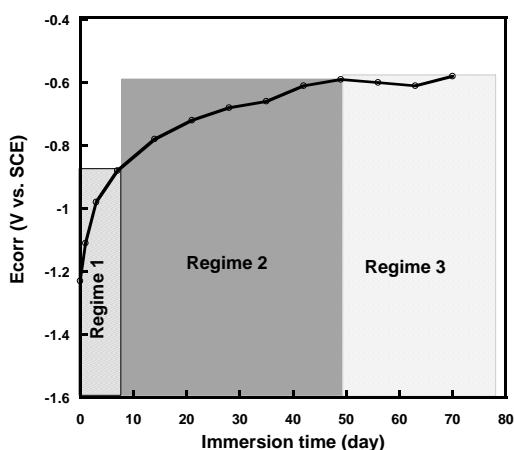


Figure 55. A long term OCP measurement of the optimized two-component Mg-rich primer, H-Ad-1-50, on AA2024-T3 using diluted Harrison's solution

This time period for the OCP transition from -1.25 V to -0.6V is assumed to be the life-time of the primer (50 days) for active cathodic protection, which is much longer than that reported for the three-component Mg-rich primer (30 days).[3]

A long term study of corrosion protection for the coating system based on the two-component Mg-rich primer and the polyurethane topcoat was conducted by using EIS in conjunction with salt spray exposure. As shown in Figure 56, the coating system showed excellent barrier properties prior to salt spray exposure.

The low frequency impedance was quite high (more than $10^9$ ohm) and the linearity of the Bode plot indicated highly capacitive behavior. As salt spray exposure time increased, the coating resistance slowly decreased as indicated by the reduction in low frequency impedance. However, after 125 days of salt spray exposure, the low frequency impedance only dropped

about one order of magnitude, indicating that the coating system maintained good barrier

properties over the course of the exposure. This conclusion was supported by visual

observation of the coating which showed no evidence of coating delamination, blistering, or

corrosion products.
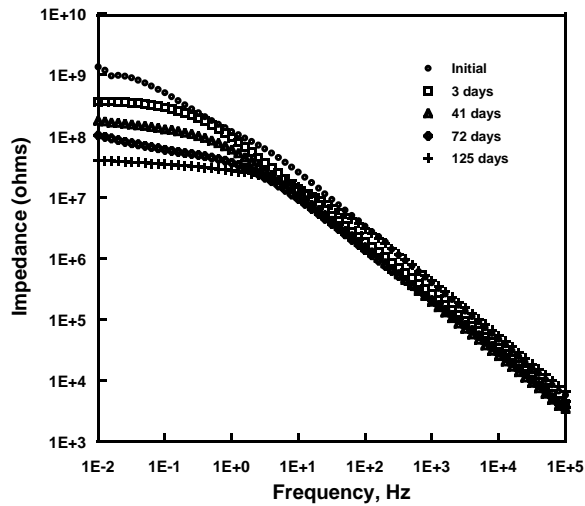


Figure 56. Bode plots of the topcoated, optimized Mg-rich primer, H-Ad-1-50, as a function of salt spray exposure time

SEM and EDX were used to correlate corrosion performance of the two-component Mg-

rich coating with coating morphology. Figure 57 shows a surface and cross section SEM image

of the coating before salt spray exposure. From both the surface SEM image and the cross

section image, it can be seen that the Mg particles were in direct contact with one-another

allowing for the efficient electron transfer needed for galvanic protection. In addition, the cross

section image shows a high concentration of Mg particles in direct contact with the Al substrate

allowing for galvanic coupling with the substrate.

Figure 58 shows a cross section image of the coating system after 3,000 hours of salt

spray exposure and provides EDX mapping for Mg, Al, oxygen, and chlorine. From Figure 58, a

higher oxygen content was found in the primer than in the topcoat, indicating the generation

of Mg oxidation products as a result of salt spray exposure.
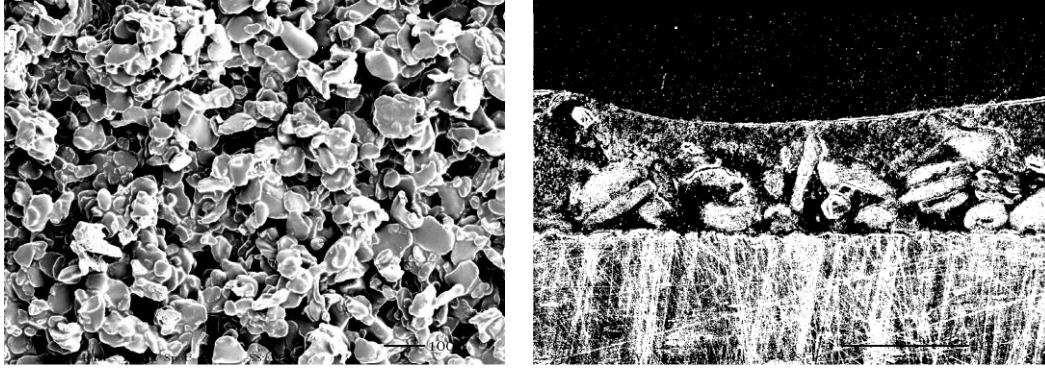
Figure 57. Surface (left) and cross-section (right) SEM image of sample H-Ad-1-50 coated on Al-2024

The Mg oxide or derivative compounds may affect corrosion performance by at least two mechanisms. Similar to zinc-rich coatings for the galvanic protection of steel, Mg corrosion products may fill porosity within the primer and, thereby, enhance barrier properties of the coating.[8, 9, 10] The Mg oxide generated as a result of Mg oxidation may also precipitate at the substrate and modify the Al surface by filling pores within the Al oxide layer, increasing the stability of the oxide layer to ions ($Cl^-$).[11] Due to the excellent corrosion performance of the coating system, no Al species were found in the primer or topcoat as shown by EDX Al mapping (Figure 58).
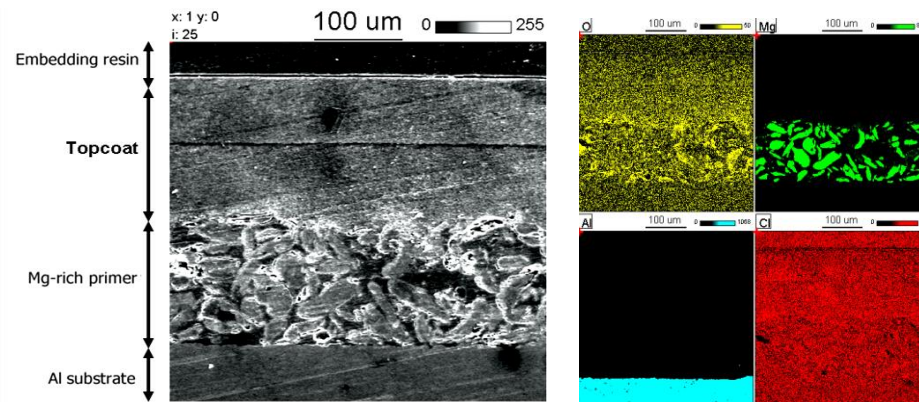


Figure 58. SEM cross section image (left) and EDX mapping (right) of sample H-Ad-1-50 after 3,000 hours of salt spray exposure

## Conclusions

A two-component Mg-rich primer coating was developed that showed excellent corrosion protection of Al 2024 when used in conjunction with a polyurethane topcoat. The development involved an investigation of the effects of most all of the compositional variables on corrosion protection. The variables investigated were epoxy resin MW, curing agent functionality, epoxy/NH ratio, and Mg content. A number of techniques such as OCP measurement, EIS, B117 salt spray, pull-off adhesion, SEM, and EDX were used to study and evaluate corrosion protection. All of the variables investigated had a significant effect on coating system performance and an optimized coating composition was identified that showed very good corrosion protection for at least 3,000 hours of B117 salt spray exposure. The optimized coating composition was based on the high MW epoxy resin, amide-functional curing agent, 1.0 epoxy/NH ratio, and Mg volume content of 50%. Detailed characterization of the optimized coating system clearly showed that corrosion protection occurs through galvanic coupling between Mg in the primer and the Al substrate. In addition, SEM-EDX mapping results in conjunction with electrochemical measurements indicate that Mg oxidation products may also be playing a role in corrosion protection by increasing barrier properties over the lifetime of the coating.

## References

[1] D. Battocchi, A. M. Simoes, D. E. Tallman, G. P. Bierwagen, Corrosion Science 2006, 48, 5, 1292-1306

[2] D. Battocchi, A. M. Simoes, D. E. Tallman, G. P. Bierwagen, Corrosion Science 2006, 48, 8, 2226-2240

[3] M. E. Nanna, G. P. Bierwagen, J. Coatings Technology Research 2004, 1

[4] L. M. Farrier, S. L. Szaruga, Materials Characterization 2005, 55, 179

[5] W. D. o. N. Resources, (Ed.: W. H. W. M. Program), 1993, pp. PUBL

[6] R. E. Lobnig, W. Villalba, K. Goll, J. Vogelsang, I. Winkels, R. Schmidt, P. Zanger, J. Soetemann, Progress in Organic Coatings 2006, 55, 363

[7] A. E. Hughes, R. J. Taylor, B. R. W. Hinton, Surface and interface analysis 1997, 25, 223

[8] S. M. A. Shibli, R. Manu, Surface and Coatings Technology 2006, 201, 2358

[9] Focus on Powder Coatings 2004, 2004, 3

[10] H. Marchebois, C. Savall, J. Bernard, S. Touzain, Electrochimica Acta 2004, 49, 2945

[11] C. Dornfest, F. C. Redeker, M. A. Fodor, C. Brecaw, H. S. Tomizawa, Vol. 648866 (Ed.: E. P. Appl.), 1995

CHAPTER 7. THERMAL STABILITY OF MAGNESIUM–RICH PRIMERS BASED ON GLYCIDYL

CARBAMATE RESINS

Neena Ravindran,[1] Dipak Chattopadhyay,[2] Dante Battocchi,[1,2] Dean C. Webster,[2] Gordon P.

Bierwagen[1,2]

## Abstract

Coatings of outstanding thermal stability were obtained on combining two novel

technologies, that of magnesium-rich primer composites and a silane-modified glycidyl carbamate

binder. The objective of the study was to evaluate a new binder system, specifically with respect to

overall film properties in the magnesium rich primer technology. However, during

thermogravimetric analysis of samples, previously unobserved properties were discovered. The

samples transformed into an intact residue, with the amount of the residual char ranging between

60 to 90% weight depending on the PVC of the composition. The hitherto unobserved property is

essentially a function of the metallic pigment particles in the composite. The discovery of the

outstanding thermal stability potentially increases the range of application for these primers.

Keywords: Thermal stability, metallic primers, anti-corrosion primers, metallic pigments,

magnesium pigments, glycidyl carbamate resin

## Introduction

Mg-rich alloys were developed in response to a requirement for chrome-free replacements

for aircraft alloys.[1] Currently chrome based materials are used to impart corrosion protection

properties either as pigments or in the form of a pretreatment. Development of magnesium

particles for Al2024 alloy is a major paradigm shift in coatings technology with respect to corrosion

---

[1] NDSU, Center for Surface Protection, Fargo ND 58105-5376, USA

[2] NDSU, Department of Coatings and Polymeric Materials, Fargo, ND 58105-5376, USA

protection of metals. The Mg-rich primer provides cathodic protection to the substrate and the polymer matrix provides good adhesion and barrier properties. Electrochemical behavior investigations of the system confirmed that the connecting magnesium particles provide corrosion protection by two mechanisms: polarizing the aluminum cathodically and by offering barrier protection from oxidation products.

Therefore, as opposed to the traditional zinc-rich systems wherein cathodic protection can only be obtained at Pigment Volume Concentration (PVC) greater than the Critical Pigment Volume Concentration (CPVC), cathodic protection can still be obtained at PVC lower than CPVC in case of the magnesium rich system.[2] The original system developed for a Mg-rich primer was a three part system which included a silane-pretreatment for the metal substrate and hybrid binder and a silanised crosslinker.1 Most of the research since this innovation has focused on expanding the understanding of pigmentary properties and other pigment modifications. This study is focused on the evaluation of an alternate binder in trying to enhance the barrier properties and thereby significantly increasing the lifetime of the coating. The binder chemistry under consideration is the glycidyl carbamate (GC) chemistry [3].[3] GC chemistry has the potential of combining polyurethane and epoxy chemistry into a single system.

It has been previously demonstrated that the coatings based on GC resins exhibit outstanding chemical resistance and mechanical properties. For this particular study, silanised-GC resin was used as the binder keeping in line with the characteristics of the original system which had an additional inorganic component in the coating system which effectively made it a three-part system.

However, the use of a silanised resin has the benefit of yielding of a two-part system with potentially comparable or better results. As this was meant as feasibility screening study, and the focus was on obtaining trends of final coating properties due to variation in formulation parameters. This paper focuses on the thermal properties of these coatings.

Experimental

*Materials*

Glycidyl carbamate resins containing 10, 15 and 20% silanization (aminopropyltrimethoxy silane) of the free isocyanate groups were synthesized. The reaction details are outside the scope of this study and will be addressed in a separate publication. Anacamide 2353 was obtained from Air Products and Epicure 3164 from Shell Chemical Company. The magnesium pigment powder (3820) was obtained from Ecka Granules. Methyl ethyl ketone was purchased from Sigma Aldrich. All materials were used as received without further purification.

*Preparation of coatings*

Formulations were prepared by mixing calculated quantities of the GC resin, magnesium filler particles and crosslinker and thinned to spray application viscosity using methyl ethyl ketone. The final film thickness ranged between 50 to 70 microns. The pigment volume concentrations of the formulations were fixed at 20, 30 and 40%. The crosslinkers used were identified from a separate study and were Epicure 3164 and Ancamide 2353. The formulations for the screening study evaluation were selected such that the effect of increasing % silane, the effect of PVC and the chemical nature of the crosslinker could be obtained.

The formulations were spray-coated onto Al2024 and glass substrates for further tests. The Al2024 substrates were prepared by sanding (first using 220 grit followed by 600 grit) followed by a hexane wash. The resultant coatings were evaluated for thermal properties through thermogravimetric analysis (TGA), differential scanning calorimetry (DSC), photoelectron spectroscopy (XPS) and energy diffractive Xray (EDAX).

*Nomenclature*

The formulations have been designated as GCSilX_YPVC_Crosslinker wherein, X= % of NCO groups modified with silane and Y= % PVC. PVC is the pigment volume concentration and is calculated as follows:

$$\%PVC = 100 \times V_{pigment}/(V_{pigment}+V_{non\text{-}volatile\ binder}) \qquad \text{(Equation 9)}$$

The samples without the PVC term are the control samples and do not contain pigments. These controls were included in the evaluation to delineate the properties in terms of binder and pigmentary contributions to the extent possible. The crosslinkers Ancamide 2353 and Epicure 3164 are notated as 2353 and 3164 respectively.

*Characterization*

DSC measurements were conducted using a TA Instruments Q1000 series DSC. The testing method used was a heat-cool-heat cycle. The samples were first equilibrated at -75°C and then subjected to a heat cycle at the rate of 10°C/min to 200°C, followed by cooling to -75°C and held isothermally for 5 minutes, and a final heating cycle at a rate of 10°C/min to 250°C. TGA was determined using a TA Instruments Q500 Thermogravimetric Analyzer. Samples were heated in air from 25°C to 800°C, at a rate of 10°C/min. XPS measurements were carried out with a PHI Quantera XPS microprobe system. It was equipped with an electron neutralize gun and an Ar ion sputter gun. The base pressure of chamber was less than $1 \times 10^{-8}$ torr during measurement. All the results were obtained with an Al $K_\alpha$ (h$\nu$ = 1486.6 eV) X-ray beam at beam diameter of 200 microns.

The pass energy of analyzer was fixed at 55 eV and scanning step was 0.1eV.  The binding energy was calibrated by using Au $4f_{7/2}$ = 84.0 and Cu $2p_{3/2}$ = 932.67 eV. Scanning electron microscopy (SEM) was carried out with a Jeol JSM-6490LV microscope, equipped with an energy dispersive X-ray analyser (EDAX). The samples were mounted on aluminum mounts and coated with gold using a Technics Hummer II sputter coater (Anatech Ltd., Alexandria, Virginia.) Images were obtained using a JEOL JSM-6490LV Scanning Electron Microscope (JEOL USA, Inc., Peabody, Massachusetts.)   X-ray information was obtained via a Thermo Nanotrace Energy Dispersive X-ray detector with NSS-300e acquisition engine.

## Result and Discussion

The thermal behavior of the magnesium-rich primer based on silane-modified glycidyl carbamate resin was investigated. As this was meant to be a screening study, selected formulations

were evaluated to understand the effect of parameters such as % silane, PVC and type of crosslinker on performance properties. The glass transition temperature ($T_g$) data obtained from differential scanning calorimetry is included Table 7.

Table 7. Glass transition temperature ($T_g$) data obtained from differential scanning calorimetry

| Sample | $T_g$ (°C) |
|---|---|
| GCSil10_2353 | 72.0 |
| GCSil10_20PVC_2353 | 77.6 |
| GCSil10_30PVC_2353 | 78.6 |
| GCSil10_40PVC_2353 | 81.2 |
| GCSil15_2353 | 76.3 |
| GCSil15_40PVC_2353 | 81.3 |
| GCSil10_3164 | 41.0 |
| GCSil10_20PVC_3164 | 43.0 |
| GCSil10_30PVC_3164 | 47.9 |
| GCSil10_40PVC_3164 | 50.7 |
| GCSil15_3164 | 42.1 |
| GCSil15_30PVC_3164 | 43.1 |
| GCSil15_40PVC_3164 | 41.1 |
| GCSil20_3164 | 43.1 |
| GCSil20_30PVC_3164 | 43.3 |

The first conclusion that can be drawn from the $T_g$ values is that the $T_g$ varies with type of the crosslinker, as expected. Coatings containing Ancamide 2353 had a higher $T_g$ as compared to those containing Epicure 3164 and can be attributed to the difference in chemical compositions of the two crosslinkers.

It was also found that generally the introduction of the magnesium pigment resulted in an increase in $T_g$ value and further with the increase in the PVC, there was a further increase in the $T_g$.

*Thermogravimetric Analysis (TGA) of primers*

TGA experiments on samples from 25°C-800°C in air, showed a residual weight gain in samples containing magnesium pigments after 600°C. It was also found that the residue yield ranged from 60 to 90 weight % depending on the PVC. A representative TGA thermogram is shown in Figure 59.
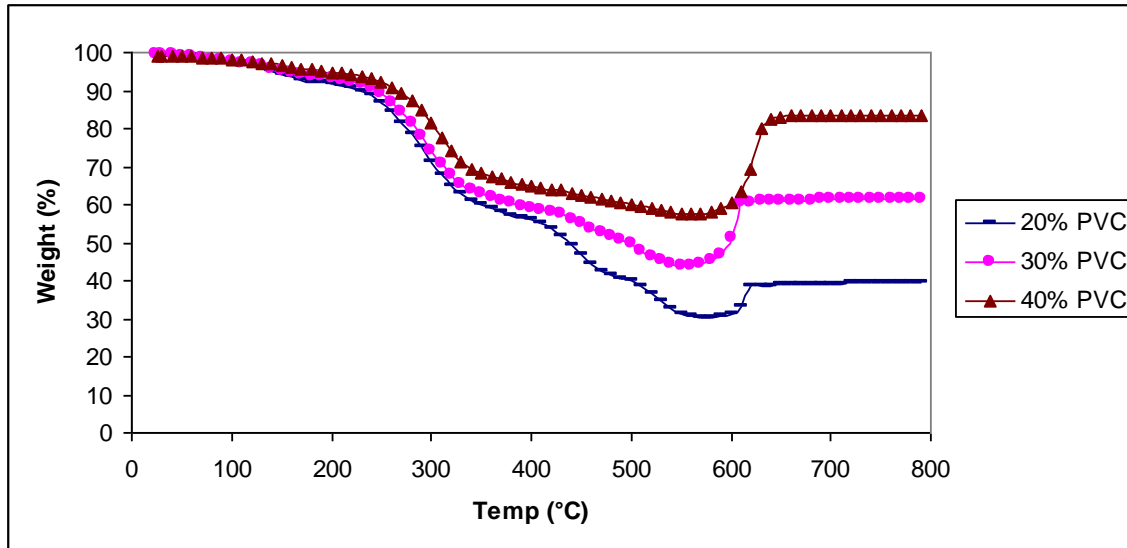
Figure 59. Thermogravimetric analysis curves in air for formulations with PVC= 20%, 30% and 40%

The plot indicates that perhaps an oxidation reaction causes the increase in residual weight at higher temperatures. Another observation concluded that the residue was visually intact and looked similar to the starting material.

*Energy Dispersive XRay Results (EDAX)*

In order to further investigate the mechanism at work, we analyzed the residue obtained from the thermogravimetric analysis using EDAX to understand its composition. As stated earlier, the residue looked intact in terms of appearance and there were no visible signs of deterioration due to the thermal exposure. Figures 60 and 61 are images of the residue mounted on a carbon tape and the cracks appeared after pressure was applied to make it adhere to the tape. High magnification images of the residue are also included.

High magnification image suggest a sintering of the coating material and this behavior possibly contributes to the sample integrity post high temperature exposure. The elemental analysis scans as illustrated in Figures 62 and 63 indicate that the major components of the residue are Mg and O both in case of 30% PVC and 40% PVC. From the values obtained composition from elemental analysis, it could be concluded that Mg and O were present in a ratio of 1:1 suggesting that the residual material was constituted of MgO.
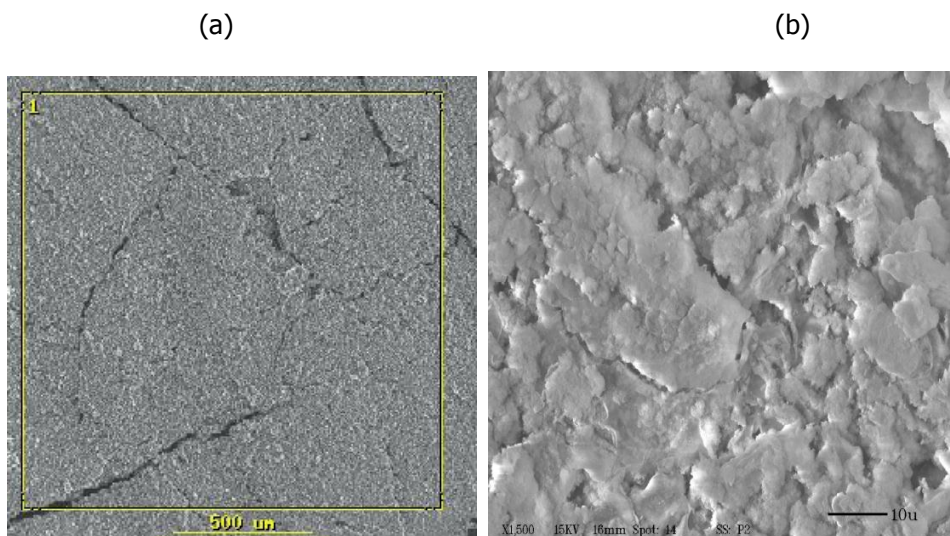
Figure 60. (a) Residue of 10% Silane (aminopropyltrimethoxy silane) modified glycidyl carbamate resin with 30% PVC and crosslinker Epicure 3164 observed from EDAX after TGA at 800 °C. (b) High magnification image of the same sample

(a) (b)
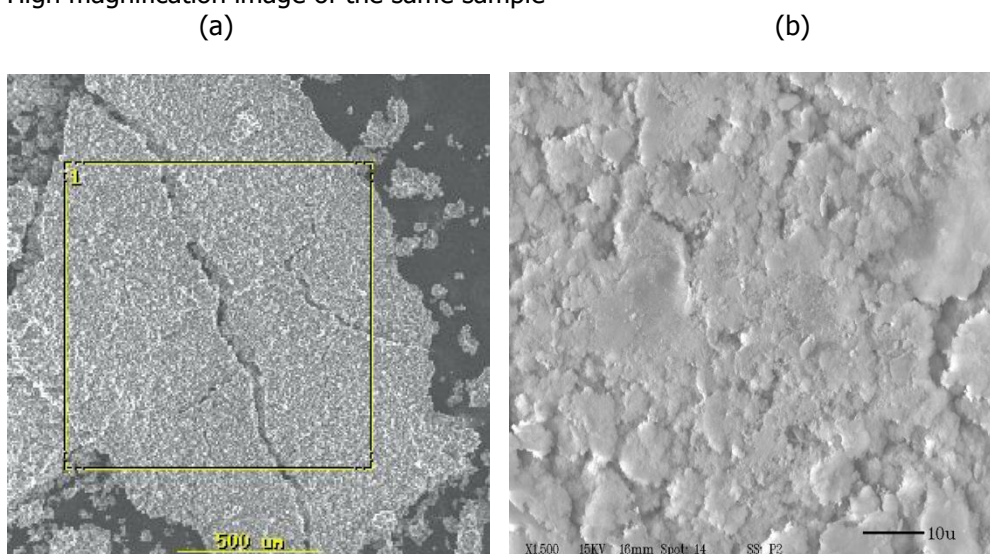


Figure 61. (a) Residue of 10% Silane (aminopropyltrimethoxy silane) modified glycidyl carbamate resin with 40% PVC and crosslinker Epicure 3164 observed from EDAX after TGA at 800 °C. (b) High magnification image of the same sample

*XRay Photolectron Spectroscopy*

To further confirm the composition of the residue a sample (30% PVC) coated on an Al2024 substrate was subjected to an indirect flame. The residue of both the intact material and the thermally degraded materials were analyzed using XPS. The XPS findings are depicted in Figure 64.
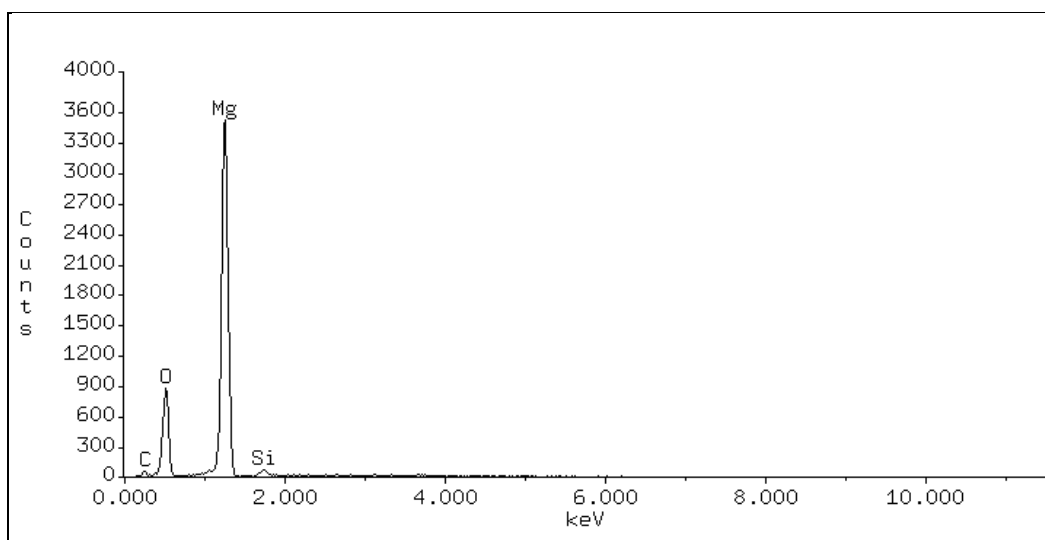
Figure 62.  Scan from EDAX showing the elemental composition of the residue @ 800°C from TGA 10% silane modified glycidyl carbamate resin with 30% PVC and crosslinker Epicure 3164 sample
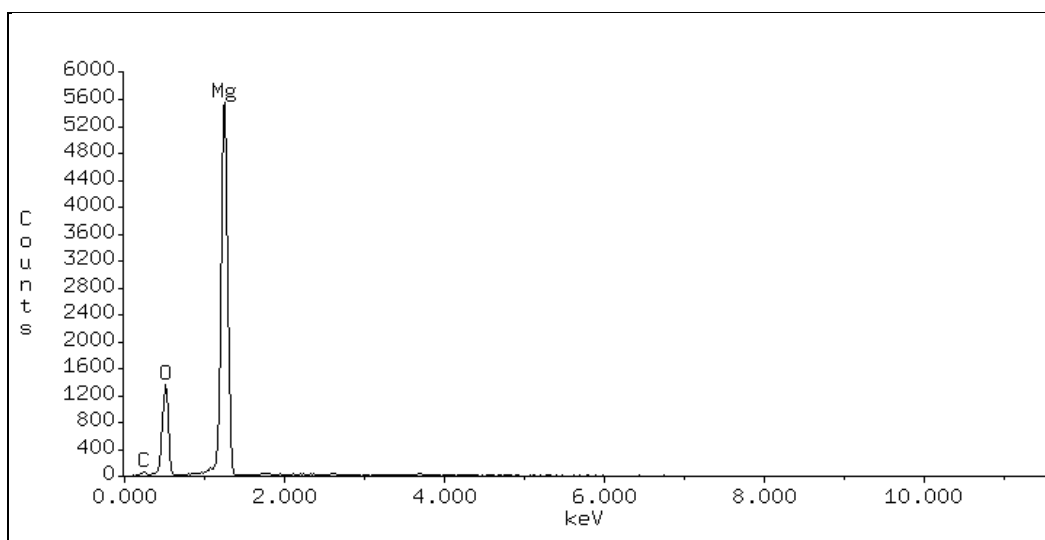


Figure 63. Scan from EDAX showing the elemental composition of the residue at 800°C from TGA 10% silane modified glycidyl carbamate resin with 40% PVC and crosslinker Epicure 3164 sample

In the Mg 2p spectrum obtained with deconvolution from XPS, two distinct signals were obtained before flame exposure corresponding to metallic magnesium and oxidized magnesium. After exposure to the indirect flame, a single signal was obtained corresponding to oxidized magnesium. This provides further confirmation that the material degrades into a MgO residue.

103
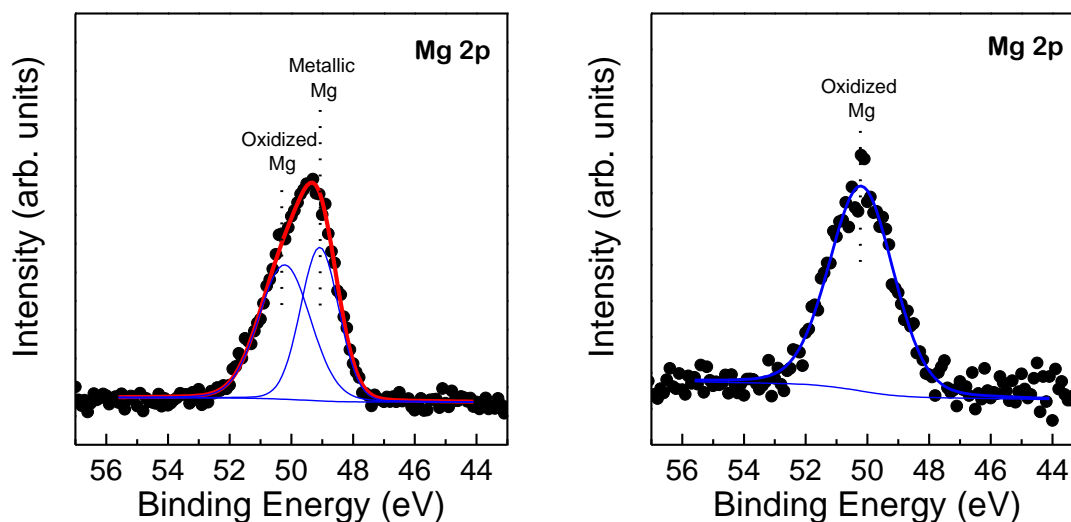
Figure 64. Deconvoluted XPS spectrum before and after indirect flame exposure of samples

This is an important finding from the perspective of coating properties. Mg-rich primers have been shown to exhibit outstanding corrosion protection properties. The thermal stability attribute of the coating system can further increase the range of applications for the system. For example these coatings can be potentially developed to be flame resistant systems in addition to its established corrosion protection properties.

## Conclusions

Silane-modified glycidyl carbamate resins were evaluated as a potential binder for magnesium-rich primer system. It was found to be a promising system in a screening study. However, in addition to the regular coating properties, an unexpected finding was the excellent thermal stability of the material at high temperatures. This finding has a potential to significantly increase the scope of application for this material especially in the areas of high temperature applications or as a potential anti-flammable material.

## Acknowledgements

The authors would like to thank Mark Hatzenbeller for the assistance in the coating application. We would also like to thank Scott Payne of the USDA microscopy laboratory at NDSU for characterization with EDAX and Jinhai Wang of the department of Coatings and Polymeric Materials at NDSU for characterization with XPS.

## References

[1] M. E. Nanna, G. P. Bierwagen, J. Coatings Technology Research, 1 (2004) 69-80

[2] D. Battocchi, A. M. Simões, D. E. Tallman, G. P. Bierwagen, Corrosion Science (2006), 48(5), 1292-1306

[3] P. A. Edwards; G. Striemer, D.C. Webster, JCT Research (2005), 2(7), 517-527

CHAPTER 8. MODELING OF ELECTROCHEMICAL IMPEDANCE DATA OF A MG-RICH PRIMER

Kerry N. Allahar,[1] Dante Battocchi,[1] Mark E. Orazem,[2] Gordon P. Bierwagen,[1] Dennis E. Tallman[1]

Abstract

The application of Mg-rich primers (MRPs) for the protection of aluminum structures represents an attractive alternate to the environmentally unfriendly Cr-rich primers that are presently used.  The protective modes of MRPs are similar to those of Zn-rich primers (ZRPs) on steel and include cathodic protection driven by the more active Mg particles compared to the Al substrate, and a barrier-type protection due to the insulation of the substrate from the environment. Interpretation of ZRP EIS data has been accomplished using a transmission-line model that accounted for the contact impedance between the zinc particles, the impedance associated with the zinc dissolution, and the percolation resistance of the coating. EIS experiments results are presented here for a MRP on a gold substrate under immersion in dilute Harrison's solution.

The data was analyzed using the measurement model technique to determine the consistency with respect to Kramer-Kronig relationships. The transmission-line model was used to analyze the data to demonstrate its applicability for analyzing the protection afforded by the MRP. Gold was used as a noble substrate and to promote the electromotive degradation of the MRP as the mixed potential of a MPR/gold system was more positive than that of a MRP/Al system.

[1] NDSU, Department of Coatings and Polymeric Materials, Fargo, ND 58105-5376, USA

[2] University of Florida, Department of Chemical Engineering,
  Gainesville, FL 32611, USA.

Introduction

Available commercially, non-chromate inhibitor pigments have been shown to be much less effective in corrosion protection as compared to the industrial standard of $SrCrO_4$. A non-chromate pigment has been reported to perform as effective as $SrCrO_4$ on Alodine 1200 treated AA 2024-T3.[1] The use of Alodine does expose the substrate to chromates and as such the influence of chromate cannot be discounted. The application of Mg-rich primers (MRPs) for the protection of aluminum structures has been demonstrated by Bierwagen and co-workers and represent an attractive alternate to the environmentally unfriendly Cr-rich primers that are presently used for such protection.[2-6] This system does not require an Alodine pre-treatment and represents a Cr-free system.

The protective modes of MRPs include cathodic protection driven by the more active Mg particles compared to the Al substrate and a barrier-type protection due to the insulation of the substrate from the environment by products of the hydroxide and hydroxy carbonate species of Mg that fill in pores and voids.[3,7,8] The behavior of the MRPs on Al substrate has been characterized using open circuit potential evolution, potentiodynamic polarization, and electrochemical impedance spectroscopy (EIS), scanning vibrating electrode technique (SVET) and scanning electrochemical microscopy (SECM).[2-6] Interpretation of the EIS data has been limited to two and three time-constant equivalent circuit models where parameters attributed to coating resistance and charge-transfer resistance were observed to reduce with time immersed in 0.1% wt. NaCl.[3]

The protective modes of MRPs are similar to those that have been associated with Zn-rich primers (ZRPs).[3,4] The cathodic and barrier-type protection provided by ZRPs for steel substrates have been extensively investigated by electrochemical methods.[9-18] Early interpretation of EIS data was accomplished using Randles type circuits[9-11] but recently the transmission-line model has been shown to be applicable to ZRPs.[13,14] This model includes parameters that were attributed to the contact impedance between the zinc particles, the impedance associated with

the zinc dissolution, and the percolation resistance of the coating. An extended transmission-line model has also been presented that accounted for the oxygen reduction on the zinc particles at the outermost part of the coating.[13]

Experiments were conducted to gather EIS data associated with the evolution of the electrochemical behavior of MRPs on a gold substrate exposed to immersion in dilute Harrison's solution. The objective of this work was to determine the applicability of the transmission-line model for characterizing EIS data of MRPs. The EIS data obtained in the 1 mHz-100 kHz frequency range was shown to be consistent with Kramers-Kronig relationships using the measurement model technique that was developed by Orazem and co-workers.[19-23] The transmission-line model was shown to be applicable to a 1 mHz-10 kHz frequency range for the MRP investigated. The evolutions of the contact impedance, dissolution impedance, and percolation resistance demonstrated the use of the transmission-line model for analyzing the protection afforded by the MRP and demonstrate the similarity between the protective modes of MRPs and ZRPs.

## Experimental

The MRP primer was applied unto a gold substrate that consisted of sputtered gold on a silica disk. The MRP coating consisted of a 10 $\mu$m average sized Mg particulate in a two-component epoxy of Epon resin 828 and Encamide 3164 that was supplied by Resolution Performance Products, Houston TX. The Mg particulate was supplied by Ecka-granules of America, Louisville KY, and was covered by a thin layer of MgO that limited its reactivity.[2] The dispersion of the Mg particles was aided by an anti-settling agent.[2] The coating was formulated at 45% pigment volume concentration that was approximately equal to the critical pigment volume concentration.[2] The primer was applied using a compressed air spray gun to a thickness of approximately 50 $\mu$m. A drying period in excess of three days was used.

The experimental apparatus included a perspex cylinder cell that exposed a 7.07 cm$^2$ area of the primer. The cell was clamped to the coating with an O-ring housed between cell and

coating that prevented leakage. Three-probe electrochemical measurements were performed with the gold substrate, a saturated calomel electrode and an approximate 1 $cm^2$ Pt mesh as the working, reference, and counter electrodes, respectively. The electrolyte was diluted Harrison's Solution (DHS) which comprised of 0.35 wt.% $(NH_4)_2SO_4$ and 0.05 wt% NaCl in distilled water. A Gamry FAS2 potentiostat was used in conjunction with EIS300 software to conduct the experiments with both potentiostat and software supplied by Gamry Instruments Inc, PA. EIS data were collected for the 100 kHz to 1 mHz frequency range with a 10 mV(rms) amplitude at 10 points per decade. The experimental procedure involved monitoring the MRP under constant immersion in DHS by performing replicated EIS experiments daily.

## Results and Discussion

The evolution of the open circuit potential (OCP) is shown in Fig. 65 with the value and all potential values in the text referenced to the standard calomel reference. The OCP value for the Mg particulate was reported as −1.6 V[3] while the measured OCP value for the gold/silica substrate used was 0.5 V. The OCP value decreased from 0.55 V to −0.5 V within the first 15 minutes of immersion and remained at that value for the following 15 minutes. The OCP value increased from −0.5 V to −0.22 V over the first day and from −0.22 V to 0.05 V from day 1 to day 7.



Figure 65. OCP ($E_{oc}$) as a function of immersion time for MRP in diluted Harrison's solution
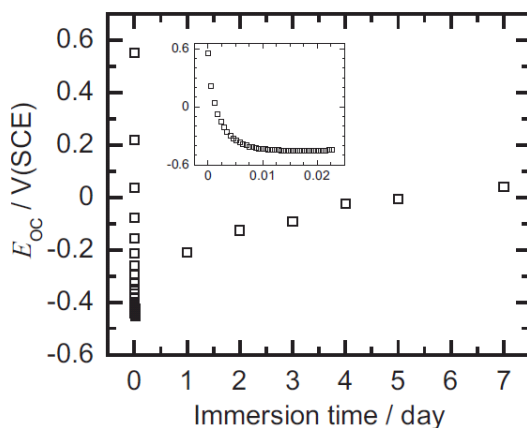
The initial decrease in OCP value during the first 15 minutes represented a period where the mixed potential between the Mg particles and the gold substrate developed. The mixed potential OCP value of −0.5 V, between 0.05 and −1.6 V, was maintained for less than a day as the OCP value of −0.22 V on day 1 indicated that the mixed potential was moving toward that of the gold substrate. The measured values evolved to the OCP of the gold substrate indicating the decrease in cathodic protection provided by the Mg particulate.

Experiments conducted for Mg-rich primers of AA 2-2024-T3 substrates under immersion in DHS have shown cathodic protection for 20 days.[24] The change in OCP from the mixed potential value of −0.5 V to the 0.05 V associated with the gold substrate took 7 days. The faster loss of the cathodic protection for the Mg-rich primer on the gold substrate was attributed to the larger potential difference between the mixed potential and the OCP value associated with Mg.

The EIS data obtained for days 1 through 5 and day 7 immersion times are shown in Fig. 66(a). The spectra associated with days 1 to 4 overlapped with high and low frequency features observable. The spectra for days 5 and 7 indicated that the low-frequency features became more dominant with time. The EIS data for three replicated scans designated *a*, *b*, and *c* on day 1 are shown in Fig. 66(b). The scans were taken sequentially approximately 20 minutes apart. The three scans overlapped and this demonstrated the reproducibility of the EIS data on a particular day.
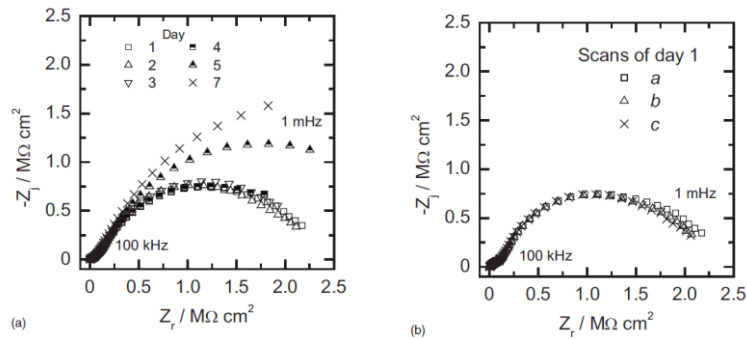


Figure 66. Impedance spectra for MRP immersed in diluted Harrison's solution. (a) The first spectra of a set of three sequential scans obtained daily. (b) Sequential scans obtained on day 1

*Measurement model analysis*

In this work the EIS data associated with a MRP was regressed to a transmission-line model which is an equivalent circuit model representative of the impedance of a particulate network.[13] The regression of EIS data associated with a coating to an equivalent circuit model is performed under the assumptions that the data is free of instrument artifacts due to non-stationary behavior, that the noise level in the data is acceptable, and that the weighting strategy is appropriate. Application of the measurement model technique can be used to qualify these assumptions by analysing the residual error between the measurement model impedance fit and the measured impedance data. The technique has been applied in literature to identify the contributions of systematic, bias, and stochastic errors to the residual error.[19]

The measurement model technique involves using a generalized Voigt model to analyze the error associated with replicated EIS data. The model is shown in Fig. 67 and consists of a series of Voigt elements comprising of a parallel arrangement of a resistor $R_k$ and capacitor $C_k$, in series with a resistor $R_0$ that represents the solution resistance. The characteristic time constant associated with a Voigt element is $\tau_k = R_k C_k$ and the impedance of the model can be expressed as[19]

$$Z = R_0 + \sum_{k=1}^{K} \frac{R_k}{1 + j\omega\tau_k} \qquad \text{(Equation 10)}$$
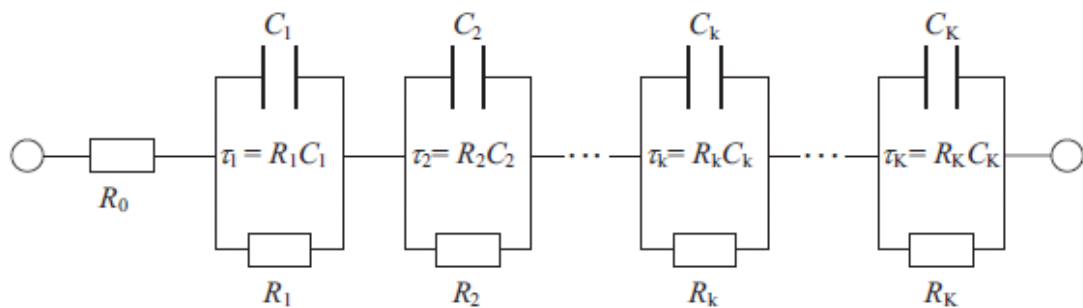


Figure 67. A schematic representation of a Voigt measurement model used by Agarwala et. al.[20, 21 ,22] The time constant for a given element is included

The Voigt measurement model is consistent with Kramers-Kronig relations, and the application of the technique can determine the internal consistency of the measured EIS data without need for explicit integration of the Kramers-Kronig relations.[21] The technique involves using a weighting strategy for the complex non-linear least squares regression that is based on the measured error structure associated with replicated EIS data.

*Technique*

The measurement model technique is demonstrated here using the replicated EIS data associated with day 1 that are shown in Fig. 66(b). The maximum number of elements that could be regressed to scans *a*, *b* and *c* was 12. There were good agreements between the fit of the measurement model and the data associated with the scans and an example of this agreement can be seen in Fig 68(a). The resistor and time constant values obtained for the regression using modulus weighting are given in Table 8. The resistance associated with the solution is also given. The parameters are arranged in order of increasing time constant with an error of $\pm\sigma$ included with each parameter. The $R$ and $\tau$ parameters for a given Voigt element were similar among the scans and indicated that there was no significant difference among the scans.
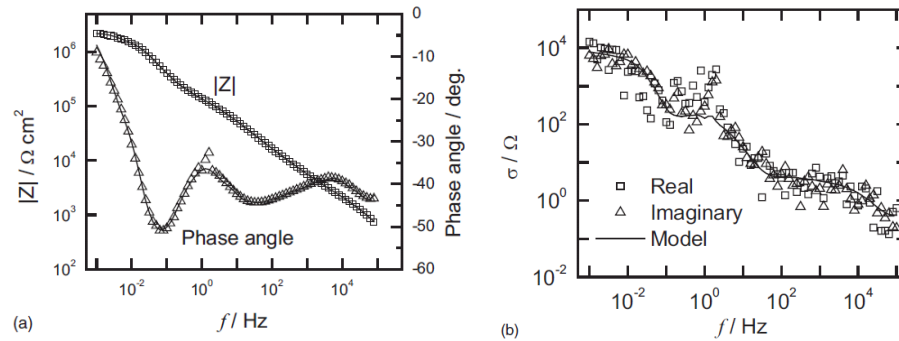


Figure 68. (a) Bode plot of impedance data for scan *a* of day 1 shown in Fig. 66(b). The superimposed lines on the data represent the 12 element Voigt measurement model that was regressed to the data using modulus weighting. (b) Standard deviation of real and imaginary parts of the impedance data associated the scans of day 1 shown in Fig. 66(b). The line through the data is a fit of the model given by equation to the data

The data shown in Table 8 was used to calculate the standard deviations of the real and imaginary parts as functions of frequency. The standard deviation that is calculated can be used

to calculate the standard deviation of the residual errors from which the standard deviation of the stochastic error can be identified.

Table 8. Model parameters for a fit to a 12 element Voigt measurement model for the impedance data associated with scans *a*, *b*, and *c* after 1 day of immersion

| Parameter | Scan *a* | Scan *b* | Scan *c* |
|---|---|---|---|
| $R_1$ ($\Omega$ cm$^2$) | $663 \pm 115$ | $646 \pm 113$ | $639 \pm 127$ |
| $\tau_1$ ($\mu$s) | $3.4 \pm 0.5$ | $3.4 \pm 0.5$ | $3.4 \pm 0.5$ |
| $R_2$ (k$\Omega$ cm$^2$) | $1.1 \pm 0.2$ | $1.0 \pm 0.2$ | $1.0 \pm 0.2$ |
| $\tau_2$ ($\mu$s) | $15 \pm 4$ | $15 \pm 4$ | $14 \pm 5$ |
| $R_3$ (k$\Omega$ cm$^2$) | $1.6 \pm 0.5$ | $1.5 \pm 0.5$ | $1.4 \pm 0.5$ |
| $\tau_3$ ($\mu$s) | $67 \pm 29$ | $64 \pm 27$ | $61 \pm 31$ |
| $R_4$ (k$\Omega$ cm$^2$) | $3.0 \pm 1.1$ | $2.9 \pm 1.0$ | $2.8 \pm 0.9$ |
| $\tau_4$ (ms) | $0.28 \pm 0.13$ | $0.26 \pm 0.13$ | $0.24 \pm 0.13$ |
| $R_5$ (k$\Omega$ cm$^2$) | $5.8 \pm 1.9$ | $5.5 \pm 1.8$ | $5.4 \pm 1.7$ |
| $\tau_5$ (ms) | $1.1 \pm 0.5$ | $1.1 \pm 0.5$ | $1.0 \pm 0.5$ |
| $R_6$ (k$\Omega$ cm$^2$) | $12 \pm 4$ | $12 \pm 4$ | $11 \pm 3$ |
| $\tau_6$ (ms) | $4.6 \pm 2.0$ | $4.3 \pm 2.0$ | $4.2 \pm 1.8$ |
| $R_7$ (k$\Omega$ cm$^2$) | $31 \pm 5$ | $28 \pm 5$ | $28 \pm 5$ |
| $\tau_7$ (ms) | $19 \pm 6$ | $17 \pm 5$ | $17 \pm 5$ |
| $R_8$ (k$\Omega$ cm$^2$) | $61 \pm 6$ | $57 \pm 6$ | $55 \pm 5$ |
| $\tau_8$ (ms) | $81 \pm 15$ | $71 \pm 13$ | $75 \pm 14$ |
| $R_9$ (k$\Omega$ cm$^2$) | $79 \pm 10$ | $77 \pm 8$ | $74 \pm 9$ |
| $\tau_9$ (s) | $0.52 \pm 0.11$ | $0.46 \pm 0.08$ | $0.49 \pm 0.10$ |
| $R_{10}$ (M$\Omega$ cm$^2$) | $0.41 \pm 0.17$ | $0.37 \pm 0.14$ | $0.38 \pm 0.14$ |
| $\tau_{10}$ (s) | $4.1 \pm 1.0$ | $3.8 \pm 0.8$ | $4.0 \pm 0.9$ |
| $R_{11}$ (M$\Omega$ cm$^2$) | $1.0 \pm 0.1$ | $1.1 \pm 0.1$ | $1.1 \pm 0.1$ |
| $\tau_{11}$ (s) | $12 \pm 2$ | $12 \pm 2$ | $12 \pm 2$ |
| $R_{12}$ (M$\Omega$ cm$^2$) | $0.65 \pm 0.08$ | $0.60 \pm 0.06$ | $0.55 \pm 0.06$ |
| $\tau_{12}$ (s) | $67 \pm 11$ | $70 \pm 10$ | $78 \pm 14$ |
| $R_{sol}$ ($\Omega$ cm$^2$) | $356 \pm 15$ | $352 \pm 14$ | $351 \pm 15$ |

This procedure is based on the assumptions that the model parameters account for systematic differences with the systematic errors associated with lack of fit, non-stationary

behavior and instrument artifacts being unchanged from one scan to another. The standard deviations of the real and imaginary parts as functions of frequency are shown in Fig 68(b). The expression

$$\sigma_{Z_r} = \sigma_{Z_j} = \alpha |Z_j| + \beta |Z_r| + \gamma \frac{|Z|^2}{R_q} + \delta \qquad \text{(Equation 11)}$$

was used to model the standard deviation where $R_q$ is the current measuring resistor used in the experiment, and $\alpha$, $\beta$, $\gamma$, $\delta$ are constants to be determined by regressing the real and imaginary parts to the expression.[19] The values of −0.0040, 0.0041, 0.0005, and 1.68 were obtained for $\alpha$, $\beta$, $\gamma$, and $\delta$, respectively, and the value of $10^5$ Ω was used for $R_q$.

*Consistency with Kramers-Kronig relations*

The consistency of the impedance data to the Kramers-Kronig relations was performed by fitting the Voigt measurement model to the data using the error structure as the weighting strategy. The approach suggested by Orazem is to fit the model using the maximum number of Voigt elements to the imaginary part of the data.[19] A 12-element Voigt model was fit to the imaginary part of the EIS data associated with scan *a* of day 1. The measurement model values and data are shown in Figure 69 together with dashed lines that represent the 95.4 % confidence interval for the model obtained by Monte Carlo simulation using the confidence interval associated with the estimated parameters.

The parameters obtained from the fitting of the imaginary part were used to predict the real part. There was agreement between the fit and measured data for the imaginary part as expected while there was also agreement between the predicted and measured real parts. The width of the 95.5% confidence interval band at the low frequency end for both the imaginary and real parts was representative of the greater uncertainty with the parameters associated with the low frequency end as compared with the high frequency end.

114

Figure 69. Results of the fit of a 12-element Voigt measurement model (MM model) to the impedance data associated with the scan *a* of day 1 shown in Fig. 2b. The error structure was used as the weighting strategy. The experimental data and model are represented by open symbols and a superimposed solid line, respectively. The dashed line represents the 95.4% confidence interval for the model obtained by Monte Carlo simulation using the calculated confidence interval for the estimated parameters. (a) fit to the imaginary part; (b) prediction of the real part

The relative residual error between the fitted and measured imaginary data and the relative residual error between the predicted and measured real data are shown in Figure 70. The relative imaginary residual error was within the 95.4% confidence interval, which demonstrated the confidence associated with the regression of the imaginary measured impedance to the 12-element Voigt measurement model. The relative real imaginary error associated with the highest frequency at 100 kHz was not within the 95.4% confidence interval and was attributed to start-up transients associated with the experiment.[17] Two points of the predicted real values were outside of the 95.4% confidence interval at frequencies close to 1 Hz.

The Bode phase plot of the impedance data for scan *a* shown in Fig. 68(a) indicated that the measurements at these frequencies were not consistent with the trend in the measurements before and after these frequencies. Although these points were inconsistent with the Kramer-Kronig relations they were not excluded from the spectra during further analysis as the technique has only been used in literature to truncate data at high and low frequency ends.

*Transmission Line Model*

The transmission line model has been shown to be applicable to ZRPs and a schematic diagram of the model used is shown in Fig. 71.[13,14]

115

(a) (b)

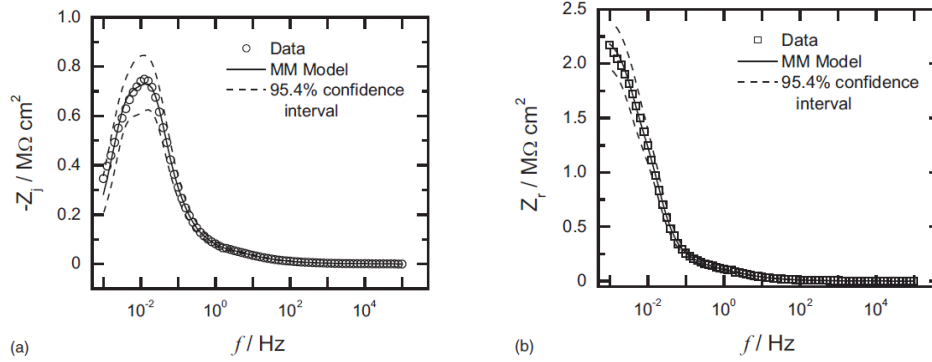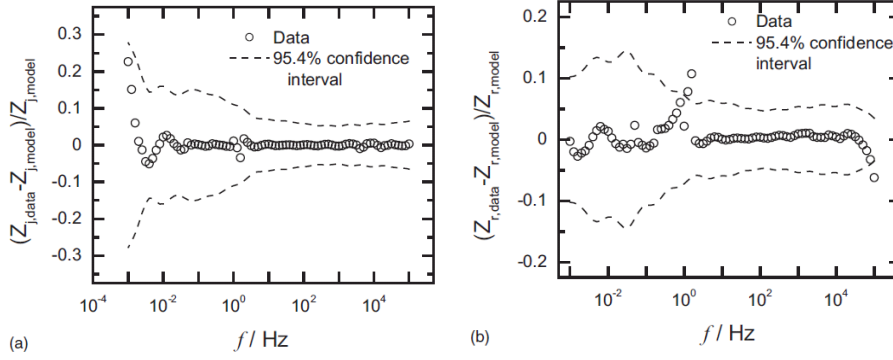Figure 70. Relative residual errors for the fit of a 12-element Voigt measurement model to the impedance data associated with scan *a* of day 1 shown in Fig. 2b. The experimental data are represented by open symbols and the dashed lines represent the 95.4% confidence interval for the model obtained by Monte Carlo simulation using the calculated confidence interval for the estimated parameters. (a) Imaginary part and (b) Real part

The ZRP was viewed as zinc particles distributed in a poorly conducting polymer matrix with a behavior as a porous electrode.[13] This provided justification for using the model as the transmission line model is applicable to a porous electrode. However, the circuit that is shown in Fig. 71 includes a contact impedance between the particles. The inclusion of this contact impedance is attributed to Gabrielli who applied it to analyze the EIS data associated with electroactive fluidized beds.[25,26]
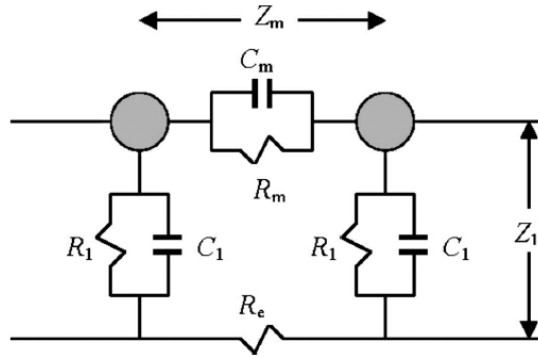


Figure 71. Schematic representation of the transmission-line model given by Abreu et. al[13]

The circuit shown in Fig. 71 includes the contact impedance $Z_m$ with

$$Z_m = \frac{R_m}{1+\left(j\omega R_m C_m\right)^{\alpha_m}}$$

(Equation 12)

where $R_m$ and $C_m$ are resistance and capacitance components and $\alpha_m$ is included for the dispersion of the time-constants associated with the contact impedance.

116

The impedance between the particles and the electrolyte in the pores for a small segment is given by $Z_1$ with

$$Z_1 = \frac{R_1}{1 + (j\omega R_1 C_1)^{\alpha_1}}$$

(Equation 13)

where $R_1$ and $C_1$ are the faradaic resistance and double layer capacitance associated with the particle dissolution. The parameter $\alpha_1$ is included to account for dispersions of the time-constants associated with the dissolution process. The inclusion of the $\alpha_m$ and $\alpha_1$ parameters was done to avoid complications arising from non-uniform transmission-line behavior.[13]

The impedance of a uniform transmission-line is given by

$$Z = \frac{Z_m R_e L}{Z_m + R_e} + \frac{(Z_m^2 + R_e^2)\cosh(L\sqrt{\gamma}) + 2Z_m R_e}{(Z_m + R_e)\sqrt{\gamma}\sinh(L\sqrt{\gamma})}$$

(Equation 14)

where $L$ is the thickness of the coating, $R_e$ the electrolyte resistance in the pores of the coating and $\gamma$ given by

$$\gamma = \frac{Z_m + R_e}{Z_1}$$

(Equation 15)

The expression given by Equation 10 was regressed to the EIS data of the MRP using an algorithm developed by Nelder and Mead that is based on the Downhill-Simplex method.[27]

A modulus weighting strategy was used in the minimization of the impedance data. The results for the regression of the transmission line model to the data of scan $a$ of day 1 are shown in Figure 72 for the frequency range of 1 mHz-100 kHz. There was agreement between the modulus of data and model as shown by the Bode modulus plot. It was observed from the Bode phase angle plot that the data and model were in agreement for the 1mHz-10 Hz frequency range but at frequencies greater that 10 Hz the model was not in agreement with the data.

This dissimilarity for frequencies greater than 10 Hz was also observed from fits of the model to the impedance data associated with days 2 through 4. Observation of the phase angle experimental data in Figure 72(b) indicated that there was an increase in phase angle from 100 Hz to 5 kHz followed by a decreased from 5 kHz to 100 kHz. The fit of the model for the 1 mHz-

100 kHz range exhibited an increase in phase angle for frequencies greater that 100 Hz without any decrease at higher frequencies. The results of the fit of model to the data for the frequency range 1 mHz-10 kHz is also shown Figure 72. There was agreement between the model and data for this frequency range.
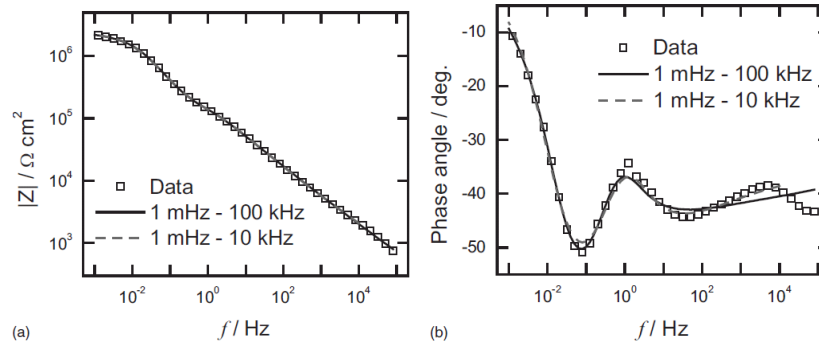


Figure 72. Bode plots of impedance data of scan *a* of day 1 with superimposed lines for the fit of the transmission-line model for frequency ranges 1 mHz-10 kHz and 1 mHz-100 kHz. (a) Magnitude and (b) phase angle

The parameters from the fit of the model to the data for the frequency ranges 1 mHz-100 kHz and 1 mHz-10 kHz are given in Table 9. There were no significant differences between the values associated with the two frequency ranges for a given parameter. The similarity between the parameters was attributed to the transmission-line model of Equation 11 being adequate for the 1 mHz-10 kHz range. As seen in Fig. 72(b) the model was suitable up to 10 kHz after which the data exhibited a decrease in phase angle with frequency which was not accommodated by the model as shown by the fit for the 1 mHz-100 kHz range.

The experimental data associated with the frequency range 10 kHz-100 kHz was shown to be consistent with the Kramers-Kronig relations. The influence of truncating the 10 data points at the high frequency end was determined by fitting a measurement model to the data of scan *a* of day 1 for the frequency range of 1 mHz-10 kHz. A Voigt model of 11 elements maximum was fit to the data in this frequency range. The value of the resistance as a function of time constant for the Voigt models used for the 1 mHz-100 kHz and 1 mHz-10 kHz ranges are given in Figure 73.

Table 9. Parameters associated with the regression of the transmission-line model to the impedance data of scan *a* of day 1 for the frequency ranges 1 mHz-100 kHz and 1 mHz-10 kHz

| Frequency range | $R_m$ (G·xcm) | $C_m$ (nFxcm$^{-1}$) | $\cdot_m$ | $R_1$ (k· cm$^{-3}$) | $C_1$ (·F cm) | $\cdot_1$ | $R_e$ (M· cm) |
|---|---|---|---|---|---|---|---|
| 1 mHz -100 kHz | 0.79 | 61 | 0.67 | 6.1 | 1670 | 0.87 | 59 |
| 1 mHz - 10 kHz | 0.92 | 22 | 0.72 | 5.1 | 2650 | 0.81 | 45 |

There were 12 time constants associated with the 1 mHz-100 kHz and only 9 were

common with the 11 time constants of the 1 mHz-10 kHz range.
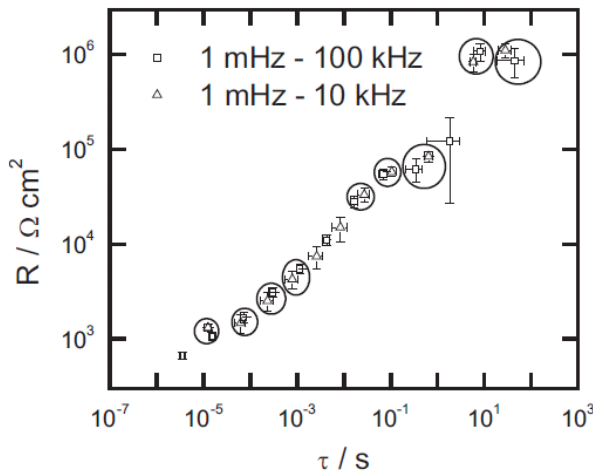


Figure 73. Distribution of the time constants for the fits of measurement model to the impedance data of scan *a* of day 1. A 12-element Voigt model was used to fit the data in the frequency range of 1 mHz-100 kHz and a 11-element Voigt model was used to fit the data in the frequency range of 1 mHz-10 kHz. The error bars correspond to ±σ and were calculated using a linear approximation.  Nine circles/ovals are used to identify the nine time constants that were similar between the fit results

This demonstrated that the truncated data set of 1 mHz-10 kHz range did not contain all

the information as the 1mHz-100 kHz data set. It was concluded that the data in the range 10

kHz-100 kHz, which was Kramers-Kronig consistent, contained information for processes with

small time constants that could not be resolved from the transmission-line model given by

Equation 11. It would be necessary to adjust the model to accommodate data in the 10 kHz-100

kHz range.

A modification to the transmission line model given by Equation 11 was used by Abreu

et. al. to model the EIS data associated with a ZRP where the OCP was above that of the OCP

associated with the steel substrate.[13] This was based on the assumption that the zinc particles in the upper part of the film were isolated from the substrate such that the cathodic oxygen reduction reaction took place on the particles in the upper part. This assumption was supported by the larger distribution of time constants that was observed.

The type of modification used by Abreu et. al. may not be suitable to address the inability of the transmission line model to fit the EIS data of the MRP in the 10 kHz-100 kHz range. It may be necessary to incorporate the influence of a salt film that precipitates on the Mg particles into the transmission line model. This is supported by the observation of porous magnesium oxides in scribed regions of an MRP on an aluminum substrate.[3]

The parameters for the fit of the transmission-line model to the impedance data associated with days 1 through 5 are shown in Figures 74 and 75 with the parameters given as functions of the open circuit potential. There was a poor fit obtained when the transmission line model was regressed to the data associated with day 7.

The open circuit potential increased monotonically with time. There was little change observed in the resistance and capacitance parameters over the first 4 days up to an open circuit potential of −0.025 V(SCE). There was a noticeable drop in contact resistance $R_m$ and a smaller drop in electrolyte resistance $R_e$ from day 4 to 5 at which the open circuit potential was close to a 0 V(SCE). The interfacial resistance $R_1$ had a small increase for this period.

The drop in contact resistance coupled with the open circuit potential moving toward a more positive value was attributed to the products of the Mg dissolution between Mg particles providing conductivity thereby reducing the contact resistance while at the same time the level of galvanic protection would be decreased. The small increase in interfacial resistance was consistent with the reduction in the active surface area of the Mg particles as they are being consumed. Changes in the values of $\alpha_m$ and $\alpha_1$ were observed in Figure 75(b). The departure from unity for these parameters is an indication of the dispersion in the time constants of the processes involved. The larger change in the $\alpha_m$ parameter as compared to the $\alpha_1$ parameter

120

indicated that there were more changes occurring in the processes contributing to the contact

impedance as those contributing to the interfacial impedance.
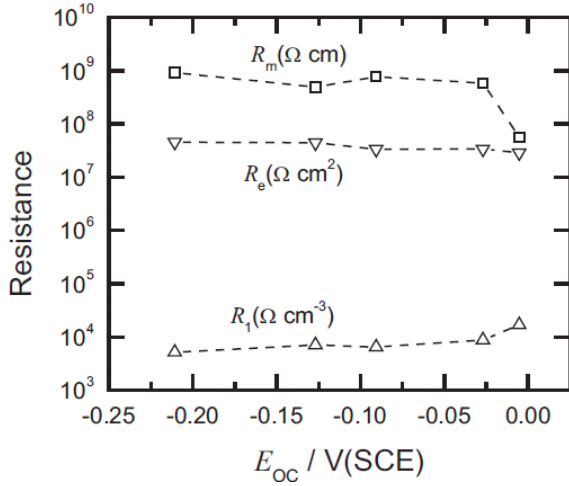


Figure 74. Resistance values of the contact impedance, interfacial impedance and the electrolyte resistance parameters obtained from the fit of the transmission-line model to the daily impedance data shown in Figure 66(a) as functions of the open circuit potential
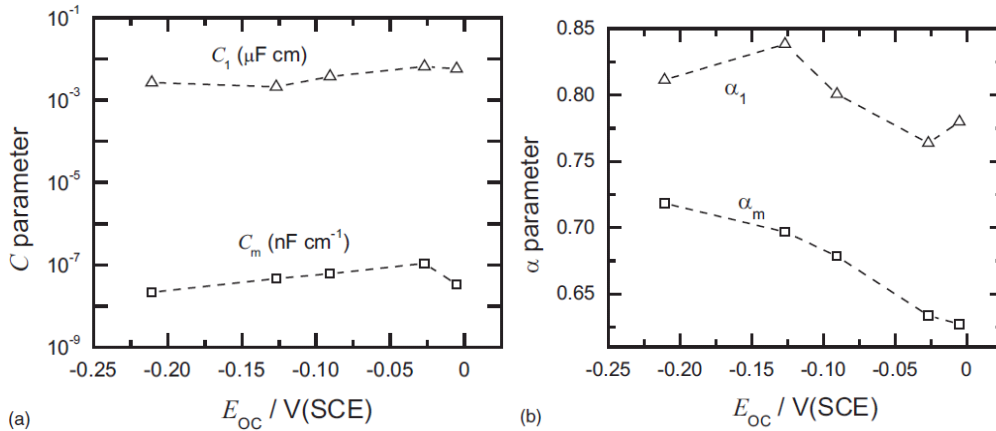


Figure 75. Parameter values of the contact impedance, interfacial impedance and the electrolyte resistance parameters obtained from the fit of the transmission-line model to the daily impedance data shown in Figure 66(a) as functions of the open circuit potential. (a) Capacitance parameters and (b) parameters associated with the dispersion of the contact and interfacial impedance

## Conclusions

Experimental EIS data of a MRP on an inert gold substrate was analyzed for consistency

with Kramers-Kronig relations and applicability for use with a transmission- line model.  The

Kramers-Kronig consistency was determined with the use of the measurement model technique and its application yielded that the data in the frequency range of 1 mHz-100 kHz was Kramers-Kronig consistent.

The reproducibility of the data at the low frequency end of 1mHz-10 mHz indicated that the processes with the large time constants were stable.  The transmission-line model reported by Abreu et. al. was shown to be applicable for the 1 mHz-10 kHz frequency range.[13] The data of the 10 kHz-100 kHz range was consistent with the Kramers-Kronig relations and was not resolvable by the transmission-line model used.  Additional features may be required to be included in the transmission-line model that can resolve these processes at the high frequency end of the spectra.

The model in its present form was applicable to determine the contributions of the contact and interfacial impedance, and the electrolyte resistance of a MRP on a gold substrate for the period where the potential changed from a mixed potential value to a value more associated with the gold substrate.

## Acknowledgements

## References

[1]  J. Sinko, Prog. Org. Coat., 42, 267 (2001).

[2]  M.E. Nanna, G.P. Bierwagen, J. Coating Technol. Res., 1, 69 (2004).

[3]  D. Battocchi, A.M. Simoes, D.E. Tallman, G.P. Bierwagen, Corros. Sci., 48, 1292 (2006).

[4]  D. Battocchi, A.M. Simoes, D.E. Tallman, G.P. Bierwagen, Corros. Sci., 48, 2226 (2006).

[5]  G. Bierwagen, D. Battocchi, A. Simoes, A. Stamness, D. Tallman, Prog. Org. Coat., 59, 172 (2007).

[6] A.M. Simoes, D. Battocchi, D.E. Tallman, G.P. Bierwagen, Corros. Sci., (2007). 49, 3838 (2007).

[7] N.C. Hosking, M.A. Strom, P.H. Shipway, C.D. Rudd, Corros. Sci., (2007), 49, 3669 (2007).

[8] M. Jonsson, D. Persson, D. Thierry, Corros. Sci., 49, 1540 (2007).

[9] S. Feliu, R. Barajas, J.M. Bastidas, M. Morcillo, J. Coat. Technol., 61, 775 (1989).

[10] S. Feliu, R. Barajas, J.M. Bastidas, M. Morcillo, J. Coat. Technol., 61, 71 (1989).

[11] C.A. Gervasi, A.R. Di Sarli, E. Cavalcanti, O. Ferraz, E.C. Ducharsky, S.G. Real, J.R. Vilche, Corros. Sci., 36, 1963 (1994).

[12] S.G. Real, A.C. Elias, J.R. Vilche, C.A. Gervasi, A. di Sarli, Electrochim. Acta, 38, 2029 (1993).

[13] C.M. Abreu, M. Izquierdo, M. Keddam, X.R. Novoa, H. Takenouti, Electrochim. Acta, 41, 2405 (1996).

[14] C.M. Abreu, M. Izquierdo, P. Merino, X.R. Novoa, C. Perez, Corrosion, 55, 1173 (1999).

[15] D. Pereira, J.D. Scantlebury, M.G.S. Ferriera, E. Almedia, Corros. Sci., 30, 1135 (1990).

[16] S.E. Faidi, J.D. Scantlebury, P. Bullivant, N.T. Whittle, R. Savin, Corros. Sci., 35, 1319 (1993).

[17] X.R. Novoa, M. Izquierdo, P. Merino, L. Espada, Mater. Sci. Forum, 44, 223 (1989).

[18] M. Izquierdo, X.R. Novoa, G. Pena, L. Espada, Mater. Sci. Forum, 111, 257 (1992).

[19] M.E. Orazem, J. Electroanalytical Chem., 572, 317 (2004).

[20] P. Agarwal, M.E. Orazem, L.H. Garcia-Rubio, J. Electrochem. Soc., 139, 1917 (1992).

[21] P. Agarwal, O.D. Crisalle, M.E. Orazem, L.H. Garcia-Rubio, J. Electrochem. Soc., 142, 4149 (1995).

[22] P. Agarwal, M.E. Orazem, L.H. Garcia-Rubio, J. Electrochem. Soc., 142, 4159 (1995).

[23] K.N. Allahar, D.P. Butt, M.E. Orazem, H.A. Chin, G. Danko, W. Ogden, R. Yungk, Electrochim. Acta., 51, 1497 (2006).

[24] K.N. Allahar, D. Battocchi, G.P. Bierwagen, D.E. Tallman, in preparation.

[25] C. Gabrielli, F. Huet, A. Sahar, G. Valentin, J. App. Electro., 24, 481 (1994).

[26] C. Gabrielli, F. Huet, A. Sahar, G. Valentin, J. App. Electro., 22, 801 (1992).

[27] W.H. Press, S.A. Teukolsky, W.T. Vetterling, and B.P. Flannery, Numerical Recipes in Fortran 77, 2nd edition (Cambridge UK: Press Syndicate of the University of Cambridge, 1992).

CHAPTER 9. SUMMARY AND CONCLUSIONS

The previous chapters, based on published manuscripts, present experimental evidence of the development and testing of one of the few materials that can be considered a valuable candidate for replacing Chromium VI (CrVI) as the active ingredient in corrosion protective coatings for Al. Chromium was used as ingredient in paints and coatings in a number of industrial applications and now is heavily regulated and there are waivers in place for its use in the aerospace market, until a suitable replacement can be brought to light.

With the objective to demonstrate that the Mg rich primer is indeed a suitable replacement, our work in the laboratory was focused on demonstrating the behavior and the efficacy of this new material in the protection of Al and its alloys used in aerospace applications.

The mechanism of cathodic protection, one of the bases of our primer, is very common for the protection of steels, but it was believed not possible for Al and its alloys.

To overcome this common belief, the first manuscripts were aimed to demonstrate the basic principles that the Mg-rich primer is based on. The published manuscripts have been cited by many other groups, as our work is the first documented evidence that the mechanism of cathodic protection can be used for Al and its alloys. The number of the citation of each chapter is reported in Table 1.

We used electrochemical techniques to study and demonstrate the behavior of the Mg-rich primer and these techniques allowed us to quantify numerically the effect of the protective primer on the Al substrate. Open circuit potential and Electrochemical Impedance Spectroscopy were used and it was found that the effect of Mg is based upon two different mechanisms, each one associated with one stage.

First, Mg polarizes cathodically the aluminium substrate, shifting its potential below the pitting corrosion potential and therefore protecting it from corrosion. Second, there is a barrier effect, likely due to the formation of a porous layer during Mg reaction with Al

substrate. Also, the typically high dissolution rate of Mg is significantly decreased by its incorporation in the polymer.

Subsequently, we combined the data from Open Circuit Potential (OCP), Electrochemical Impedance Spectroscopy (EIS), Scanning Vibrating Electrode Technique (SVET), Scanning Electron Microscopy (SEM) and Energy Dispersive Spectroscopy (EDAX), to further demonstrate the cathodic protection mechanism.

SVET shows that in damaged areas of the Mg rich primer the bare exposed substrate becomes cathodically protected shortly after exposure to electrolyte. SEM and EDAX were used to identify the oxidation products of the Mg particles after exposure of MRP in damaged areas. Open Circuit Potential measurements showed that the Mg particles were electronically coupled to the Al alloy substrates, and by this connection the substrates were polarized to potentials that provided them cathodic protection.

One important feature of a protective system is not being specific toward a particular environment, and to study this aspect, two different solutions were used to study the corrosion behavior of AA2024 and AA7075 Al alloys. 0.1% NaCl was used to emulate a marine/costal environment and Dilute Harrison Solution (DHS) was used to simulate an industrial environment. It was shown that the change from 0.1% NaCl to Dilute Harrison Solution (DHS) affected the open circuit potential, the corrosion rates and the equivalent circuits of the systems studied. However, the Mg-rich primer maintained its protective ability to cathodically polarize the underlying substrate. The exposure to DHS caused a faster degradation, probably due to the presence of sulphates, but the sacrificial action of the primer remained the main protection mode.

Further development of this technology was focused on the composition of the metal pigment and it was demonstrated that Mg alloys could be used as active pigments instead of pure Mg; therefore the metal composition could be varied without sacrificing the protection ability. EIS results showed that the metal-rich primers with the Mg alloys as pigments had the mixed potentials between the OCPs of Mg alloys and the bare Al 2024 T3, indicating that the

125

Mg alloy pigments provided sacrificial protection to the Al alloy substrates. These investigations of the properties of the Mg alloys gave a good understanding of the effects of the particle size, the particle shape and the chemical composition on the particle packing efficiency, CPVC and electrochemical behaviour of the primer system, suggesting that pigments with smaller particle size and better controlled shape would result in a better primer system.

After the work dedicated to the metal pigments, the development was directed to the optimization of the binder system, and a two-component Mg-rich primer coating was developed that showed excellent corrosion protection of Al 2024 when used in conjunction with a polyurethane topcoat. The variables investigated were epoxy resin MW, curing agent functionality, epoxy/NH ratio, and Mg content. A number of techniques such as OCP measurement, EIS, B117 salt spray, pull-off adhesion, SEM, and EDX were used to study and evaluate corrosion protection. The optimized coating composition showed very good corrosion protection for 3,000 hours of B117 salt spray exposure.During the study of alterative polymers we evaluated a Silane-modified glycidyl carbamate resins as a potential binder for Mg-rich primer system. In addition to the regular coating properties, an unexpected finding was the excellent thermal stability of the material at high temperatures.

The last section of the scientific approach we followed for the primer development was that of data modeling. Experimental EIS data of a MRP on an inert gold substrate was analysed for consistency with Kramers-Kronig relations and applicability for use with a transmission- line model. The Kramers-Kronig consistency was determined with the use of the measurement model technique and its application determined that the data in the frequency range of 1 mHz-100 kHz was Kramers-Kronig consistent. The transmission-line model, was shown to be applicable for the 1 mHz-10 kHz frequency range. The data of the 10 kHz-100 kHz range was consistent with the Kramers-Kronig relations and was not resolvable by the transmission-line model used.

The model in its present form was applicable to determine the contributions of the contact and interfacial impedance, and the electrolyte resistance of a MRP on a gold substrate for the period where the potential changed from a mixed potential value to a value more associated with the gold substrate.

CHAPTER 10. FUTURE WORK

Several manuscripts have been generated from the study and the development of the Mg-rich primer but some basic research is still necessary to fully understand the behavior of this system when protecting the Al substrate. The last phase of the present work was somewhat directed to commercial development of the material. There are three main areas of interest that could be expanded with basic research studies:

1. Galvanic coupling: We used electrochemical means to monitor the behavior of the Mg-rich primer when applied onto Al alloys. Some attention could be dedicated to the electrical current that is passed between Mg and Al in presence of a corrosive environment. The monitoring of the current and other parameters during the galvanic coupling could be helpful to better understand the life time of the protective system. Knowing the minimum of the current needed from the Mg to keep the Al protected from corrosion could be correlated to the amount of Mg consumed in a time unit and therefore lifetime could be, maybe, assessed.

2. Oxidation products: some of the reaction products generated during the weathering of Al samples coated with Mg rich primer were identified, such as Mg oxides, hydroxides and Mg carbonates but there is space left for an analytical study of the differences of the reaction products generated during weathering in different environments. We noticed that the reaction products increased the barrier effect of the primer, possibly sealing the voids that naturally are formed in the coating during exposure to the environment.

3. Extension to other structural metals: the development of this protective primer was sponsored and generated by the US Air Force and its need for a replacement for the toxic Chromate based primers for Al alloys. Because of time and limitation in funds, it was not possible to look deeply at other applications and other fields that use structural Al alloys. Aluminum alloys are used in several other applications, costal

structures, outdoor windows, high speed trains naval applications and other uses

definitely exist that we did not identify.